

University of Naples Federico II



School of Engineering
Department of Chemical Engineering, Materials and Industrial Production
Ph.D. in
INDUSTRIAL PRODUCT AND PROCESS ENGINEERING
33° Cycle

*Engineering novel micro-scaffolds and bottom up
strategies for in vitro building of vascularized
hybrid tissues*

Ph.D Candidate: **Parisa Pedram**

Supervisor: **Prof. Dr. Paolo Antonio Netti**

Advisor: **Dr. Aurelio Salerno**

Coordinator: **Prof. Dr. Andrea D'Anna**

Academic years 2018-2021

Table of contents

Abstract	10
-----------------	-----------

Chapter 1

State of the art about micro-scaffolds design, fabrication and application in modular tissue engineering	12
---	-----------

1.1	Introduction to tissue engineering, scaffolds, and bottom-up approaches	14
1.2	Micro-particles and their use as scaffolding modules for <i>in vitro</i> and <i>in vivo</i> tissue engineering	17
1.2.1.	Micro-particles fabrication by advanced processes	17
1.2.2.	Porous scaffolds prepared by micro-particles sintering (cell-free strategies)	20
1.2.3.	Porous micro-particles as micro-scaffolds for <i>in vitro</i> tissue building (cell-laden strategies)	26
1.3	Research hypothesis and objectives	37
1.4	References	39

Chapter 2

Bioinspired design of novel micro-scaffolds for fibroblasts guidance towards <i>in vitro</i> tissue building	47
---	-----------

2.1	Introduction to porous micro-scaffolds for <i>in vitro</i> tissue engineering	49
2.2	Experimental part	51
2.2.1	Materials	51
2.2.2	Fluidic device and porous polycaprolactone micro-scaffolds fabrication	51
2.2.3	Morphological and microstructural characterization	52
2.2.4	<i>In vitro</i> degradation	53
2.2.5	Cells expansion, seeding and culture	53
2.2.6	Cell viability and proliferation	54
2.2.7	Cell morphology, colonization and tissue production	54
2.2.8	Statistical analysis of data	56
2.3	Results and discussion	56

2.3.1	Fabrication of porous polycaprolactone micro-scaffolds	56
2.3.2	Modulation of micro-scaffolds diameter and porous structure	59
2.3.3	<i>In vitro</i> degradation and biocompatibility	66
2.4	Conclusion	74
2.5	References	75

Chapter 3

***In vitro* microscale engineering of 3D vascularized hybrid tissues by micro-scaffolds patterning and co-culture of fibroblasts and endothelial cells**

3.1	Introduction to micro-scaffolds patterning and modular tissue vascularization	88
3.2	Experimental part	92
3.2.1	Materials	92
3.2.2	Porous polycaprolactone micro-scaffolds fabrication and characterization	92
3.2.3	Polydimethylsiloxane patterned moulds design and fabrication by soft lithography	92
3.2.4	Fibroblasts and endothelial cells culture and expansion	94
3.2.5	Vascularized hybrid mono-layer constructs fabrication by micro-scaffolds patterning onto polydimethylsiloxane moulds and co-culture of fibroblasts and endothelial cells	94
3.2.6	Analysis of monolayer constructs morphology and growth by MicroCT and histology	95
3.2.7	Characterization of cells growth and tissue vascularization by confocal and multiphoton analyses	95
3.2.8	Collagen biosynthesis evaluation by second harmonic generation test	96
3.2.9	Fabrication of vascularized hybrid bilayer constructs by monolayers assembly and bonding into de-novo designed culturing chamber	96
3.2.10	Analysis of bilayer constructs morphology and growth by MicroCT and histology	99
3.2.11	Characterization of cells growth, proliferation and tissue vascularization by confocal and multiphoton analyses	99

3.2.12	Collagen biosynthesis evaluation by second harmonic generation test	99
3.2.13	Statistical analysis of data	100
3.3	Results and discussion	100
3.3.1	Micro-scaffolds morphology and pore structure features	100
3.3.2	Monolayer constructs morphology, composition and vascularization	102
3.3.3	Collagen amount and density of monolayer constructs	109
3.3.4	Monolayers discussion	113
3.3.5	Bilayer constructs morphology, composition and vascularization	114
3.3.6	Collagen amount and density into bilayer constructs	122
3.3.7	Bilayers discussion	125
3.4	Conclusion	126
3.5	References	128
Chapter 4		
Conclusions		132
<hr/>		
Chapter 5		
Future perspectives		135
<hr/>		
5.1	Control of hybrid tissues composition and growth by the modulation of micro-scaffolds degradation	136
5.2	Control of hybrid tissues vascularization by the incorporation of growth factors delivering micro-scaffolds	137
5.3	References	138

Acronyms list (alphabetic order)

<i>Abbreviation</i>	<i>Expanded form</i>
μPs	Microparticles
μ-scaffolds	Micro-scaffolds
μTPs	Micro tissue precursors
3D	Three-dimension
AL	Alendronate
ALP	Alkaline phosphatase activity
BMP-2	Bone morphogenetic protein-2
BSA	Bovine serum albumin
CAD	Computer-aided design
CLSM	Confocal laser scanning microscopy
Dex	Dexamethasone
ECM	Extracellular matrix
FBS	Fetal bovine serum
Gel-MA	Gelatin-methacrylate
HA	Hydroxyapatite
HAMSCs	Human amniotic
HDFs	Human dermal fibroblast
HepG2	Human hepatocellular carcinoma cells
HMSCs	Human mesenchymal stem cells
HUVECs	Human umbilical vein endothelial cells
MEM	Minimum Essential Medium Eagle
MG63	Human osteosarcoma
MSCs	Mesenchymal stem cells

<i>Abbreviation</i>	<i>Expanded form</i>
NCMS	Nanofibrous chitosan μ -scaffolds
PBS	Phosphate-buffered saline
PCL	Polycaprolactone
PDMS	Polydimethylsiloxane
PEG	Polyethylene glycol
PEGDMA	Polyethylene glycol dimethacrylate
PEO	Polyethylene oxide
PLA	Poly-lactic acid
PLGA	Poly-lactic-co-glycolic acid
PTFE	Polytetrafluoroethylene
PVA	Polyvinyl alcohol
QCP	Continuous phase
QDP	Dispersed phase
RT	Room Temperature
SEAL	StampEd Assembly of polymer Layers
SEM	Scanning electron microscope
SF	Silk fibroin
SHG	Second Harmonic Generation
SLS	Selective laser sintering
TE	Tissue engineering
TGF	Transforming growth factor
UV	Ultraviolet

DEDICATIONS

TO MY SUPPORTIVE HUSBAND AND BEST FRIEND

ACKNOWLEDGEMENTS

I would like to convey my sincere and heartfelt gratitude to my supervisor, Professor Dr. Paolo Antonio Netti for giving me exceptional support and assistance during this challenging multidisciplinary project. I am honoured to have had the opportunity to work as a Ph.D. candidate under his supervision at the Italian Institute of Technology (IIT), center in Naples.

I would also like to thank my advisor, Dr. Aurelio Salerno, whose full support, vast knowledge, and professionalism, helped me to fully succeed in this project. I am blessed to have worked under his direction. I am extremely lucky to have learned from him through his continuous professional assistance during this research project. He has always been there for me whenever I needed help both personally and professionally.

I would like to thank my coordinator Prof. Dr. Andrea D'Anna for his constant support and guidance during my studies.

I would also like to acknowledge Dr. Claudia Mazio, who have greatly contributed to the accomplishment of this work. Precious her contributions have surely paved the way to the accomplishment of my Ph.D. project.

I would like to say a big thank you to all the technician's group members at the IIT for their supporting throughout my project, especially to Dr. Valentina Mollo for the guidance throughout the SEM and MicroCt analysis, Dr. Fabio Formiggini for the help with CLSM imaging. My thanks also go to the Dr. Chiara Attanasio of the department of veterinary medicine, University of Naples Federico II, for providing the best possible opportunity to do an important part of my experiment in this interesting project.

My deep and special gratitude goes to Dr. Arash Moeini my supportive husband and my best friend, who helped me in various aspects during my Ph.D. I would like to thank him for her love, patience, and encouragement, and having faith in me when I was down, and pushing me to stand up and continue.

To conclude, I would like to thank my family for always supporting me and I cannot forget to thank my closest friends, Laura Matino and Claudia Lubrano for all the unconditional support in these very intense academic years.

Abstract

There is a significant demand of de-novo engineered tissue grafts capable of replacing biological tissue and/or organ functions for clinical applications. The major obstacle to achieve this goal is the difficulty of recreating all of the complex biochemical and biomechanical functions of the tissue to regenerate, together with transport limitations into the bulk of these newly synthesized tissues. Oxygen and nutrients are supplied to cells and tissues naturally by the microvasculature, which is composed of branching, variable diameter blood vessels. Replicating the complex architecture and functionalities of native tissue vasculature is therefore one of the most important challenge in tissue engineering strategies.

To date, bottom up techniques are strong powerful tools to build large viable tissue constructs by packing and sintering cell-laden scaffold-based micro-modules (μ -scaffolds) in a mould. In fact, after sintering and further μ -scaffolds degradation it is possible to achieve large viable tissues *in vitro*, replicating the composition and structure of native tissue and suitable for studying biological processes involved in new tissue genesis, maturation and remodelling.

The aim of this work is to design and engineering novel μ -scaffolds and bottom up assembly techniques to fabricate vascularized layered tissues and to study the effect of μ -scaffolds spatial distribution and co-culture of human dermal fibroblasts (HDFs) together with human umbilical vein endothelial cells (HUVECs) on new tissue growth and vascularization *in vitro*. To achieve these aims, in first part of this study, we fabricated porous polycaprolactone (PCL) μ -scaffolds with bioinspired trabecular structure and we demonstrated that these newly developed μ -scaffolds supported the *in vitro* adhesion, growth, and biosynthesis of HDFs. The μ -scaffolds were fabricated by using a fluidic emulsion/porogen leaching/particle coagulation process and by using polyethylene oxide (PEO) as a biocompatible pore-generating agent. In particular, the effect of the composition of the polymeric solution and the flow rate of the continuous phase on μ -scaffolds size distribution, morphology and architectural properties were assessed with the aim to find the best preparation conditions for biological characterization. *In vitro* culture of HDFs showed that μ -scaffolds supported cells adhesion, colonization, proliferation and biosynthesis in the entire three-dimensional porosity up to 25 days.

The second part of this study involved the development of a soft-lithography approach to control the spatial assembly of μ -scaffolds and to create two distinctive μ -scaffolds patterns, namely ordered and disordered. The as obtained patterns were used as substrate for culturing HDFs and

HUVECs aiming to develop viable monolayers and bilayers tissue constructs *in vitro*. The results of this study demonstrated that μ -scaffolds patterning directed cells colonization and biosynthesis and guided the morphology and distribution of newly formed vasculature. All of the findings reported in this work demonstrated the vital role of μ -scaffolds architectural features and assembly on *in vitro* tissue growth and, pay the way about the possibility to create in silico-designed vasculatures inside modularly engineered biohybrids tissues.

Chapter 1

*State of the art about micro-scaffolds
design, fabrication and application in
modular tissue engineering*

The following Chapter 1 includes data and information that have been published in the review article:

Aurelio Salerno, Giuseppe Cesarelli, Parisa Pedram, Paolo Antonio Netti. Modular Strategies to Build Cell-Free and Cell-Laden Scaffolds towards Bioengineered Tissues and Organs. Journal of Clinical Medicine. 2019, 8, 1816; [doi:10.3390/jcm8111816](https://doi.org/10.3390/jcm8111816).

1.1. Introduction to tissue engineering, scaffolds, and bottom-up approaches

Tissue engineering (TE) is an interdisciplinary research field aiming to restore, maintain, or enhance the functionalities of damaged tissues or organs [1]. Since its birth in the 1980s, the field of TE has applied the principles of biology, medicine, and engineering science to find clinical solutions for enhancing wound healing and stimulate the own body`s capability of repairing tissues like skin, nerve, cardiovascular tissue, bone and cartilage among others [1-5].

Cells, biodegradable scaffolds, and biochemical cues, like growth factors and stem cell differentiation molecules, are the three key components of engineered tissues in TE as they are usually combined to replicate natural processes of tissue regeneration and development. The interactions among these three main components are critical to obtaining de-novo regenerated tissues with proper biochemical and biomechanical functionalities [6].

Biological tissues are normally composed of cells residing in an extracellular matrix (ECM). This ECM provides adequate structural support for anchorage-dependent cells, organizes cells in a three-dimensional (3D) space, and acts as a reservoir of growth factors for cell growth and morphogenesis. Synthetic scaffolds must therefore mimic the features of the native ECM of the target tissue. However, ECM in native tissues possesses complex compositions and dynamic nature, which bring multiple biological functions such as cell adhesion, migration, proliferation, and differentiation. This is a critical aspect as ECM complexity is challenging to be enclosed in a single scaffolding device, finally limiting the actual implementation of scaffolds into the clinic [7].

Literature review regarding scaffolds for TE applications allow us to resume the main scaffolds functions, as follows: (1) serving as space holders to prevent undesired tissue invasion from the immediate vicinity into the affected site; (2) providing a temporary biomechanical support structure for the growing tissue; (3) creating a substrate for cells anchorage as well as cells grow, proliferation, migration, and differentiation; (4) serving as cell delivery platform to the defect site; (5) providing 3D space for blood vessel growth and infiltration, neotissue formation, and remodelling, (6) enabling the transport of nutrients and growth factors in the entire volume together with the removal of cellular metabolic wastes [8-10].

All of the previous basic functions require well definite scaffolds features such as [9-14]: (1) biocompatibility, intended as the capability of the scaffold to stimulate a positive interaction with cells and host tissues; (2) biodegradability, that is get broken down into small molecules to eliminate from the body via naturally occurring processes; (3) controlled degradation kinetic and

mechanical properties, matching the growth rate of the new tissue while ensuring biomechanical stability during naturally occurring *in vivo* stresses at the site of implantation; (4) surface bioactivity to enable cell attachment, growth, proliferation, and differentiation as well as ECM biosynthesis; (5) have a 3D porous architecture with optimal pore size, porosity, pore interconnectivity, and permeability to allow adequate diffusion of nutrients, growth factors, and wastes; (6) desired shape, size, and morphology.

TE scaffold-based approaches can be conveniently classified into two big groups: top-down and bottom-up [15]. In top-down approaches, the scaffolds are fabricated into a pre-formed porous monolith with size and shape close to the tissue's size and shape to regenerate. The scaffold is composed of biocompatible and biodegradable materials, such as polymeric composites or ceramics, and encodes inside the porous architecture drug delivery carriers for proper bioactivation. Therefore, this even complex scaffold can be implanted directly into the defect site and guide tissue regeneration by cell homing and blood vessel migration from surrounding tissues (*in vivo* strategy). Alternatively, cells are seeded into the scaffold *in vitro* and allowed to create the appropriate ECM with bioreactors aid before *in vivo* implantation (*ex vivo* strategy) [7]. Both top-down approaches using prefabricated scaffolds have several advantages. First, the scaffolds can be manufactured using materials of different origins, mainly synthetic and natural polymers and ceramics. This aspect ensures a large variety of compositions to match degradation and biomechanical requirements for each specific application. Furthermore, scaffolds can be produced by a wide range of processing techniques, such as gas foaming, phase separation, and porogen leaching, among others. Combining different materials and manufacturing processes may allow obtaining porous scaffolds with high mechanical properties by altering the porosity and pore architecture [7].

Nevertheless, top-down approaches still have important drawbacks. For example, cell proliferation and differentiation in the entire scaffold porosity is often hindered by inhomogeneous cell seeding and by nutrients diffusion into the scaffold core, finally leading to the formation of an immature and dysfunctional neotissue. Several efforts have been made in the past to overcome previously highlighted drawbacks of top-down scaffold-based approaches. For instance, Zhang and co-workers investigated the bone morphogenetic protein-2 (BMP-2) binding to 3D polycaprolactone (PCL) scaffolds by a crosslinking conjugation to enhance scaffold osteoconductivity [16]. Other efforts to improve cell seeding include flow perfusion of the cell

suspension inside the scaffold or designing scaffolds with architectural features, namely pore size, shape, and interconnection, suitable for improving cell migration and fluid transport in 3D [17-19]. Most importantly, by top-down approaches, it is difficult to reproduce all the complex functions of ECM of native tissues inside the scaffold to ensure a biomimetic dynamic microenvironment for cells and tissue guidance towards the regeneration of functional biological tissues in 3D [7, 15].

Bottom-up TE strategies aim to address the challenge of recreating biomimetic 3D structures by designing scaffold features at the nano and microscale. In particular, by using modular approaches, it is possible to build even complex scaffolds and large biological constructs by the controlled assembly of building blocks [15, 20]. These modules can be manufactured in many ways, such as through self-assembled aggregation [21], microfabrication of cell-laden hydrogels [22], creation of cell sheets, or direct printing of tissues [23-24]. Once created, these modules can be assembled into larger tissues through several methods such as random packing, stacking of layers, or directed assembly [15]. The bottom-up TE approaches hold great promise for creating functional tissues starting from every kind of material and cells by directing their assembly to mimic the complexity of living tissues. However, random or uncontrolled assembling of this structures can not allow to reproduce native hierarchical tissue organization from cellular to tissue level, so the control of the assembly process to fabricate 3D constructs is still a challenging goal.

This thesis focuses on the development of novel building blocks and bottom-up strategies to obtain tissue with control of cells distribution, ECM biosynthesis, and vasculature development at the micrometric size scale [7]. In the next paragraphs of this chapter, we will focus our attention on state of the art of building blocks for *in vitro* and *in vivo* modular scaffolds and their use in TE for the regeneration of biological tissues.

1.2. Micro-particles and their use as scaffolding modules for *in vitro* and *in vivo* tissue engineering

This part of the Introduction focuses on microparticles (μ Ps) design and fabrication technologies. In particular, it will be described the most interesting and advanced methods enabling the control of μ Ps features, namely morphology, size, shape and composition. Furthermore, we will provide a comprehensive and exhaustive description and discussion of literature data about porous μ Ps and their use as building blocks for bottom-up TE approaches, as these topics represent the basis for the research work herein described.

1.2.1 Micro-particles fabrication by advanced processes

μ Ps play a crucial role in tissue engineering and have recently received extensive interest in their clinical and medicine application, such as drug delivery systems, diagnostic purposes, and micro-scaffolds (μ -scaffolds) [25].

Polymeric biomaterials, that can be classified into natural and synthetic polymers, have been extensively used for μ Ps fabrication. Indeed, polymeric μ Ps can be designed and fabricated with appropriate morphology, size, and shape distribution, as well as degradation rate and surface properties depending on the specific application field [26]. PCL, poly-lactic acid (PLA), polylactic-co-glycolic acid (PLGA), polyethylene glycol (PEG) as well as their composites containing calcium phosphates, alumina and hydroxyapatite, are among the most used materials for μ Ps fabrication [27-32]. Natural polymers are also used for μ Ps fabrication as they have a chemical composition and structure resembling that of native biological tissues. This aspect is extremely important as it enables to replicate the composition and structure of native ECM. Natural polymeric μ Ps can be classified into two main groups: protein-based, such as silk, collagen, and fibrin, and polysaccharide-based, like agarose, chitosan, and hyaluronic acid. These kinds of μ Ps have advantages like good cellular interaction, low immunogenic response, and resorption kinetic that can be adjusted by varying μ Ps' formulation, molecular weight, and crosslinking degree [26]. μ Ps have been fabricated by conventional methods like phase separation, spray drying, and batch emulsion. However, these methods often produced materials with heterogeneous size distribution and limited control over their shape [33-34]. During last decades, advanced techniques have been developed to overcome these drawbacks. Figure 1.1 highlights three of the most interesting way to obtain μ Ps with finely tuned composition and architecture. Microfluidics is an advanced

technique that process fluids into microscale channels for fluid mixing, splitting, and chemical reaction. Microfluidic emulsion may enable the high-throughput production of monodisperse microparticles of controllable size, shape, and composition [35].

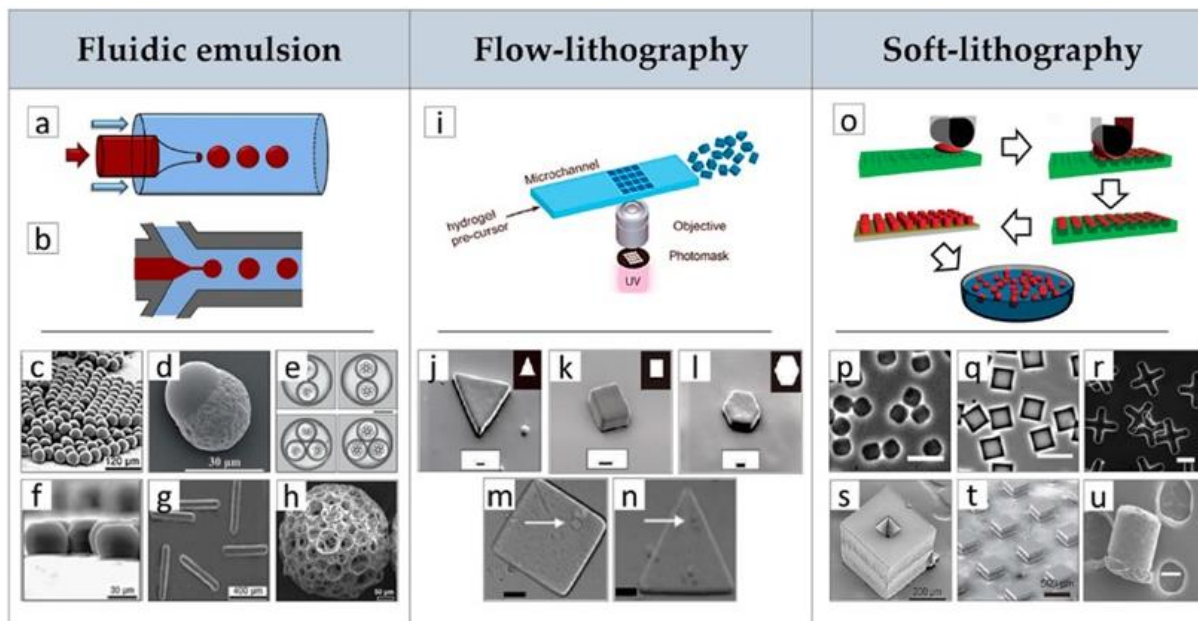


Figure 1.1: Advanced techniques for μ Ps fabrication. Fluidic emulsion: (a) co-flow and (b) flow-focusing. (c) Spherical monodisperse μ Ps, (d) Janus μ Ps, (e) core-shell μ Ps with dual and triple cores, (f) disks and (g) rods μ Ps, (h) Porous PLGA μ Ps prepared by double emulsion. (i) Flow-lithography process: (j) triangles, (k) squares and (l) hexagons μ Ps. Single-cell encapsulated within (m) square and (n) triangular μ Ps, (o) Soft-lithography: (p, q and r) effect of mold type on μ Ps shape; morphology of μ Ps obtained by SEAL process before (s) and (t) after sealing; (u) morphology of vascular endothelial growth factor (VEGF)-loaded PLGA microsphere after solvent vapor shaping process. (J. Clin. Med. 2019, 8, 1816; doi:10.3390/jcm8111816 [26]).

Microfluidic devices are usually fabricated of transparent materials that doesn't dissolve and/or deform when in contact with used chemicals, such as glass capillaries or creating channels in a silicone elastomer, e.g., polydimethylsiloxane (PDMS), through soft-lithography methods (Figures 1.1 (a) and (b)) [36]. Figures 1.1 (a) and (b) shows the single emulsion for the fabrication of μ Ps with uniform shape and size distribution. Uniform beads are formed conveniently from droplets controlling the flow rate of continuous and dispersed phases (Figure 1.1c). More importantly, beads can be formed with a variety of architectures like core-shell, patchy, and Janus

with controlling other parameters in this technique such as solvent evaporation, phase separation, and solutions' composition (Figure 1.1d) [29, 37]. For example, Cao and co-workers reported that the patchy and Janus shape of μ Ps can be formed with high-throughput and narrow size distribution by using PLGA/PCL blends. In that study, droplets formed and easily converted into beads by controlling interfacial tensions and spreading coefficients between immiscible phases of the generated droplets. Therefore, μ Ps' properties, such as hydrophilicity, degradation rate, and drug delivery, can be adjusted depending on the application [29]. Fabrication of multiple cores and impart drug delivery capabilities can be also possible in microfluidic devices by combining multiple emulsions (Figure 1.1e). Besides, the loading efficiency of hydrophobic polymeric μ Ps is improved by changing their polarity in these techniques [38]. In the microfluidic flow-focusing, droplets were formed in the PDMS and glass capillary devices with different sizes and shapes and monodispersed size distribution [39]. Defining the size of an undeformed (regular) spherical droplet as $dS = (6V/\pi)^{1/3}$, non-spherical droplets can be formed when dS is larger than one of the outlet channel's dimensions. Figure 1.1f shows a discoid shape with rounded borders formed when $w > dS$ (w = width) while the height $h < dS$. On the other hand, if h and w are smaller than dS , droplets can be formed with a rod-like morphology as shown in (Figure 1.1g) because, in this case, droplets are contacted with all channel walls.

Microfluidic techniques have been utilized for the fabrication of porous μ Ps (Figure 1.1h), with suitable features such as large surface area, good mechanical strength, and high interconnectivity. These samples were then used as μ -scaffolds for cell adhesion and proliferation [37]. In this case, porous μ Ps were produced by a water-in-oil emulsion that gelatin and poly (vinyl alcohol) (PVA) is served as a discontinuous phase and PLGA solution in dichloromethane as the continuous phase. Therefore, porous μ Ps are generated by solvent extraction and evaporation in the water phase. Other advanced techniques are the flow-lithography process for the fabrication of multifunctional Janus μ Ps as well as synthesizing different kinds of shapes and sizes of oligomers. In this process, ultraviolet (UV) photopolymerization of a fluidic bead within light transparent PDMS channel is induced by using proper UV masks to control particle size and shape [31]. However, several parameters should be optimized, such as optical resolution, microscope objective, polymerization time, and flow rate, to keep the patterned feature in the hydrogels. More importantly, these advanced techniques are not suitable for synthetic thermoplastic polymer, such as PCL and PLGA that cannot be photopolymerized by UV [26]. Recent advances in micro/nanotechnology have

allowed fabrication of μ PBs made of thermoplastic polymers with uniform sizes and well-defined shapes and composition which are otherwise impossible to fabricate using conventional μ PBs manufacturing methods, providing new building blocks libraries for modular TE. In particular, soft-lithography techniques involve the use of elastomeric PDMS stamps with topological microfeatures to fabricate μ PBs with precise control over size and geometry in a simple, versatile, and cost-effective modality (Figure 1.1o) [30, 40-42]. The cavities of the stamp were filled by polymeric solution and after solvent evaporation, the dried polymer is deposited on selective portions of the mold in form of particles and it is removed from the PDMS mold by stamping it onto a PVA sacrificial layer at temperatures and pressures in the range of 80–120 °C and 30–90 KPa, respectively [41]. The μ PBs are released from the mold by dissolving the PVA layer in water. The versatility of these fabrication methods has been demonstrated using materials of biomedical interest including thermoplastic polymers such as PCL and PLGA (Figures 1.1p-r) [42], polyethylene glycol dimethacrylate (PEGDMA) hydrogels and chitosan. An advancement in this fabrication technique was reported recently by McHugh and co-workers that developed a microfabrication method, termed StampEd Assembly of polymer Layers (SEAL), for fabricating modular micrometric structures, such as injectable pulsatile drug-delivery PLGA μ PBs with complex geometry at high resolution (Figures 1.1s,t) [43]. In another study, de Alteriis and co-workers used microspheres to obtain shaped μ PBs by a soft-lithography approach [30]. This was achieved by positioning PLGA microspheres into PDMS mold cavities with different shapes and deforming them under gentle process conditions, i.e. at room temperature using a solvent/non-solvent vapor mixture. By this approach, it was also possible to preserve the microstructure and bioactivity of molecules loaded inside the μ PBs (Figure 1.1u). In conclusion, all of the discussed advanced μ PBs fabrication methods may open new avenues for the fabrication of multifunctional building blocks for modular TE applications.

1.2.2 Porous scaffolds prepared by micro-particles sintering (cell-free strategies)

μ PBs are used as building blocks for engineering biological tissues with two different approaches: cell-free and cell-laden. In the first one, μ PBs are assembled to form a sintered porous scaffold. The scaffold can be subsequently implanted *in vivo* into the defect site and stimulate the intrinsic body's regeneration capability by delivering bioactive molecules (*in vivo* strategy). Alternatively, the sintered scaffold is seeded *in vitro* with specific cells and, the as obtained hybrid construct is maintained *in vitro* under biochemical and biomechanical stimulation to promote new

tissue development before *in vivo* implantation (*ex vivo* strategy). Conversely, the cell-laden approach involves the use of μ Ps as μ -scaffolds for *in vitro* cell culture and new tissue fabrication. In particular, cells are seeded onto the μ Ps that, in this case are use as μ -scaffolds, and the cell-laden μ -scaffolds are assembled *in vitro* by promoting cell-to-cell and cell-to-ECM interlocking. The final μ -scaffolds degradation and new tissue remodeling allow to obtain fully biological tissues trying to reproduce native tissues' composition and structure [26]. Both approaches require μ -scaffolds assembly into the 3D structure (centimeter scale) by two main ways, random and ordered. This part of the dissertation will describe cell-free TE strategies and highlighted some of the most investigated studies up to date while paragraph 1.2.3 will focus on cell-laden approaches that are the main objective of the work.

There are several literature works reporting the design and fabrication of scaffolds by assembling biodegradable and biocompatible μ Ps to achieve tailored porous structure, full interconnected porosity, high mechanical stiffness and, ultimately, drug loading and controlled release features. In a typical process, researchers prepared bioactive and biodegradable μ Ps using traditional or advanced methods, such as those described in the previous section. The μ Ps were then poured into appropriate molds and sintered together to form a continuous matrix [26, 27]. Sintering depended on the motion of polymeric chains from μ Ps surface to contact points that leads to chain inter-diffusion and subsequent formation of connecting necks between μ Ps. This mechanism depends on polymer plasticization and can be promoted by heat, organic solvents or high pressure fluids [44-49]. As shown in (Figure 1.2a), PCL scaffolds were fabricated using thermal sintering of spherical μ Ps with two different size ranges, smaller (300-500 μ m) and larger (500-630 μ m) at 60°C for 1h. A double emulsion process was also implemented for bovine serum albumin (BSA) encapsulation inside the depots of smaller (50-180 μ m) PCL particles for drug delivery purposes. The authors reported the decrease of scaffolds porosity and pores size as well as the increase of compression moduli with the decrease of μ Ps size. This effect is ascribable to an enhanced μ Ps compaction and a concomitant higher number of fusion points between smaller μ Ps [27]. However, low porosity and pore size may result in decreased cell adhesion and colonization. The use of porous μ Ps enable to overcome this limitation and achieve higher scaffolds' porosity. For instance, Qutachi and co-workers, fabricated porous PLGA μ Ps by the double emulsion process using phosphate-buffered saline (PBS) as the internal aqueous phase and treating the μ Ps by utilizing 30% 0.25 M NaOH:70% absolute ethanol to enhance surface pores opening.

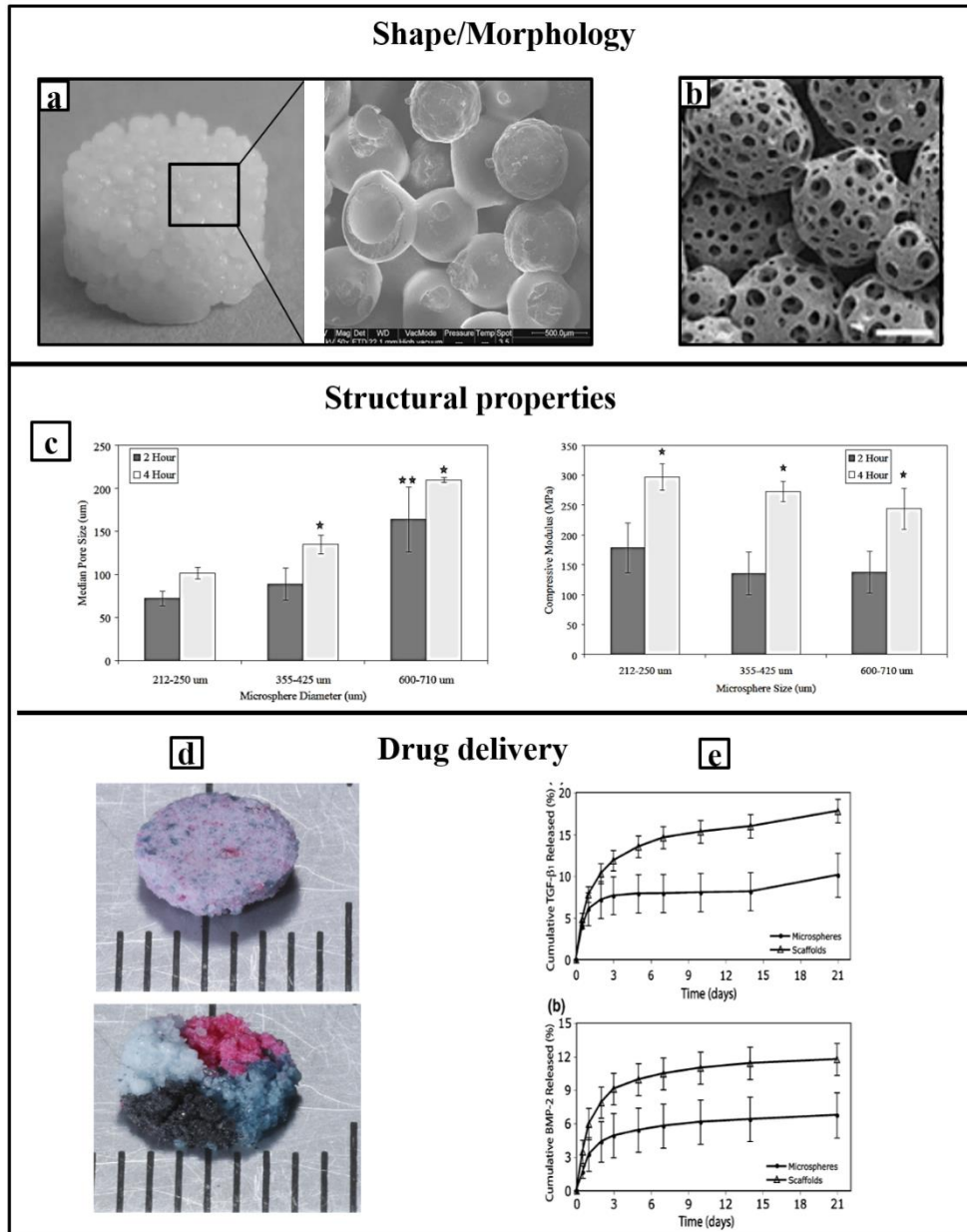


Figure 1.2: μ Ps applications in tissue engineering (TE) of cell-free scaffold-based approach by the random assembly (a) PCL scaffold obtained by thermal sintering and the morphology of sintered PCL μ Ps (b) Morphology of porous PLGA μ Ps' in sintered PLGA scaffold (c) the influence of diameter and thermal sintering time of PLGA μ Ps on average pore size and compressive modulus of PLGA scaffolds. (d) Optical images of sintered scaffolds with the homogeneous and heterogeneous spatial distribution of loaded μ Ps. (e) Release profiles of (BMP)-2 and transforming growth factor (TGF) beta1 from μ Ps'-sintered scaffolds for osteochondral interface TE. (Adapted from: J. Clin. Med. 2019, 8, 1816; doi:10.3390/jcm8111816 [26]).

As shown in Figure 1.2b, PLGA μ Ps were also able to form a sintered matrix at body temperature, therefore opening the use of these materials as injectable fillers [44]. The sintering process is an important issue to fabricate the scaffolds by using μ Ps as it affects the scaffolds' structure as well as porosity and mechanical properties. Therefore, controlling the sintering process is the most crucial step to fabricate scaffolds by μ Ps. Many studies tried to develop and optimize the sintering step for melt-sintered, solvent-sintered, and high-pressure CO₂ sintering [45, 50-51]. Figure 1.2c shows that the mechanical properties of PLGA scaffolds are directly related to fusion time as, increasing fusion from 2 to 4 h, lead to an increase in the mechanical properties. However, the pore structure completely collapsed with increasing treatment time resulting from the extensive polymer melting [50]. These scaffolds, having elastic compression moduli in the range of 137.44 to 296.87 MPa, appeared to be capable of sustaining loads in the mid-range of cancellous bone [50]. Another method of scaffold setting is solvent/non-solvent chemical sintering and can be used to obtain TE scaffolds from a wide variety of the polymeric μ Ps at low temperatures for drug delivery applications [51]. Brown et al. have investigated the assembly of polyphosphazene exhibiting glass transition temperatures from -8 to 41 °C and PLGA by solvent/non-solvent sintering process. They optimized the parameter of solvent/non-solvent mixing and treatment time based on the affinity between polymer and solvent mixtures and observed that scaffolds' pore size and porosity were close to the scaffolds prepared by thermal sintering [51]. However, the toxic organic solvent is the main problem in this process and, in such cases, low-temperature solvent-free sintering is the preferred method [44-45]. High-pressurized CO₂ is applied for the sintering of μ Ps such as PCL, PLGA, and PLA [45]. For example, PLGA scaffolds have been sintered at room temperature by using CO₂ pressure in the 15–25 MPa range, and sintering increase with the increase of the pressure, finally resulting in scaffolds with higher mechanical properties [45]. As described in the paragraph 1.1, the design of bioactive molecules releasing scaffolds has to consider that spatial patterning of bioactive signals is vital to some of the most fundamental aspects of life, from embryogenesis to wound healing, all involving concentration gradients of signaling molecules that have to be replicated by scaffolds. μ Ps have been long studied as drug delivery systems for a variety of molecules as they enable an easy control of the release kinetics of loaded therapeutics. For instance, Shi and co-workers reported the use of Alendronate (AL)- and dexamethasone (Dex)-loaded PLGA μ Ps for bone regeneration [52]. These molecules were selected as AL is a bisphosphonate that improves the activity and maturation of osteoblasts and

mesenchymal stem cells (MSCs) differentiation, while Dex is a glucocorticoid with osteogenic features. Scaffolds can release AL and Dex for two months in a sustained fashion. Therefore, these scaffolds have advantages such as a higher expression of bone-related proteins and genes, such as alkaline phosphatase activity (ALP), type-I collagen, osteocalcin, and (BMP)-2, by transplanted cells, if compare to unloaded scaffolds. Besides, drug-loaded scaffolds evidenced significantly higher new bone creation at 8 weeks of implantation into rabbit femurs bone defects [52]. Figure 1.2d shows another advantage of μ Ps sintered scaffolds for the spatially controlled distribution of bioactive molecules in the porous structure [53]. These results were obtained by Singh and co-workers that developed a fluidic device for the controlled deposition of functional microspheres to create gradients of releasing molecules for interfacial tissues' regeneration [54]. By controlling suspensions composition and flow rates during pumping, it was possible to engineer multiple gradient configurations of BMP-2 and (TGF) beta1, to match the requirements of anisotropic tissues like osteochondral tissue (Figure 1.2e) [55]. MSCs-seeded scaffolds revealed regionalized gene expression of major osteogenic and chondrogenic markers after 6 weeks of *in vitro* culture. Overall, scaffolds based on the assembly of μ Ps are versatile for wide range of TE applications, from soft to hard tissues. For instance, the use of synthetic polymers resulted in high mechanical stiffness and a slow degradation rate for *in vivo* load bearing implantation, such as bone and osteochondral tissue [56-57]. Conversely, soft biopolymeric chitosan μ Ps scaffolds were proposed as 3D functional neuronal networks regeneration platform [58]. Even if all these studies clearly evidenced the potential of μ Ps-based scaffolds in TE applications, some key issues have to be still addressed for their successful clinical translation. As previously discussed, biological tissues are characterized by hierarchical ordered architectures at both nano- and micro-metric size scales, that can be replicated only in part by μ Ps random assembly. Furthermore, μ Ps-based scaffolds require multiple steps of fabrication, from μ Ps fabrication up to assembly and sintering. Therefore, the possibility to reduce scaffolds fabrication time by automated processes will be a great step towards clinical implementation.

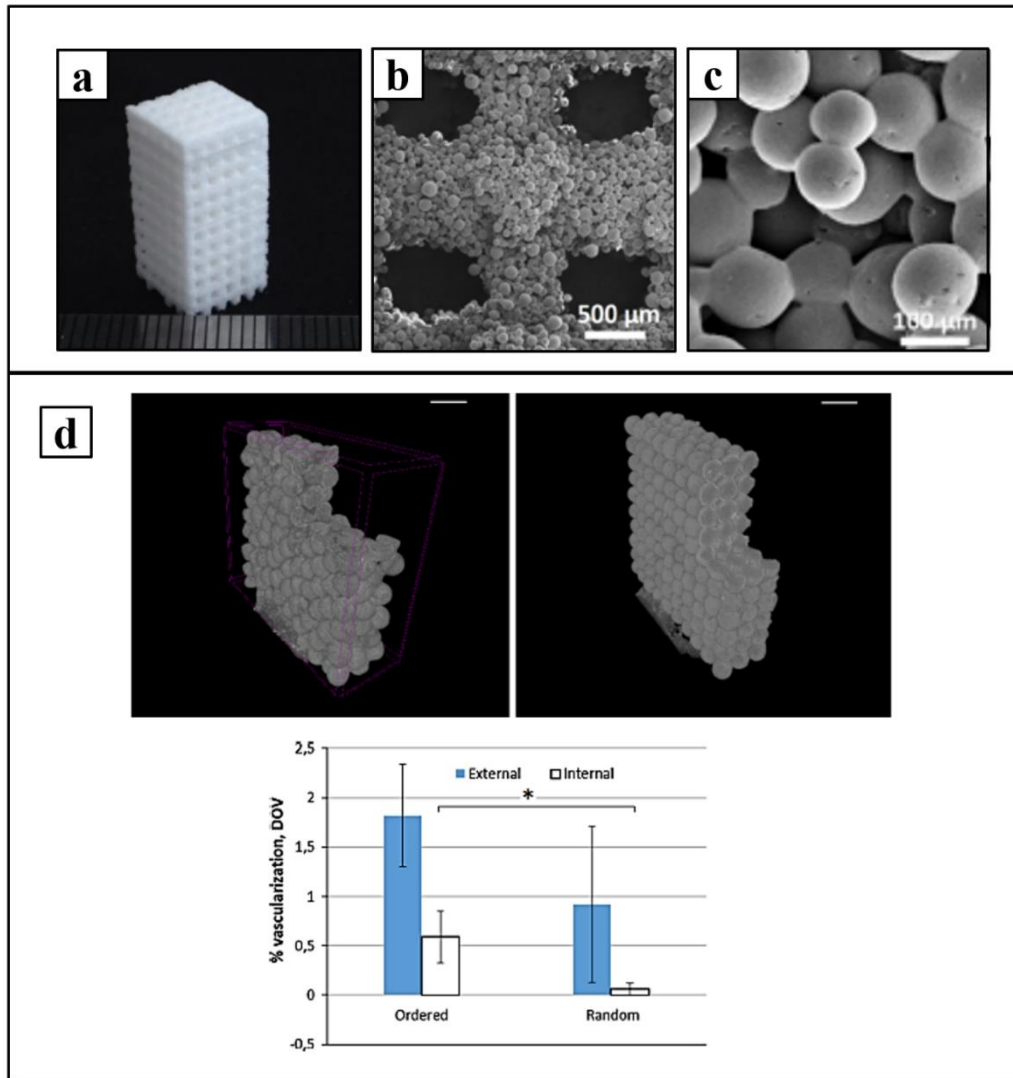


Figure 1.3: μ Ps applications in tissue engineering (TE) of cell-laden scaffold-based approach by ordered assembly (a) Optical image ordered scaffold made of PCL μ Ps, performed by SLS. (b) morphology of SLS ordered scaffold structure (c) morphology of SLS random scaffold structure (d) the degree of vascularization of random and ordered PCL scaffolds *in vivo*, The results evidenced that better vascularization in the inner core of the ordered scaffold in comparison with the random scaffolds. (Adapted from: J. Clin. Med. 2019, 8, 1816; doi:10.3390/jcm8111816 [26]).

As previously discussed, biological tissues are characterized by hierarchical-ordered architectures at both nano and micrometric size scales, that can be replicated in a limited way by random μ Ps' assembly. Furthermore, μ Ps-based scaffolds require multiple steps of fabrication, from μ Ps' fabrication up to assembly and sintering. Therefore, the possibility to reduce scaffolds'

fabrication time by automated processes represent a great step towards the clinical implementation of these materials. One of the most investigated methods to obtain ordered scaffolds from sintered μ Ps is selective laser sintering (SLS) [59]. SLS uses a CO₂ laser beam to selectively sinter a powder bead, following a computer-aided design (CAD) scaffold model. Du and co-workers fabricated PCL and PCL-hydroxyapatite scaffolds for bone TE [60]. However, the SLS method provides an ordered structure (Figure 1.3b) within a random assembly of μ Ps (Figure 1.3c) as μ Ps cannot be precisely positioned in the inner part of the scaffold structure. To address this issue, not so far Rossi and co-workers reported a new way to manipulate polymeric microspheres and achieve highly ordered scaffolds for *in vivo* vascularization [61]. They used PCL μ Ps with size in the 425–500 μ m range to fabricate ordered and randomly assembled structures. After implantation in a rat subcutaneous pocket model, the ordered PCL scaffolds provided better vascularization and blood vessels infiltration than the random one [61]. This approach was tested with large μ Ps (500 μ m), as smaller μ Ps require the implementation of new advanced automated manufacturing. These recent results pave the way on the importance on μ Ps' scaffold design features and provide the basis for the future development in this extremely promising scaffold design research field.

1.2.3 Porous micro-particles as micro-scaffolds for in vitro tissue building (cell-laden strategies)

Modular TE uses porous μ -scaffolds as cell-laden building blocks to recreate large tissues *in vitro*. In fact, μ -scaffolds size, shape and porosity guide cells distribution and ECM biosynthesis in 3D. Moreover, complex manipulation and assembly of these cell-laden μ -scaffolds inside appropriate bioreactors enabled to generate tissues with desired composition and morphology *in vitro*. Therefore, this approach may allow overcoming cell seeding and culturing limitation in 3D scaffolds porosity for a wide range of applications, such as dermis, bone tissue and vascular tissue [26].

As shown in Figure 1.4, the use of cell-laden μ -scaffolds for *in vitro* tissue building involves two main steps. In the first step (Step1), cells are seeded and cultured onto the μ -scaffolds under dynamic conditions to stimulate cell adhesion, proliferation and ECM production and to allow the formation of small aggregates named micro tissue precursors (μ TPs) [62]. In the second step (Step2), 3D tissues are obtained by bio-fusion and assembly of μ TP in suitable molds as consequence of cell-cell and cell-ECM linking (Figure 1.4).

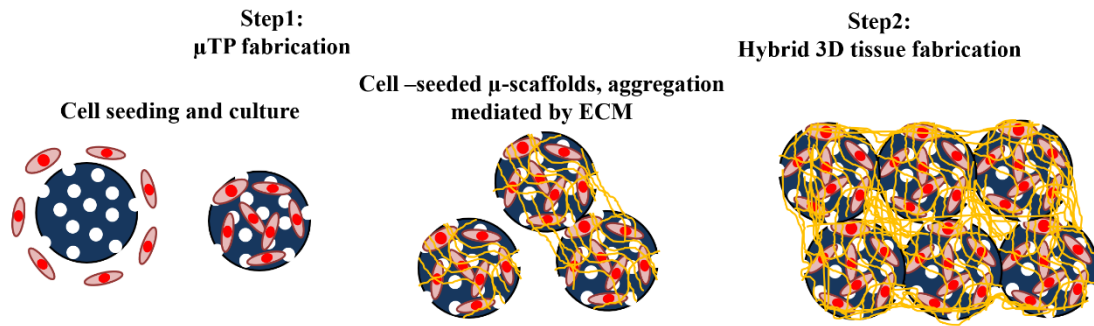


Figure 1.4: schematic of 3D tissues fabrication *in vitro* by using two steps processes.

In this paragraph the description of the literature work about random assembly of cell-seeded μ Ps is structured depending on the specific application, starting from dermal tissues and then discussing musculoskeletal tissues and possible strategies for enhancing tissue vascularization.

Urciuolo et al. manufactured a dermis-equivalent tissue by culturing human dermal fibroblast (HDFs) onto gelatin μ -scaffolds [62]. More importantly, a 3D tissue construct with a well-defined shape could fabricate after few days of μ TPs assembly in a spinner culture [62]. Dynamic cell seeding was performed in a spinner flask bioreactor by loading cells and porous gelatin μ -scaffolds in the ratio of 50 cells per μ -scaffolds and operated at 30 rpm. The result showed that the fibroblasts cell density in the spinner flask decreased 60% after the first 6 hours because of cell attachment to the μ -scaffolds wall and cell death. Furthermore, the μ -scaffolds promoted cell proliferation over culture time and biosynthesis of new ECM components leaving to the formation of μ TP [62].

Kim and co-workers used PLGA μ -scaffolds as transplantation vehicle of human keratinocytes, and HDFs for the regeneration of full-thickness skin wounds [63]. PLGA μ -scaffolds were fabricated by using oil/water emulsion and solvent evaporation/extraction achieving average size of 11.96-24.2 μ m. Cells were seeded onto PLGA μ -scaffolds in a spinner flask and cultured at 50 rpm for 2 weeks. Cell-seeded μ -scaffolds were used to treat full thickness skin wounds created on the back of athymic mice. Dermal regeneration with positive staining for vimentin, a marker of dermal fibroblast, was observed in the cell-transplanted group [63].

In another study, Tang et al. constructed microfabricated tissue by seeding the HDFs onto the microporous cellulose μ -scaffolds able to degrade slowly *in vivo* [64]. In that study, μ -scaffolds were fabricated and sterilized according to the manufacturer instruction and subsequently, microtissue was created by inoculating HDFs in a spinner flask. In this culturing system, cell density onto μ -scaffolds increased even after 8 h of culture time and reached maximum after 20

days of culture time. Moreover, cells colonized the inner porosity of the samples while, large-scale tissue was created by reassembly of the engineering microtissue in the perfusion system. By this approach the authors obtained cylindrical shaped macro-tissue with more than 5 mm thickness and characterized by a homogenous distribution of cells and ECM in the entire construct [64].

Using a similar approach Matsunaga and co-workers reported that tissue shape can be precisely manipulated by using shaped molds as reported in (Figure 1.5) [65].

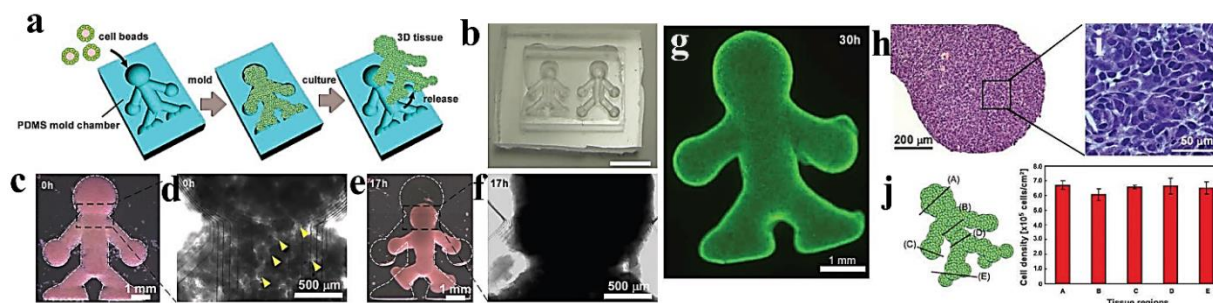


Figure 1.5: Fabrication of millimeter-scale 3D tissue in well-defined shape, (a) schematic of producing the 3D tissue architecture utilizing of monodispersed μ -scaffolds, (b) microscopy image of PDMS doll-shaped mold, (c, d) microscopy images of cell/ μ -scaffolds after stacking. Yellow arrows show cavities among cell/ μ -scaffolds, (e, f) microscopy images of cell/ μ -scaffolds, 17 h after stacking. (g) live/dead assay of 3D tissue after 30 h of culture time, (h, i) microscope images of tissue section after reconstruction, (j) cell density of 3D tissue architecture at different regions of tissue. (Reproduced with permission from: Adv. Mater. 2011, 23, 90–94; doi:10.1002/adma.201004375 [65]).

In the first step of that study, monodispersed collagen gel μ -scaffolds were fabricated by microfluidic technology (section 1.2.1). Cell-laden μ -scaffolds were prepared by seeding the NIH 3T3 cells on the collagen gel μ -scaffolds with the size of 100 μ m. Then these formed cell-laden μ -scaffolds were randomly assembled into the PDMS chamber within a specific shape of a doll by micropipette (Figures 1.5 (a) and (b)). Cell-laden μ -scaffolds immediately fused to each other and enabled rapid formation of macroscopic cell-dense tissues, without necrosis during tissue formation (Figures 1.5 (c-f)) [65]. Figures 1.5 (h) and (i) and graph of (Figure 1.5j) shows cell viability within the 3D construct after removal PDMS mold (Figure 1.5g). Most importantly, the proposed method is highly compatible with the formation of vascularized complex tissues, since the samples can be easily molded with different types of microtissue units.

Bone TE cell-laden μ -scaffolds were also reported in the recent literatures. For instance, Porous PCL μ -scaffolds functionalized with hydroxyapatite (HA) were obtained by means of a bio-safe versatile thermally-induced phase separation process [66]. In the first step of this study, PCL-HA nanocomposite μ -scaffolds with different HA concentrations were prepared and characterized to assess the morphological and microstructural properties. PCL-HA nanocomposite μ -scaffolds with the 30% HA concentration were subsequently chosen to stimulate bone regeneration by human mesenchymal stem cells (hMSCs). The nano composite μ -scaffolds promoted hMSCs differentiation *in vitro* even without the addition of osteogenic growth factor. More importantly, the formation of bone μ TP after 28 days in dynamic spinner culture demonstrated that PCL-HA nanocomposite μ -scaffolds can represent an excellent physical platform for cell adhesion and a 3D microenvironment to arrange the cells and make signals for cellular differentiation and ECM mineralization. These results demonstrated that μ -scaffolds provided a suitable supporting structure for cell attachment while, the presents of an inorganic cue (HA) on the μ -scaffolds surface stimulated cell differentiation towards an osteogenic lineage [66].

Chen et al. created a large bone tissue (centimeter-sized) by culturing human amniotic (hAMSCs) onto gelatin μ -scaffolds in a dynamic culture system [67]. Within a total culture period of 28 days, using a two-stage culture strategy, hAMSCs-laden μ -scaffolds with a high cell density were prepared at the first stage and the cells were then directly induced to undergo osteogenic differentiation in the same culture flask. The results demonstrated that after 8 h of cell seeding, cells can tightly adhere on the surface of μ -scaffolds (Figures 1.7a (8h)) and with culture time at day 8, cells can proliferate and coated the microcarriers (Figures 1.7a (8d)). More importantly, histology analysis of the ECM osteogenic differentiation of hAMSCs on μ -scaffolds proved that ECM occupied around the μ -scaffolds and interior part of them after 8 days of culturing time (Figure 1.7b). During *in vitro* dynamic culture cell-laden μ -scaffolds undergo aggregation, forming μ TPs of 700-800 μ m in size suitable to maintain high cell viability. These μ TPs were characterized by high mineral deposition with cells expressing osteogenic markers. As shown in (Figure 1.7c) these modular bone-like μ TPs were used as building blocks to fabricate a macroscopic bone construct in a cylindrical perfusion culture chamber (2 cm in diameter). After a 7-day perfusion culture, these building blocks assembled into a centimeter-sized constructs with good cell viability and fairly homogenous distribution of cellular content and bone matrix [67].

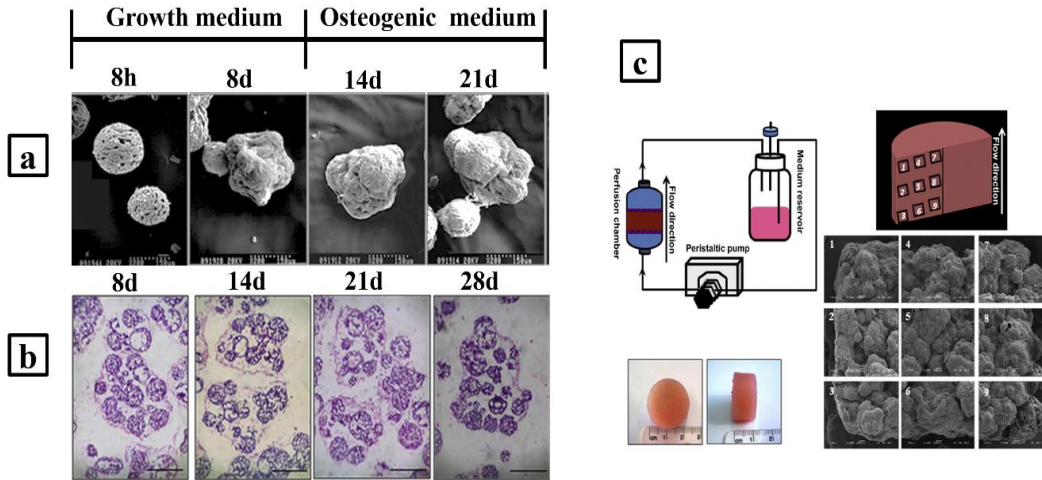


Figure 1.7: culture device utilized to fabricate three-dimensional (3D) bone *in vitro* by cell-laden μ Ps' assembly and morphological and optical visualization of corresponding tissue. A, morphology and proliferation of cell on the microcarriers during the cultivation. B, Osteogenic differentiation of hAMSCs on microcarriers on day 8, 14, 21 and 28. C, assembly of modular tissues into a macro-tissue (Reproduced with permission from: *Biomaterials*, 2011, 32, 7532–7542; doi: 10.1016/j.biomaterials.2011.06.054 [67]).

Therefore, these results demonstrated that macroscopic bone constructs were created by modular tissues after a short time of the perfusion culture [67].

In another study, Zhou and co-workers fabricated the chitosan μ -scaffolds with ECM-mimicking nanofibrous structure for cartilage tissue regeneration [68]. In that study nanofibrous chitosan μ -scaffolds (NCMS) with uniform size and controlled nanofibrous structure were obtained by microfluidic technology (section 1.2.1) and physical crosslinking. NCMS with sizes from 165 to 425 μ m were tested by seeding cells *in vitro*. Up to 90% cell adhesion was observed after 6 h from seeding. More importantly, it was found that chondrocytes cultured with smaller NCMS were more easily to form into cell-NCMS aggregates.

Chondrocytes completely covered the surface of NCMS after 7 days of culture time and showed a flat morphology indicating a good adhesion and spreading onto the nanofibrous structure [68]. These results demonstrated that ECM-mimicking μ -scaffolds can be designed for enhancing cell behavior and modular microtissue features of bottom-up TE approaches.

To successfully generate functional tissue constructs and to ensure proper ECM and cells survival in 3D engineered tissue, the capability to stimulate vascular network by the μ -scaffolds is required [69]. In view of this aim, Zhong et al. developed the engineered bone-like constructs by

self-assembly of osteon-like modules and by utilizing the gelatin μ -scaffolds as fast degradation biomaterials [70]. Firstly, human osteosarcoma (MG63)-laden hydrogel μ -scaffolds were prepared using an electrostatic droplet method, and then human umbilical vein endothelial cells (HUVECs) were seeded onto the hydrogel μ -scaffolds surface for co-culture. Subsequently, the samples were mixed with gelatin microspheres and randomly assembled into a macrotissue. The μ -scaffolds with MG63 cells inner and HUVECs on the surface were designed to mimic the complex structure of osteon with both bone part and vascular part. Due to the fast degradability of gelatin at 37 °C, the introduced gelatin microspheres would gradually dissolve over time, thus providing additional space among the spherical modules to naturally form vessel-like channels [70]. In fact, the authors found that co-culture of MG63 and HUVECs together with the incorporation of gelatin microspheres showed better vasculogenic function if compared to microtissue formed without HUVECs and without gelatin microspheres used as control.

An interesting modification of this approach was reported by Scott and co-workers that investigated the effect of modularity, biological activity, and porosity at multiple length scales by mixing human liver cancer cell line, human hepatocellular carcinoma cells (HepG2), and three different types of PEG μ Ps with different functionalities [71]. The entire scheme of this process is highlighted in (Figure 1.6) together with images of the resulting assembly of modular μ -scaffolds. Indeed, the first type of PEG μ Ps provides μ -scaffolds mechanical support, another type used for controlling the delivery of the sphingosine 1-phosphate (S1P), an angiogenesis-promoting molecule, other type lead to dissolving of non-cytotoxic porogen materials slowly. Macroporous samples formed after components centrifugation into the mold and overnight incubation at 37 °C that promoted dissolution of the porogen (Figure 1.6b) [71].

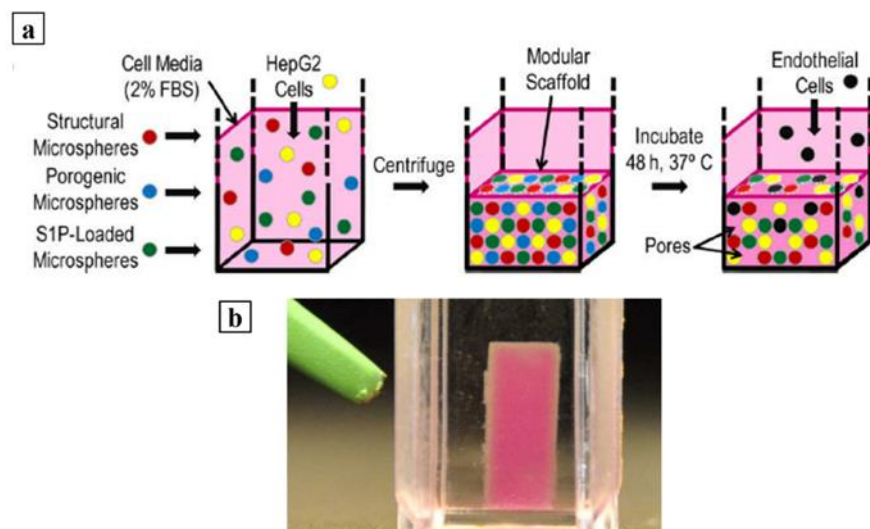


Figure 1.6: Assembly of μ -scaffolds into bioactive modular scaffolds. (a) assembly of cell and multifunctional PEG μ Ps to investigate of cells migration *in vitro* as a function of scaffolds porosity and S1P release. (b) photograph of a scaffold created by centrifuging μ Ps in the presence of medium with 2% FBS. (Reproduced with permission from: Acta Biomater. 2010, 6, 29–38; doi: 10.1016/j.actbio.2009.07.009 [71]).

The absence of surfactants and organic solvents during the manufacturing process allowed the assembly of μ -scaffolds with cells, resulting in a homogenous cellular distribution. Bioactivity was enhanced via RGD peptide conjugation and S1P delivery that promoted HDFs infiltration [66]. The use of porosity gradient was produced by varying μ -scaffolds density, indicating the potential to fabricate complex system for TE application [71].

In another research work, pre-vascularized endogenous human dermis model was produced by seeding HUVECs on endo dermis tissue [72]. In that study, gelatin μ -scaffolds were fabricated by double emulsion technique, cross-linked with 4% glycerinaldehyde and seeded with HDFs in a spinner flask. Cells attached and proliferated onto the surface and into the inner part of the μ -scaffolds and synthesized new collagenous ECM that promoted μ TPs formation [72]. The formed μ TPs were assembled into customized bioreactor system to stimulate tissue growth and μ -scaffolds degradation. Samples were cultured for 3 weeks to obtain dermis equivalent tissue. Pre-vascularized dermis model was achieved by HUVECs seeding onto the dermis samples and subsequently implanted *in vivo* to study functional anastomosis with host vasculature process [72].

Wang and co-workers developed a 3D endothelialized hepatic tumor microtissue model by using porous PLGA μ -scaffolds seeded with HepG2 and HUVECs [73]. This 3D liver tumor

microtissue model was used for drug screening proposes. It was found that the drug evaluation capability of the tissue model was significantly enhanced compared to the 2D plate culture method while using doxorubicin and cisplatin as model drugs. The enhancement of drug evaluation was not only evidenced by the ability of the tumor microtissue model to significantly prolong the time of internalization of the drug molecules into the interior, but also by the different availability of the drugs for the cells in the different locations [73].

Similar to the work reported by Zhong et al., Liu and co-workers fabricated a bioinspired 3D gelatin-methacrylate (Gel-MA) hydrogel incorporating pore generating gelatin microspheres and co-culturing HMSCs and HUVECs which was used to investigate whether HMSCs could play a pericytes-like role and enhance vascularization within the engineered scaffolds [74]. The results showed that co-culture of HMSCs and HUVECs enhanced tissue vascularization when compared to either HUVECs or HMSCs monoculture. Moreover, when implanting the pre-vascularized scaffolds *in vivo*, co-culture system integrated more successfully with host tissue and showed higher host tissue invasion. More importantly, MSCs differentiated towards pericytes to enhance vascularization [74].

As previously commented, the final properties of biohybrids can be improved and customized by controlling the spatial assembly of cell-laden μ -scaffolds. This can be achieved, for instance, by using bioprinting. In fact, this technique allows CAD cells and materials in powder form with microscale resolution following predefined virtual models of evenly complex tissues like osteochondral [75]. By using bioprinting, Levato and co-workers obtained a bilayer biohybrids characterized by porosity and 3D cells distribution mimicking the architecture and composition of cartilage and bone portions of osteochondral tissues [75]. In particular, building blocks made of PLA μ -scaffolds and mesenchymal stromal cells (MSCs) were obtained by static or spinner flask culture and they were encapsulated in a gelatin methacrylamide-gellan gum (GelMA)-GG bioinks and processed in the bioprinting machine. This technique allowed the creation of constructs with high cell concentration and cell viability. μ -scaffolds encapsulation improved the compressive modulus of the hydrogel constructs, facilitated cell adhesion, and supported osteogenic differentiation and bone matrix deposition by MSCs. As shown in Figures 1.8 (a) and (b), μ -scaffolds, MSCs, and cells seeded μ -scaffolds were distributed homogeneously in the gel matrix and proved excellent cell viability.

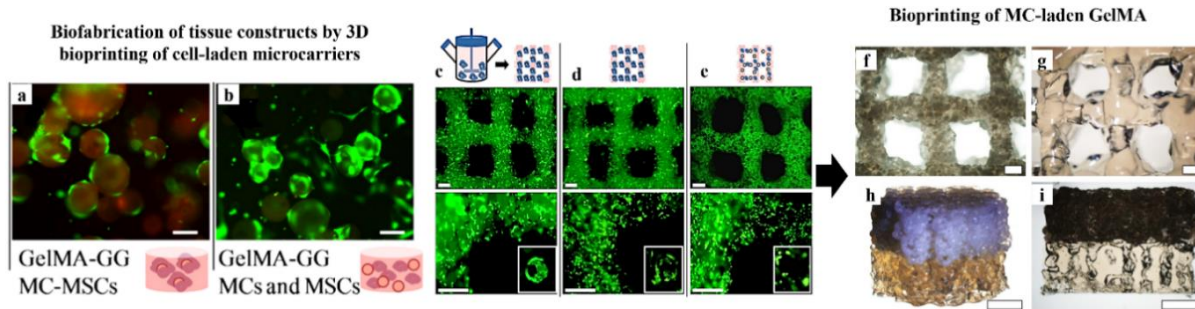


Figure 1.8: (a) gels loaded with pre-cultured μ -scaffolds and (b) with cells and μ -scaffolds separately. (c-e) Immunofluorescence analysis on bioprinted GelMA-GG hydrogels with encapsulated cells and μ -scaffolds. (c) MSCs were precultured on μ -scaffolds either in a spinner flask bioreactor (d) under static conditions (e) directly mixed in the hydrogel solution without preculture. (f-i) Bilayered GelMA-GG cylindrical osteochondral graft model. (f) μ -scaffolds-laden layer top view, (g) GelMA-GG layer top view, (h) perspective, (i) cross-section. (Reproduced with permission from: Biofabrication, 2014, 6, 035020, doi:10.1088/1758-5082/6/3/035020 [75]).

The results demonstrated MSCs were found onto μ -scaffolds after 4 h in presence of GelMA. Figure 1.8 show MSCs precultured on μ -scaffolds in a dynamic culture condition (c), static condition (d), and directly mixed in the hydrogel solution (e). These results revealed that obtained constructs were characterized by a homogeneous distribution of cells and μ -scaffolds among the gel matrix for all the conditions. Besides, for all conditions, constructs were fabricated with homogeneous distribution of cells and μ -scaffolds through the gel matrix, comparable overall dimensions, strands orientation, struts and pore sizes, with respect to the original CAD design. Bilayer osteochondral graft model was fabricated by using the μ -scaffolds based biofabrication strategy. In this regard, GelMAGG was used for printing the cartilage region and GelMA-GG with encapsulated μ -scaffolds to represent the bone region [75]. Bilayered GelMA-GG cylindrical osteochondral graft model showed a homogenous distribution of PLA μ -scaffolds through the whole structure (Figures 1.8 (f) and (h)).

Tan et al. introduced a similar strategy for recreation of vascular tubular tissues by the micropipette extrusion bioprinting technique [76]. The entire scheme of this process is highlighted in Figure 1.9 together with images of the resulting vascular construct. Cell-laden μ -scaffolds encapsulated within agarose-collagen hydrogels were used to make bioink. Besides, the capability to utilize the C2CL2 and Rat2 cell-laden μ -scaffolds are examined simultaneously. In this regard, cells were seeded on the PLGA μ -scaffolds in the stirred or perfused culture to create cell-laden

μ -scaffolds. The as prepared composite bioink was printed to obtain tightly packed constructs. As shown in Figure 1.9 (a) bioink with various cell types were made in separate centrifuge tubes and then they were loaded into a printer with controlling the temperature and gentle stirring.

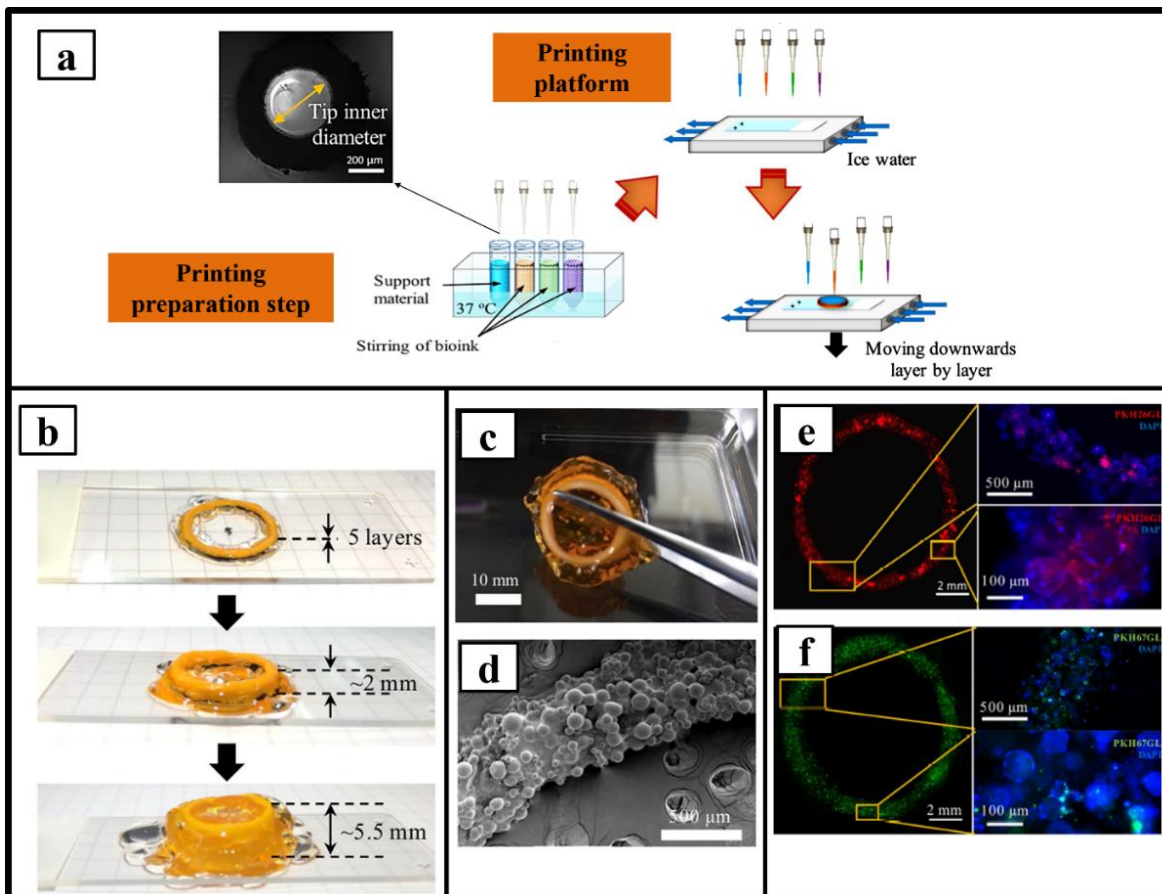


Figure 1.9: (a) schematic of an automated bioprinting system and the 3D-printed prototype. (b, c) 3D-printed tubular construct with gelatin. (d) SEM image of printed construct. (e, f) C2C12 cells and Rat2 cells labelled with red and green fluorescent cell linker respectively. (Mater. Lett. 2018, 228, 360–364, <https://doi.org/10.1016/j.matlet.2018.06.045> [76]).

This design prevented cell-laden μ -scaffolds from fusing before printing. Extrusion-based printing was obtained manually in this study. However, complex 3D constructs can be bioprinted by utilizing an automated printer [76]. Figures 1.9 (b) and (c) show optical images of 3D printed tube, while Figure 1.9 (d) reported SEM analysis of tightly packed PLGA μ -scaffolds printed by utilizing micropipette extrusion technique. Figures 1.9 (e) and (f) show constructs filled with live cells after 3days of *in vitro* culture time. Cells continued proliferation within cell-laden μ -scaffolds

and migrated to the hydrogel after 7 days and were populating the whole bioprinted construct after 14 days of culture time. These results revealed that printed construct provided a desirable microenvironment for cell proliferation.

Manipulation of cell-laden μ -scaffolds at the micro-scale was studied to fabricate precisely designed 3D constructs for TE. μ -scaffolds were immersed in an inert medium, such as mineral oil whereas their assembly was achieved by geometrical constraints, particularly by using of guiding structures. For example, Xiao and co-workers obtained 3D structure by assembling cell-laden μ -scaffolds created by UV-lithography and using UV-photo-cross-linkable GelMA solution [77]. They introduced silk fibroin (SF) into GelMA for controlling the matrix stiffness and swelling feature of the microgels. For fabrication GelMA-SF μ -scaffolds, homogeneous prepolymer (6wt.% GelMA, 1wt.% photoinitiator and 1wt.% SF) was pipetted onto the hydrophobic PDMS surface treated glass side then a photomask with a special shape was arranged on the top and exposed to UV. Thus, GelMA-SF μ -scaffolds obtained after methanol treatment and lyophilization of patterned microgels. Cell-laden μ -scaffolds fabricated by seeding MG63 cells on the GelMA-SF μ -scaffolds. These cell-laden μ -scaffolds were immersed in the mineral oil after 1day of culture time [77]. μ -scaffolds assembly complexes were obtained by surface tension-driven assembly technique. Figure 1.10 show the schematic of the two assembly processes of μ -scaffolds and images of the resulting 3D construct.

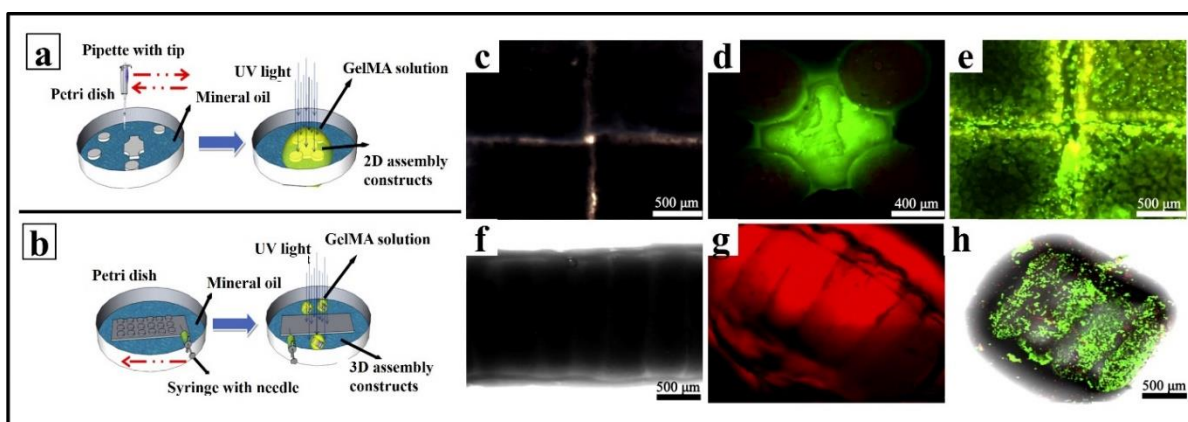


Figure 1.10: Scheme of μ -scaffolds assembly process (a, b), two similar cell-friendly approaches for assembly of μ -scaffolds. (c, f), fluorescence pictures. (d, g), assembly of μ -scaffolds. (e, h), stained assembly after 3days of culture time. (Reproduced with permission from: Mater. Lett. 2018, 228, 360-364, <https://doi.org/10.1016/j.matlet.2018.06.045> [77]).

2D complex created by mechanical agitation utilizing the tip of pipette to aggregate individual μ -scaffolds and 2D surface assembly (Figure 1.10a). Therefore, a syringe needle was swiped uniaxially against the linear array of μ -scaffolds on the glass slide for 3D sequential assembly then μ -scaffolds were packed. Subsequently, GelMA solution was added dropwise on the assembly structure and μ -scaffolds assembly was fixed after performing of secondary photo crosslinking (Figure 1.10b). The result demonstrated μ -scaffolds were fabricated with open porous structure and high interconnectivity that suitable for cellular ingrowth and vascularization. Besides, the morphology of MG63 cells on μ -scaffolds revealed that cells attached after 1 days and proliferated for 5 days of culture time to the μ -scaffolds. As shown in figures 1.10 (c), (d), (f), and (g), μ -scaffolds were closely regulated into assembly complexes. Besides, as can be observed, GelMA provided a bonding role in the assembly of μ -scaffolds. Results revealed that cells were distributed in constructs after 3 days of culture time with excellent viability (Figure 1.10 (e) and (h)). These results are ascribable to the biosafe process develop based on the use of inert and safe reagent, such as the mineral oil [77]. In conclusion, the two assembly processes (Figures 1.10 (a) and (b)) have the potential to be used for building block assembly.

Lui et al. presented a technique for assembly of shape-controllable microcapsule by utilizing an untethered magnetic microcapsule-robot [78]. This microcapsule-robot with shape-matching structure can grab the building components during assembly process. The core-shell alginate-chitosan-alginate microcapsule-encapsulated magnetic nanoparticles act as a magnetic microcapsule-robots. These core-shell microcapsules separated bioactive materials from magnetic nanoparticles, so no necessity to release of magnetic nanoparticles from cell-loaded hydrogel microstructures. Several microcapsules are assembled, and posture controlled at the interface between water and perfluorodecalin. Construction of the 3D heterogenous liquid-like core-shell microcapsule was carried out with using programmable microcapsule fabrication device [78]. The orientation and position of building blocks was adjusted by the microcapsule-robot dynamically. Furthermore, authors demonstrated that the presented manipulation method can be applied to cell-loaded microcapsules without damage and toxicity. From the above, the proposed method of 3D heterogeneous microcapsule fabrication and assembly holds great promise to build bioartificial architectures for promoting the development of tissue regeneration and drug screening applications [78].

1.3. Research hypothesis and objectives

The research activity carried out in this work aim to provide new knowledge in the field of modular TE and, in particular, on the control of new tissue properties at the micro-scale. In fact, by designing new types of porous μ -scaffolds and by developing novel cell/ μ -scaffolds assembly techniques, it is possible to enhance the control of the spatial organization of cells, ECM and blood vessels distribution in 3D. To address this challenging goal, we pursued the following objectives:

- 1) Implement a fluidic emulsion technique suitable to design and fabricate 3D porous biocompatible μ -scaffolds with controllable size, shape, pore size and interconnectivity. The μ -scaffolds were prepared starting from PCL and by using polyethylene oxide (PEO) as biocompatible porogen agent. The control of μ -scaffolds features was achieved by studying the effect of emulsion conditions, namely the composition of the polymeric solution, the flow rate of the continuous phase, the temperature of the coagulation bath and the ultrasounds post processing. The final materials were characterized to assess their morphological and micro-structural properties. Furthermore, cellular biocompatibility tests were used by seeding HDFs cells on μ -scaffolds to validate their use as building blocks for *in vitro* tissue building.
- 2) Set-up a new approach to control the spatial assembly of μ -scaffolds and HDFs and study the effect of μ -scaffolds patterning on new tissue development. In particular, μ -scaffolds spatial distribution was achieved by the use of patterned molds. The structure of the molds was designed in-silico while their fabrication was obtained by soft-lithography technique. This last step involved the use of micromilling and PDMS replica techniques and enabled the achievement of two μ -scaffolds patterned layers: ordered and disordered. *In vitro* co-culture of HDFs and HUVECs was subsequently used to create ordered and disordered hybrid vascularized layered constructs and to study the effect of the different array design on cells proliferation, distribution, ECM biosynthesis and blood vessels formation. As a final objective, thick vascularized hybrid constructs were built by the controlled assembly of two ordered layered samples. This was achieved by designing a layers bonding chamber that provide the desired alignment of the samples and the correct tissue culture and growth *in vitro*. In addition, the effect of culture time on 3D vascularized hybrid constructs features, such as layers bonding interface development, ECM and blood vessels growth into samples core, were examined.

1.4. References

- [1]. Isla, N.de.; Huseltein, C.; Jessel, N.; Pinzano, A.; Decot, V.; Magdalou, J.; Bensoussan, D.; Stoltz, J-F. Introduction to tissue engineering and application for cartilage engineering. *Biomed. Mater. Eng.* **2010**, *20*, 127-33.
- [2]. Price, R.; Anthony, E.; Myers, S.; Navsaria, H. Tissue engineering for skin transplantation. *Tissue engineering.* **2008**, 507-532.
- [3]. Gaalen, S.V.; Kruyt, M.; Meijer, G.; Mistry, A.; Mikos, A.; Beucken, J.V.D.; et al. Tissue engineering for bone. *Tissue engineering.* **2008**, 559-610.
- [4]. Dalton, P.; Harvery, A.; Oudega, M.; Plant, G. Tissue engineering of the nervous system. *Tissue engineering.* **2008**, 611-647.
- [5]. Nugent, H.M.; Edelman, E.R. Tissue engineering therapy for cardiovascular disease. *Circulation. Res.* **2003**, *92*,1068-1078.
- [6]. Costa, J.B.; Pereira, H.; Espregueira-Mendes, J.; Khang, G.; Oliveira, J. M.; Reis, R. L. Tissue engineering in orthopaedic sports medicine: current concepts, *Jisakos.* **2017**, *2*, 1–7.
- [7]. Kang, Y.; Jabbari, E.; Yang, Y. Integrating top-down and bottom-up scaffolding tissue engineering approach for bone regeneration. *Micro and Nanotechnologies in Engineering Stem Cells and Tissues.* **2013**, *22*, 142-158.
- [8]. Muschler, G.F.; Nakamoto, C.; Griffith, L.G. Engineering principles of clinical cell-based tissue engineering. *The Journal of Bone and Joint Surgery.* **2004**, *86-A*, 1541-1558.
- [9]. Stella, J.A.; D'Amore, A.; Wagner, W.R.; Sacks, M.S. On the biomechanical function of scaffolds for engineering load bearing soft tissues. *Acta. Biomater.* **2010**, *6*, 2365-2381.
- [10]. Bose, S.; Roy, M.; Bandyopadhyay, A. Recent advances in bone tissue engineering scaffolds. *Trends in Biotechnology.* **2012**, *30*, 546-554.
- [11]. Karande, T.S.; Agrawal, M. Functions and requirements of synthetic scaffolds in tissue engineering. *Nanotechnology and Regenerative Engineering: The Scaffold,* **2016**, 63-102.
- [12]. Agrawal, C.M.; Ray, R.B. Biodegradable polymeric scaffolds for musculoskeletal tissue engineering. *J. Biomed. Mater. Res.* **2001**, *55*, 141-150.
- [13]. Hutmacher, D.W.; Schantz, T.; Zein, I.; Ng, K.W.; Teoh, S.H.; Tan, K.C; Mechanical properties and cell cultural response of polycaprolactone scaffolds designed and fabricated via fused deposition modeling. *J. Biomed. Mater. Res.* **2001**, *55*, 203-216.

- [14]. Boccaccini, A.R.; Blaker, J.J. Bioactive composite materials for tissue engineering scaffolds. *Expert. Rev. Med. Devices.* **2005**, *2*, 303-317.
- [15]. Nichol, J.W.; Khademhosseini, A. Modular tissue engineering: engineering biological tissues from the bottom up. *Soft Matter.* **2009**, *5*, 1312-1319.
- [16]. Zhang, H.; Migneco, F.; Lin, C.; Hollister, S.J. Chemically-Conjugated Bone Morphogenetic Protein-2 on Three-Dimensional Polycaprolactone Scaffolds Stimulates Osteogenic Activity in Bone Marrow Stromal Cells. *Tissue. Eng. Part A.* **2010**, *16*, 3441-3448.
- [17]. Voronov, R.S.; VanGordon, S.B.; Sikavitsas, V.I.; Papavassiliou, D.V. Distribution of flow-induced stresses in highly porous media. *Appl. Phys. Lett.* **2010**, *97*, 024101-3.
- [18]. VanGordon, S.B.; Voronov, R.S.; Blue, T.B.; Shambaugh, R.L.; Papavassiliou, D.V.; Sikavitsas, V.I. Effects of scaffold architecture on preosteoblastic cultures under continuous fluid shear. *Ind. Eng. Chem. Res.* **2011**, *50*, 620-629.
- [19]. Alvarez-Barreto, J.F.; Landy, B.; VanGordon, S.; Place, L.; DeAngelis, P.L.; Sikavitsas, V.I. Enhanced osteoblastic differentiation of mesenchymal stem cells seeded in RGD functionalized PLLA scaffolds and cultured in a flow perfusion bioreactor. *J. Tissue. Eng. Regen. Med.* **2011**, *5*, 464-475.
- [20]. Elbert, D.L. Bottom-up tissue engineering. *Curr. Opin. Biotechnol.* **2011**, *22*, 647-80.
- [21]. Dean, D.M.; Napolitano, A.P.; Youssef, J.; Morgan, J.R. Rods, tori, and honeycombs: the directed self-assembly of microtissues with prescribed microscale geometries. *Faseb. J.* **2007**, *21*, 4005-12.
- [22]. Yeh, J.; Ling, Y.; Karp, J.M.; Gantze, J.; Chandawarkard, A.; Eng, G.; Blumling, J.; Langer, R.; Khademhosseini, A. Micromolding of shape-controlled, harvestable cell-laden hydrogels. *Biomaterials.* **2006**, *27*, 5391-8.
- [23]. L'Heureux, N.; Paquet, S.; Labbe, R.; Germain, L.; Auger, F.A. completely biological tissue-engineered human blood vessel. *Faseb. J.* **1998**, *12*, 47-56.
- [24]. Mironov, V.; Boland, T.; Trusk, T.; Forgacs, G.; Markwald, R.P. Organ printing: computer-aided jet-based 3D tissue engineering. *Trends Biotechnol.* **2003**, *21*, 157-161.
- [25]. Chau, D.Y.S.; Agashi, K.; Shakesheff, K.M. Microparticles as tissue engineering scaffolds: manufacture, modification and manipulation. *Materials Science and Technology.* **2008**, *24*, 1031-1044.

- [26]. Salerno, A.; Cesarelli, G.; Pedram, P.; Netti, P.A. Modular Strategies to Build Cell-Free and Cell-Laden Scaffolds towards Bioengineered Tissues and Organs. *J. Clin. Med.* **2019**, *8*, article n° 1816.
- [27]. Luciani, A.; Coccoli, V.; Orsi, S.; Ambrosio, L.; Netti, P.A. PCL microspheres based functional scaffolds by bottom-up approach with predefined microstructural properties and release profiles. *Biomaterials.* **2008**, *29*, 4800-4807.
- [28]. Salerno, A.; Levato, R.; Mateos-Timoneda, M.A.; Engel, E.; Netti, P.A.; Planell, J.A. Modular polylactic acid microparticle-based scaffolds prepared via microfluidic emulsion/solvent displacement process: Fabrication, characterization, and in vitro mesenchymal stem cells interaction study. *J. Biomed. Mater. Res. A.* **2013**, *101*, 720-732.
- [29]. Cao, X.; Li, W.; Ma, T.; Dong, H. One-step fabrication of polymeric hybrid particles with core-shell, patchy, patchy Janus and Janus architectures via a microfluidic-assisted phase separation process. *RSC. Adv.* **2015**, *5*, 79969-79975.
- [30]. De Alteriis, R.; Vecchione, R.; Attanasio, C.; De Gregorio, M.; Porzio, M.; Battista, E.; Netti, P.A. A method to tune the shape of protein-encapsulated polymeric microspheres. *Sci. Rep.* **2015**, *5*, article n° 12634.
- [31]. Dendukuri, D.; Pregibon, D.C.; Collins, J.; Hatton, T.A.; Doyle, P.S. Continuous-flow lithography for high-throughput microparticle synthesis. *Nat. Mater.* **2006**, *5*, 365-369.
- [32]. Vallet-Regí, M.; Salinas, A.J; Ceramics as bone repair materials. *Bone Repair Biomaterials.* **2019**, 141-178.
- [33]. Xia, Y.; Pack, D.W. Uniform biodegradable microparticle systems for controlled release. *Chem. Eng. Sci.* **2015**, *125*, 129-143.
- [34]. Campos, E.; Branquinho, J.; Carreira, A.S.; Carvalho, A.; Coimbra, P.; Ferreira, P.; Gil, M.H. Designing polymeric microparticles for biomedical and industrial applications. *Eur. Polym. J.* **2013**, *49*, 2005-2021.
- [35]. Ma, S.; Mukherjee, N. Microfluidics fabrication of soft microtissues and bottom-up assembly. *Adv. Biosyst.* **2018**, *2*, article n° 1800119.
- [36]. Li, W.; Zhang, L.; Ge, X.; Xu, B.; Zhang, W.; Qu, L.; Choi, C.-H.; Xu, J.; Zhang, A.; Lee, H.; et al. Microfluidic fabrication of microparticles for biomedical applications. *Chem. Soc. Rev.* **2018**, *47*, 5646-5683.

- [37]. Choi, S.W.; Yeh, Y.C.; Zhang, Y.S.; Sung, H.-W.; Xia, Y. Uniform beads with controllable pore sizes for biomedical applications. *Small*. **2010**, *6*, 1492-1498.
- [38]. Baah, D.; Floyd-Smith, T. Microfluidics for particle synthesis from photocrosslinkable materials. *Microfluid. Nanofluid.* **2014**, *17*, 431-455.
- [39]. Xu, S.; Nie, Z.; Seo, M.; Lewis, P.; Kumacheva, E.; Stone, H.A.; Garstecki, P.; Weibel, D.B.; Gitlin, I.; Whitesides, G.M. Generation of Monodisperse Particles by Using Microfluidics: Control over Size, Shape, and Composition. *Angew. Chem.* **2005**, *117*, article n° 3865.
- [40]. Canelas, D.A.; Herlihy, K.P.; DeSimone, J.M. Top-down particle fabrication: Control of size and shape for diagnostic imaging and drug delivery: Top-down particle fabrication. *Wiley. Interdiscip. Rev. Nanomed. Nanobiotechnol.* **2009**, *1*, 391-404.
- [41]. Higueta, N.; Dai, Z.; Kaletunç, G.; Hansford, D.J. Fabrication of pH-sensitive microparticles for drug delivery applications using soft lithography techniques. *Mater. Res. Soc. Symp. Proc.* **2008**, *1095*, 7-12.
- [42]. Guan, J.; Ferrell, N.; Lee, L.J.; Hansford, D.J. Fabrication of polymeric microparticles for drug delivery by soft lithography. *Biomaterials*. **2006**, *27*, 4034-4041.
- [43]. McHugh, K. J.; Nguyen, T.D.; Linehan, A.R.; Yang, D.; Behrens, A.M., Rose, S.; et al. Fabrication of fillable microparticles and other complex 3D microstructures. *Science*. **2017**, *357*, 1138-1142.
- [44]. Qutachi, O.; Vetsch, J.R.; Gill, D.; Cox, H.; Scurr, D.J.; Hofmann, S.; Müller, R.; Quirk, R.A.; Shakesheff, K.M.; Rahman, C.V. Injectable and porous PLGA microspheres that form highly porous scaffolds at body temperature. *Acta. Biomater.* **2014**, *10*, 5090-5098.
- [45]. Jeon, J.H.; Bhamidipati, M.; Sridharan, B.; Scurto, A.M.; Berkland, C.J.; Detamore, M.S. Tailoring of processing parameters for sintering microsphere-based scaffolds with dense-phase carbon dioxide. *J. Biomed. Mater. Res. B*. **2013**, *101*, 330-337.
- [46]. Bhamidipati, M.; Sridharan, B.; Scurto, A.M.; Detamore, M.S. Subcritical CO₂ sintering of microspheres of different polymeric materials to fabricate scaffolds for tissue engineering. *Mater. Sci. Eng. C*. **2013**, *33*, 4892-4899.
- [47]. Ghanbar, H.; Luo, C.; Bakhshi, P.; Day, R.; Edirisinghe, M. Preparation of porous microsphere-scaffolds by electrohydrodynamic forming and thermally induced phase separation. *Mater. Sci. Eng. C*. **2013**, *33*, 2488-2498.

- [48]. Mikael, P.E.; Amini, A.R.; Basu, J.; Arellano-Jimenez, M.J.; Laurencin, C.T.; Sanders, M. M.; Carter, C.B.; Nukavarapu, S.P. Functionalized carbon nanotube reinforced scaffolds for bone regenerative engineering: Fabrication, in vitro and in vivo evaluation. *Biomed. Mater.* **2014**, *9*, article n° 35001.
- [49]. Lv, Q.; Nair, L.; Laurencin, C.T. Fabrication, characterization, and in vitro evaluation of poly (lactic acid glycolic acid)/nano-hydroxyapatite composite microsphere-based scaffolds for bone tissue engineering in rotating bioreactors. *J. Biomed. Mater. Res. A.* **2009**, *91*, 679-691.
- [50]. Borden, M. Structural and human cellular assessment of a novel microsphere-based tissue engineered scaffold for bone repair. *Biomaterials.* **2003**, *24*, 597-609.
- [51]. Brown, J.L.; Nair, L.S.; Laurencin, C.T. Solvent/non-solvent sintering: A novel route to create porous microsphere scaffolds for tissue regeneration. *J. Biomed. Mater. Res. Part B.* **2008**, *86*, 396-406.
- [52]. Shi, X.; Ren, L.; Tian, M.; Yu, J.; Huang, W.; Du, C.; Wang, D.-A.; Wang, Y. In vivo and in vitro osteogenesis of stem cells induced by controlled release of drugs from microspherical scaffolds. *J. Mater. Chem.* **2010**, *20*, 9140-9148.
- [53]. Jaklenec, A.; Wan, E.; Murray, M.E., Mathiowitz, E. Novel scaffolds fabricated from protein-loaded microspheres for tissue engineering. *Biomaterials.* **2008**, *29*, 185-192.
- [54]. Singh, M.; Morris, C.P.; Ellis, R.J.; Detamore, M.S.; Berkland, C. Microsphere-based seamless scaffolds containing macroscopic gradients of encapsulated factors for tissue engineering. *Tissue. Eng. Part C.* **2008**, *14*, 299-309.
- [55]. Dormer, N.H.; Singh, M.; Wang, L.; Berkland, C.J.; Detamore, M.S. Osteochondral interface tissue engineering using macroscopic gradients of bioactive signals. *Ann. Biomed. Eng.* **2010**, *38*, 2167-2182.
- [56]. Jiang, T.; Nukavarapu, S.P.; Deng, M.; Jabbarzadeh, E.; Kofron, M.D.; Doty, S.B.; Abdel-Fattah, W.I.; Laurencin, C.T. Chitosan–poly (lactide-co-glycolide) microsphere-based scaffolds for bone tissue engineering: In vitro degradation and in vivo bone regeneration studies. *Acta. Biomater.* **2010**, *6*, 3457-3470.
- [57]. Gupta, V.; Lyne, D.V.; Laflin, A.D.; Zabel, T.A.; Barragan, M.; Bunch, J.T.; Pacicca, D.M.; Detamore, M.S. Microsphere-based osteochondral scaffolds carrying opposing

- gradients of decellularized cartilage and demineralized bone matrix. *ACS Biomater. Sci. Eng.* **2017**, *3*, 1955-1963.
- [58]. Tedesco, M.T.; Di Lisa, D.; Massobrio, P.; Colistra, N.; Pesce, M.; Catelani, T.; Dellacasa, E.; Raiteri, R.; Martinoia, S.; Pastorino, L. Soft chitosan microbeads scaffold for 3D functional neuronal networks. *Biomaterials*. **2018**, *156*, 159-171.
- [59]. Du, Y.; Liu, H.; Shuang, J.; Wang, J.; Ma, J.; Zhang, S. Microsphere-based selective laser sintering for building macroporous bone scaffolds with controlled microstructure and excellent biocompatibility. *Colloids. Surf. B: Biointerfaces*. **2015**, *135*, 81-89.
- [60]. Du, Y.; Liu, H.; Yang, Q.; Wang, S.; Wang, J.; Ma, J.; Noh, I.; Mikos, A.G.; Zhang, S. Selective laser sintering scaffold with hierarchical architecture and gradient composition for osteochondral repair in rabbits, *Biomaterials*, **2017**, *137*, 37-48.
- [61]. Rossi, L.; Attanasio, C.; Vilardi, E.; De Gregorio, M.; Netti, P.A. Vasculogenic potential evaluation of bottom-up, PCL scaffolds guiding early angiogenesis in tissue regeneration. *J Mater Sci: Mater Med*. **2016**, *27*, article n° 107.
- [62]. Urciuolo, F.; Imperato, G.; Totaro, A.; Netti, P.A. Building a Tissue in Vitro from the Bottom Up: Implications in Regenerative Medicine. *Methodist. DeBakey. Cardiovasc. J.* **2013**, *9*, 213-217.
- [63]. Kim, S.; Gwak, S.; Choi, C.Y.; Kim, B. Skin Regeneration Using Keratinocytes and Dermal Fibroblasts Cultured on Biodegradable Microspherical Polymer Scaffolds. *J Biomed Mater Res Part B*, **2005**, *75*, 369-377.
- [64]. Tang, Q.; Zhou, Y.; Chen, F.; Tan, W.-S. Preparing engineered tissues in vitro by macroporous microcarriers. *Chin. J. Biotechnol*, **2008**, *24*, 74-82.
- [65]. Matsunaga, Y.T.; Morimoto, Y.; Takeuchi, S. Molding Cell Beads for Rapid Construction of Macroscopic 3D Tissue Architecture, *Adv. Mater.* **2011**, *23*, 90-94.
- [66]. Totaro, A.; Salerno, A.; Imperato, G.; Domingo, C.; Urciuolo, F.; Netti, P.A. PCL-HA microscaffolds for in vitro modular bone tissue engineering. *J. Tissue Eng. Regen. Med.* **2017**, *11*, 1865-1875.
- [67]. Chen, M.; Wang, X.; Ye, Z.; Zhang, Y.; Zhou, Y.; Tan, W.-S. A modular approach to the engineering of a centimeter-sized bone tissue construct with human amniotic mesenchymal stem cells-laden microcarriers. *Biomaterials*, **2011**, *32*, 7532-7542.

- [68]. Zhou, Y.; Gao, H.L.; Shen, L.L.; Pan, Z.; Mao, L.B.; Wu, T.; He, J.C.; Zou, D.H; et.al. Chitosan microspheres with extracellular matrix-mimicking nanofibrous structure as cell-carrier building blocks for bottom-up cartilage tissue engineering. *Nanoscale*, **2016**,8, 309-317.
- [69]. Novosel, E.C.; Kleinhans, C.; Kluger, P.J; Vascularization is the key challenge in tissue engineering. *Adv. Drug. Deliv. Rev.* **2011**, 63, 300-311.
- [70]. Zhong, M.; Wei, D.; Yang, Y.; Sun, J.; Chen, X.; Guo, L.; Wei, Q.; Wan, Y.; Fan, H.; Zhang, X. Vascularization in engineered tissue construct by assembly of cellular patterned micromodules and degradable microspheres, *ACS. Appl. Mater. Interfaces*, **2017**, 9, 3524-3534.
- [71]. Scott, E.A.; Nichols, M.D.; Kuntz-Willits, R.; Elbert, D.L. Modular scaffolds assembled around living cells using poly (ethylene glycol) microspheres with macroporation via a non-cytotoxic porogen. *Acta. Biomater*, 2010, 6, 29-38.
- [72]. Mazio, C.; Casale, C.; Imperato, G.; Urciuolo, F.; Attanasio, C.; De Gregorio, M.; Rescigno, F.; Netti, P.A. Pre-vascularized dermis model for fast and functional anastomosis with host vasculature. *Biomaterials*, **2019**, 192, 159-170.
- [73]. Wang, Y.; Kankala, R.K.; Zhang, J.; Hao, L.; Zhu, K.; Wang, S.; Zhang, Y.; Chen, A. Modeling endothelialized hepatic tumor microtissues for drug screening, *Adv. Sci.* **2020**, 7, article n° 2002002.
- [74]. Liu, J.; Chuaha, Y. J.; Fu, J.; Zhu, W.; Wang, D.A. Co-culture of human umbilical vein endothelial cells and human bone marrow stromal cells into a micro-cavitary gelatin-methacrylate hydrogel system to enhance angiogenesis. *Mater. Sci. Eng. C.* **2019**, 102, 906-916.
- [75]. Levato, R.; Visser, J.; Planell, J.A., Engel, E.; Malda, J.; Mateos-Timoneda, M.A. Biofabrication of tissue constructs by 3D bioprinting of cell-laden microcarriers. *Biofabrication*, **2014**, 6, article n° 035020.
- [76]. Tan, Y.J.; Tan, X.; Yeong, W.Y.; Tor, S.B. Hybrid microscaffold-based 3D bioprinting of multi-cellular constructs with high compressive strength: A new biofabrication strategy. *Sci. Rep.* **2016**, 6, article n° 39140.

- [77]. Xiao, W.; Xi, H.; Li, J.; Wei, D.; Li, B.; Liao, X.; Fan, H. Fabrication and assembly of porous micropatterned scaffolds for modular tissue engineering. *Mater. Lett.* **2018**, *228*, 360-364.
- [78]. Liu, Y.; Li, G.; Lu, H.; Yang, Y.; Liu, Z.; Shang, W.; Shen, Y. Magnetically actuated heterogeneous microcapsule-robot for the construction of 3D bioartificial architectures. *ACS Appl. Mater. Interfaces*, **2019**, *11*, 25664-25673.

Chapter 2

Bioinspired design of novel micro-scaffolds for fibroblasts guidance towards in vitro tissue building

The first objective of this study is to design, fabricate and characterize of 3D porous biocompatible μ -scaffolds. The requirements that are going to be assessed in this chapter are controlling size, shape, pore size and interconnectivity and biocompatibility assay.

Many research groups have fabricated various μ -scaffolds for *in vitro* tissue engineering studies. Yet, we believe that little attention has been given to produce highly interconnected porosity with trabecular structure that can lead to a homogeneous cell distribution within 3D μ -scaffolds.

Therefore, in this chapter, we present a developed new route to generate porous PCL μ -scaffolds with bioinspired trabecular structure that supported the *in vitro* adhesion, growth and biosynthesis of HDFs. The method involved the use of PEO as biocompatible porogen and a fluidic emulsion/porogen leaching/particle coagulation process to obtain spherical μ -scaffolds with controllable diameter and full pores interconnectivity.

This study has been published in the “**Journal of ACS Applied Materials & Interfaces**”.

Reprinted with permission from (PARISA PEDRAM, CLAUDIA MAZIO, GIORGIA IMPARATO, PAOLO A. NETTI, and AURELIO SALERNO. BIOINSPIRED DESIGN OF NOVEL MICROSCAFFOLDS FOR FIBROBLAST GUIDANCE TOWARD IN VITRO TISSUE BUILDING. <https://dx.doi.org/10.1021/acsami.0c20687>). Copyright (2021) American Chemical Society.

2.1. Introduction to porous micro-scaffolds for *in vitro* tissue engineering

The concept of TE can be considered mostly a therapeutic action whose aim is to restore the biological and biomechanical functions of lost or dysfunctional tissues by the synergic combination of cells, biomaterial scaffolds and molecular cues [1,2]. In this context, modular TE represents a strong fascinating area as it aims to build large viable tissue constructs by packing and sintering cell-laden scaffold-based μ -scaffolds in a mould [3,5]. Sintering depends on μ -scaffold contact points union and can be induced by polymer plasticization/chemical bonding [6], or by promoting cell-to-cell and cell-to-ECM interlocking [7,8] Further μ -scaffold degradation allows achieving a large viable tissue replicating the composition and structure of native tissue and suitable for studying biological processes involved in new tissue genesis, maturation and remodelling.

The importance of μ -scaffold features on *in vitro* tissue development and morphogenesis has been proved in several studies. Ideally, μ -scaffold should possess interconnected porosity and pores larger than 20 μm to accommodate most types of mammalian cells and to allow for fluids transport from the surface to the μ -scaffold's core [9-12]. Besides, μ -scaffold diameter in the 100-500 μm range are required to ensure cellular adhesion and viability [12]. The biosynthetic activity of cells and the composition, organization and maturation of de novo synthesized ECM were also dependent on μ -scaffold composition, which in turn affects cellular mechanotransduction and tissue contraction, as well as *in vitro* culture conditions [7,8].

In the past decade, several polymeric μ -scaffold were tested as building blocks for the regeneration of biological tissues, both *in vitro* and *in vivo*. Stem cells-laden gelatin μ -scaffold were used to engineer a centimetre-sized bone tissue construct [7], while fibroblasts-laden gelatin μ -scaffold were implemented to produce vascularized dermal tissues [13]. Common approaches to enhancing the biocompatibility of synthetic polymeric μ -scaffold were to functionalize their surface by topographical and biochemical cues [14-17]. For instance, nano-fibrous polylactic acid μ -scaffold were investigated as injectable chondrocyte-carrying carriers for osteochondral defect repair, demonstrating enhanced cell proliferation, chondrogenic gene expression and cartilaginous matrix production if compared to smooth-surface ones [15]. Surface coating with cell adhesive molecules was another approach to enhancing μ -scaffold biocompatibility. As such, growth factor-immobilized polycaprolactone/pluronic F127 porous μ -scaffold were used as injectable filler to stimulate muscle-derived stem cells differentiation [17].

Processing techniques based on emulsion solvent evaporation [18-20], porogen leaching [9,11], spray-drying [21], and emulsion cross-linking [22], have already been developed with more or less success to produce porous polymeric μ -scaffold for TE applications. To improve the interconnectivity between the pores, complex methods were proposed that combined particulate leaching with phase separation [23], emulsion with porogen leaching [24], or gas foaming [25]. Recently, gas bubble-mediated coaxial electrospinning was proposed to obtain PCL-gelatin biomimetic nanofiber μ -scaffold with tunable diameters and multi-scaled porosity architectures that enhanced human neural progenitor cells growth in three dimensions [16]. Despite these advances, there is still demand of new processes that allows matching all the requirements of μ -scaffold fabrication. These include, easy and reliable μ -scaffold manufacture, tunable μ -scaffold diameter and narrow size distribution, controllable μ -scaffold shape and 3D architecture with fully interconnected porosity and pore size. These novel μ -scaffold must be also combined with cells seeding and culture protocols tailored for each specific μ -scaffold structure and composition, so enabling ECM biosynthesis and cell-seeded μ -scaffold assembly for hybrid (biological/synthetic) tissue formation.

PCL is a slowly degradable synthetic polymer that has been tested for several biomedical applications, including the preparation of bone and dermis μ -scaffold for *in vitro* and *in vivo* tissue regeneration [23,24,26,27]. Most importantly, PCL biochemical stability in physiological environments may allow the use of PCL μ -scaffold *in vitro* to test the effect of μ -scaffold composition, pore structure and culture conditions on cell behaviour and cell-laden μ -scaffold assembly towards new tissue formation. The slow degradation of PCL also ensures the preservation of μ -scaffold structure and biomechanical stability necessary to manipulate the samples and, further create more complex engineered tissues with controlled cell/ECM distribution and blood vessels organization [28,29].

In this work, we aimed to address these issues by developing a robust and facile approach for the bioinspired design and manufacture of porous PCL μ -scaffold for biomedical applications. The μ -scaffold were fabricated by a fluidic oil/water emulsion and particles coagulation process and by using PEO as a biocompatible pore-generating agent. Through this process we obtained μ -scaffold provided of spherical shape, narrow diameter distribution and mean diameter easily controllable by adjusting the composition of the polymeric (oil) solution and the flow rate of the continuous (water) phase. Most importantly, PCL μ -scaffold evidenced a trabecular architecture

resembling those of biological tissues like bone, full pores interconnectivity and tunable pores size. *In vitro* cell culture tests demonstrated that μ -scaffolds promoted and guided human dermal fibroblasts (HDFs) adhesion, colonization and ECM biosynthesis towards functional hybrid tissue development, opening new opportunities for the regeneration of several connective tissues.

2.2. Experimental part

2.2.1 Materials

PCL (Mw = 80 KDa), polyethylene oxide (PEO, Mw = 100 KDa), dichloromethane (DCM) and polyvinyl alcohol (PVA, Mowiol® 40-88, average Mw ~205,000 g/mol) were purchased from Sigma-Aldrich (Milano, Italy). Polyoxyethylenesorbitan Monolaurate (Tween 20, Biochemica, Mw = 1227.72 g/m) was provided by Vetro Scientifica srl (Roma, Italy).

2.2.2 Fluidic device and porous polycaprolactone micro-scaffolds fabrication

The fluidic emulsion device used for the preparation of the μ -scaffold was fabricated by using laboratory tubing and needles, similar to the approach described in a previous work [19]. The scheme of the device is highlighted in Figure 2.1.

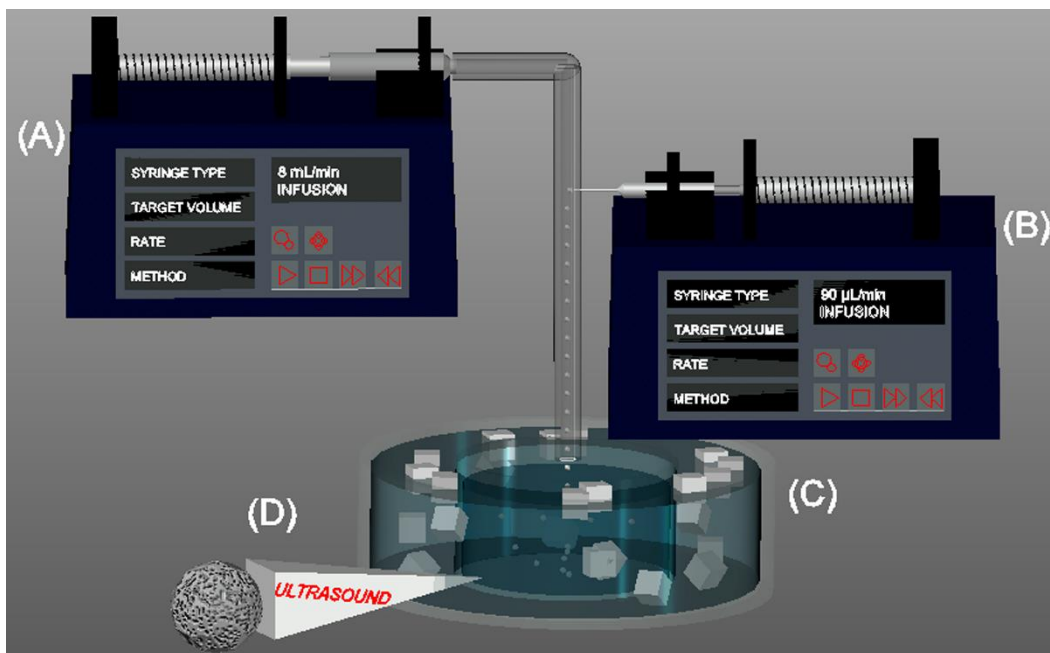


Figure 2.1: Scheme of the fluidic emulsion process developed for the design and fabrication of the porous μ -scaffold. (A) Pumping device of continuous (water) phase; (B) pumping device of dispersed (polymeric

solution) phase; (C) coagulation bath for solvent evaporation, PEO leaching and particles setting; (D) final μ -scaffold obtained after ultrasounds treatment.

As shown in Figure 2.1A, the continuous phase, consisting of water solution of Tween 20 (0.1 v/v%) and PVA (0.5 w/v%), was loaded into a 60-mL PE/PP syringe (Sigma-Aldrich, Milano, Italy) and pumped in a silicon tube (I.D. = 2 mm, O.D. = 4 mm, Sigma-Aldrich, Milano, Italy) by using a syringe pump (KDS 220-CE, KDSscientific, Holliston, MA). Concomitantly, the dispersed phase, obtained by dissolving the PCL and PEO in DCM at 50°C for 2 hours, was loaded into a 2.5 mL volume Hamilton syringe (1000 series GASTIGHT®, Sigma-Aldrich, Milano, Italy) connected to a 26G blunt tip needle (Sigma-Aldrich, Milano, Italy). The needle was inserted into the silicon tube and the dispersed phase was pumped out of the needle tip by using a syringe pump (AL300-220, World Precision Instruments Company, Friedberg, Germany) (Figure 2.1B). Droplets of the polymeric solution formed at the needle tip and dropped into a beaker containing 100 mL of Tween 20 (0.1 v/v%) and PVA (0.5 w/v%) water solution at 190 rpm (Figure 2.1C). After 3 hours stirring under the chemical hood, samples were washed three times in distilled water and treated with ultrasounds at 40 kHz for 1 minute at room temperature (RT) followed by air drying for 48 hours at ambient pressure and RT (Figure 2.1D). Several tests were carried out to find the best μ -scaffold preparation conditions. These include PCL/PEO in the 100/0 to 35/65 range, polymers concentration in the 1-10 wt% range, flow rate of the continuous phase (Q_{CP}) of either 8 or 18 mL/min, the temperature of the coagulation bath (RT or 4°C). All of the tests were carried out at the flow rate of the dispersed phase (Q_{DP}) equals to 90 μ L/min.

2.2.3 Morphological and microstructural characterization

Samples morphology was evaluated by scanning electron microscope (SEM, Ultraplus, Zeiss, Germany) analysis. PCL μ -scaffold were dried by washing in excess of absolute ethanol three times followed by air-drying under chemical hood overnight. Dried PCL μ -scaffold and their cross-sections were gold sputtered using a sputter coater (208HR, Cressington, UK) operating at 40 mA for about 10 minutes under the argon atmosphere. The mean diameter of μ -scaffold was assessed by Image analysis (Image J®) of 2X stereomicroscope (Olympus SZX16) images. One hundred particles for each condition were analysed using the “particle analysis” tools of the Image J® software pack and the diameter was then calculated from area measurement with the hypothesis of spherical shape [23]. A similar approach was used to determine the size of the surface pores of

the μ -scaffold starting from SEM pictures. In particular, high magnification SEM images showing the surface of the samples were used and converted into binary images with surface pores highlighted in black. The images were then processed by the “particle analysis” tools of the Image J[®] software pack and measurements performed as previously described. X-ray computed tomography (MicroCT, Skyscan 1172, Bruker, Milano, Italy) was used to evaluate the μ -scaffold 3D architecture and microstructural properties. Measurements were performed at a voltage of 40 kV, 250 μ A current and 3 μ m pixel size. The transmission images were reconstructed using Skyscan NRecon software and further analysed by CTAn software package to evaluate μ -scaffold porosity, pore size distribution, trabecular thickness and pores interconnectivity. The reconstruction of the 3D architecture was carried out by CTVol software package.

2.2.4 In vitro degradation

In vitro degradation tests were carried out on μ -scaffold prepared at $Q_{CP} = 8$ mL/min and from 10 w% polymeric solution to exclude possible effects of bi-products on cell survival and ECM deposition. The vacuum-dried samples were weighted by a high-accuracy balance (AB104-S; Mettler Toledo, Milano, Italy), placed in 2-mL Eppendorf vials (100 mg/vial approximately) and immersed in 1 mL of Dulbecco’s Phosphate Buffered Saline (PBS, Sigma Aldrich, Milano, Italy), and incubated at 37°C up to 40 days with gentle shaking (100 rpm) and, without refreshing media. At 10, 20 and 40 days of incubation, samples were washed in absolute ethanol three times, vacuum-dried and weighted to evaluate the weight loss with respect to the initial weight. The effect of the degradation was also assessed by the analysis of the morphology of the samples by stereomicroscope and SEM.

2.2.5 Cell expansion, seeding and culture

HDFs from healthy breast biopsies were used to assess the biocompatibility of the μ -scaffold. The cells were grown in 150 cm² polystyrene tissue culture flasks (Corning Inc., Corning, NY) in enriched Minimum Essential Medium Eagle (MEM) composed of MEM (Sigma Aldrich, Milano, Italy), 20% of fetal bovine serum (FBS) (Sigma Aldrich, Milano, Italy), 2% of Non-Essential Amino acids (EuroClone ECB3054D, Milano, Italy), 1% of L-Glutamine (Lonza 17-605E, Basel, Switzerland) and 1% of penicillin/streptomycin (Sigma Aldrich, Milano, Italy) until passage 7. The medium was changed every two days until reaching 90% confluence. Cells were washed three

times with PBS and incubated with trypsin-ethylenediaminetetraacetic acid (EDTA) (0.25% trypsin, 1 mM EDTA; Microtech, Napoli, Italy) for 5 minutes at 37°C to detach the cells.

PCL μ -scaffold were sterilized in absolute ethanol for 12 hours at RT, washed three times with sterile PBS for 20 minutes and re-suspended in the culture medium for 48 hours at 5% CO₂ and 37°C into low attachment 24 multiwell. Subsequently, each well was loaded with 80 mg of μ -scaffold and 7×10^4 cells, suspended in 1 mL of enriched MEM were seeded on the sample to obtain 200 cells/ μ -scaffold. After seeding, cycles of dynamic (5 minutes at 40 rpm) and static (30 minutes) conditions were alternated for 4 hours to promote cells attachment. For cells proliferation and hybrid tissue formation, the cell-seeded samples were maintained in static culture conditions up to 25 days and culture medium was changed at day 1 after seeding and then every two days. From the 3th day of culture, the culture medium was supplemented with Ascorbic Acid (2-O-a-DGlucopyranosyl-L-Ascorbic-Acid TCI; Cf: 0.5 mM) to stimulate collagen biosynthesis by HDFs. In fact, ascorbic acid a stimulus for collagen gene expression and many studies have evaluated the relationship between ascorbic acid and collagen expression in short- and long-term effects on cells, such as HDFs, after a single administration into the culture medium [8,13].

2.2.6 Cell viability and proliferation

The number of viable cells on the μ -scaffold was measured with Alamar blue assay (Invitrogen TM, Milano, Italy). At specific time points, namely 6 hours, 5 days, 10 days, 14 days, 20 days and 25 days, samples were washed twice with PBS and incubated in Alamar blue (10 v/v%) for 2 hours at 37°C and 5% CO₂ in the dark. After that, 200 μ L of each solution were placed into 96-well culture plate (Costar, Torino, Italy) and analysed by a spectrophotometer (Perkin Elmer, Milano, Italy) at wavelengths 570 nm and 600 nm. The number of viable HDFs on μ -scaffold was assessed by comparing fluorescence values with those of the calibration curve. Five samples were analysed for each time point.

2.2.7 Cell morphology, colonization and tissue production

Cell morphology and colonization were studied by using confocal laser scanning microscopy (CLSM). At specific time points, the constructs were fixed with paraformaldehyde (4 v/v%) at 4°C for 24 hours, washed three times with PBS solution and incubated with Triton 0.2 v/v% for 5 minutes at RT. Subsequently, the constructs were washed three times with PBS and incubated with a blocking buffer containing 3 w/v% bovine serum albumin (BSA) and 3 v/v% FBS in PBS for 1

hour at RT. Actin was stained with Phalloidin-488 (Invitrogen, 1:200 diluted in blocking buffer) for 40 minutes at RT. Samples were washed with PBS three times and the nucleus was stained with DAPI (Sigma Aldrich, 1:10.000 diluted in PBS) for 20 minutes at RT. The samples were finally washed three times with PBS and characterized by CLSM (Leica TCS SP5 II, Wetzlar, Germany) using 4x and 10x objectives to assess HDFs morphology and distribution. Multi-photon microscope was used to assay collagen biosynthesis over time, as collagen production dictate cell seeded μ -scaffolds assembly dynamic. Samples were analysed by two-photon excited fluorescence (Leica TCS SP5 II coupled with a Multiphoton Microscope stage Chamaleon Compact OPO-Vis, Coherent) to induce second harmonic generation and obtain high-resolution images of unstained collagen structures. Samples were observed by using $\lambda_{ex} = 840$ nm (two photons) and $\lambda_{em} = 415-425$ nm and a 25X water immersion objective (HCX IRAPO L 25.0, 0.95 Water, n.a. 0.95). Besides, Image analysis was used to quantify the collagen fraction in the inter- μ -scaffold regions. The Collagen Fraction (v%) was defined as the percentage of the ratio between bright pixels to total pixels in the selected regions. Cell colonization into the μ -scaffold porosity was assessed by histology analysis. To this end, hybrid tissues were fixed in 4% paraformaldehyde, washed in PBS and soaked into a 2 M aqueous sucrose solution. After 20 hours, the samples were embedded in OCT (Killik, Bio Optica, Milano, Italy), frozen in liquid nitrogen and stored at -80 °C. Frozen samples were then cryo-sectioned using a cryomicrotome (Leica CM 1850, Milan, Italy) to obtain 20- μ m-thick slices. Slice thickness was optimized to allow an optimal balance between cell detection and slice handling during the staining protocols, also considering the low adherence of PCL μ -scaffold to the glass slide. The sections were subsequently stained with hematoxylin/eosin (Bio Optica, Milano, Italy) following standard protocol, mounted with 50% glycerol instead of xylene-based histomount to overcome the problem of PCL degradation and analysed using an optical microscope (BX53; Olympus, Tokyo, Japan). 3D images of the reconstructed hybrid tissues were obtained by Micro-CT and used for quantification of the cells-tissue amount. At different time points, samples were fixed 2.5% glutaraldehyde/0.1 M cacodylate solution at 4°C overnight. Subsequently, samples were washed three times in 0.1 M sodium cacodylate solution at 4°C for 10 minutes and stained in 1% osmium tetroxide/1% potassium ferrocyanide in 0.1 M sodium cacodylate for 1 hour, at 4°C in darkness. Once staining was completed, samples were washed three times in 0.1 M sodium cacodylate, washed with chilled water and incubated with 0.15% tannic acid aqueous solution for 3 minutes at 4°C . Samples were then washed in chilled water two

times for 5 minutes and incubated with 1% uranyl acetate overnight, at 4°C in darkness. Finally, the samples were washed in chilled water three times for 15 minutes and store at 4°C before the analysis. MicroCT assay was performed at 40 kV voltage, 250 μ A current and by using a 9 μ m pixel size resolution. The transmission images were reconstructed using Skyscan NRecon software and further analyzed by CTAn/CTVol software package to evaluate the v% of new formed tissue with respect to the PCL-tissue volume and to obtain 3D reconstruction images of the hybrid tissue. Three different measurements were carried out for each time point.

2.2.8 Statistical analysis

The statistical significance of the results was assessed by one-way analysis of variance (ANOVA) and Tukey post-hoc test at the significance level $p < 0.05$.

2.3. Results and discussion

2.3.1 Fabrication of porous polycaprolactone micro-scaffolds

In the first part of this study, the operating conditions were optimized for the fabrication of PCL μ -scaffold with desired features. These include diameter in the 100-500 μ m range, surface and bulk pores with diameter and throat size larger than 20 μ m [9,11,12]. Preliminary tests were carried out starting from a 10% PCL-PEO solution, Q_{DP} and Q_{CP} set to 90 μ L/min and 8 mL/min, respectively, and changing the concentration of PEO with respect to overall polymers amount in the 0 to 65 w% range to find the best μ -scaffold morphology and architecture. The coagulation bath temperature was initially set to RT. Figure 2.2 showed the effect of PEO concentration on the morphological features of the surface and cross-section of μ -scaffold. All of the samples have rounded shape (low magnification images in Figure 2.2) and as expected, both surface and inner porosities increased with PEO concentration. As shown in the cross-section images of Figure 2.2, samples prepared by using 50 and 60 w% PEO provided the best results as they were characterized by large pores and highly interconnected trabecular architectures. However, these samples have low surface porosity considered inadequate to promote cells colonization in 3D. Samples prepared at PEO concentration of 65 w% were discharged from SEM analysis as they showed a collapsed morphology (not shown).

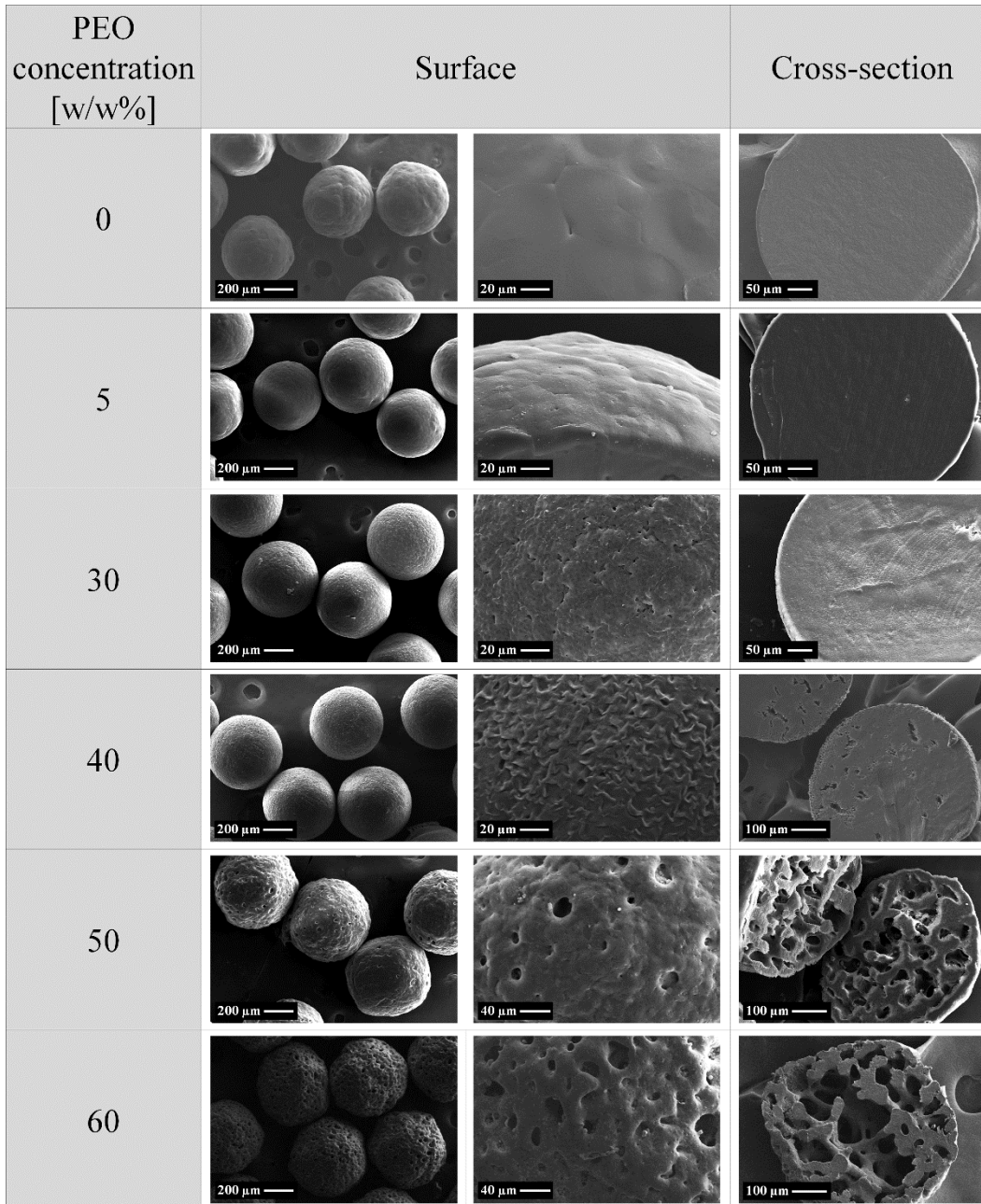


Figure 2.2: Morphology of the surface and cross-section of PCL μ -scaffold obtained from 10 w/v% polymers concentration and by varying PEO concentration in the 0 to 60 w/w% range. Fluidic emulsion was carried out by setting $Q_{DP} = 90 \mu\text{L}/\text{min}$ and by using 0.5 w/v% PVA solution as coagulation bath at RT for 3 hours.

The use of immiscible polymeric blends for the preparation of porous materials for biomedical applications has attracted large interest in the past [30-32]. This approach consisted of blending two or more polymers in the conditions required to create the so-called co-continuous morphology,

where the polymeric phases are characterized by a mutual interpenetration (percolation). The co-continuous morphology generally occurs in the 40/60 to 60/40 v% composition range and enabled the total leaching of one of the two polymeric phases using a selective solvent, finally reaching a porous structure with fully interconnected pores [30-32]. The results of this study were in agreement with literature works on PCL-PEO co-continuous blends prepared by melt blending [31,33,34]. Besides, in our knowledge, this study represents the first attempt to obtain porous PCL μ -scaffold starting from organic solution and using PEO as continuous porogen. Previous studies on miscibility and crystallization of PCL-PEO blends from solutions in organic solvents evidenced that, in the PEO range from 10 to 60 w%, PCL and PEO formed immiscible blends films after solvent evaporation [35,36]. Different from porous PCL prepared by melt blending, in our process the final PCL μ -scaffold morphology was governed by two main steps: the precipitation step and the PEO dissolution step. The precipitation step was driven by solvent evaporation and phase separation and was governed by the different solubility of the two polymers in their common solvent. Based on the Hildebrand solubility parameters, δ of dichloromethane is $19.8 \text{ MPa}^{1/2}$ [37], while δ of PEO and PCL are 20.2 and $19.7 \text{ MPa}^{1/2}$, respectively [36]. We can therefore assume that PCL is more soluble in dichloromethane than PEO. Taking this aspect into account and considering that the porous samples have a weight fraction of PEO equal or higher than PCL, it is reasonable to expect that PEO supersaturation occurred earlier than PCL and started at the polymeric solution droplet surface, where dichloromethane diffused out into the water phase. Concomitantly, the high hydrophilicity of PEO promoted its dissolution into the external water phase when PCL was still swollen by the solvent, so partially occluding the pores formed after PEO leaching. These considerations were in accord with the progressive decrease of μ -scaffold porosity from the centre towards the surface (Figure 2.2). At this point, further solvent evaporation accelerated the phase separation and the crystallization of PCL-rich regions inside the droplets. Increasing the size and distribution of surface pores of samples prepared from 60 w% PEO was a key aspect of this work and therefore, further tests were carried out to address this issue. As the surface porosity was affected by the rapid dissolution of condensed PEO at the interface between droplet and water phase, we slowed down PEO dissolution by decreasing the temperature of the coagulation bath to 4°C . As expected, the decrease of the temperature of the coagulation bath enhanced the distribution and size of the surface pores, while minor influence was observed on the inner porosity (Figure 2.3).

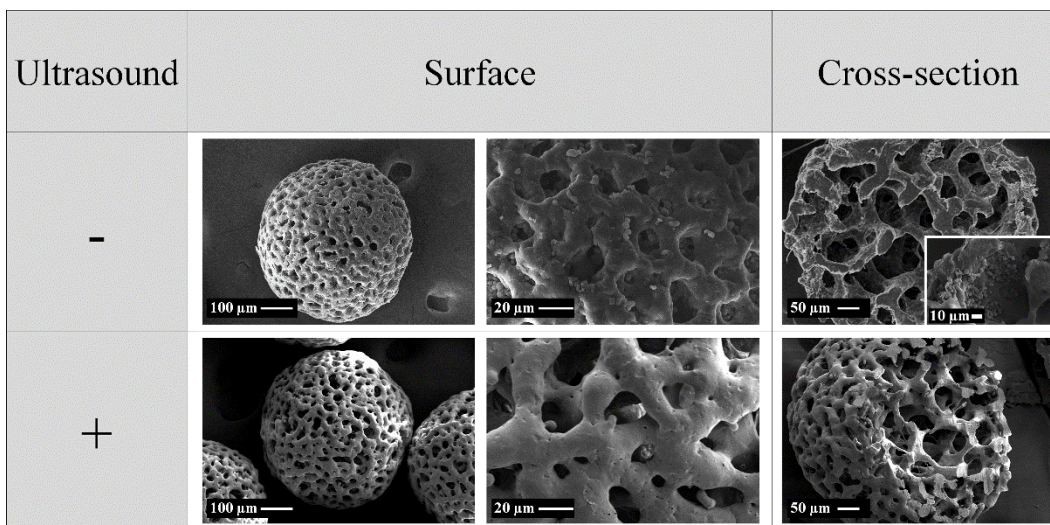


Figure 2.3: Morphology of the surface and cross-section of PCL μ -scaffold fabricated from 10 w/v% polymer concentration and 60 w/w% of PEO and by setting the particles at 4°C, before and after ultrasounds treatment.

However, morphological analysis of the sample surface evidenced that surface pores, even if larger in diameter and distribution, were partially occluded by the presence of small, few micrometres in size, PCL particles. These particles originated by the so-called “secondary phase separation”, when the increase of the viscosity of the solution limited the diffusion of the polymeric chains to only short distances [36,38]. As a direct consequence, small PCL-rich domains remained entrapped inside PEO-rich phases leading to the formation of solid PCL particles that moved from the core towards the surface of the μ -scaffold carried by dissolving PEO. These micrometric sized PCL particles accumulated/aggregated close to the μ -scaffold surface occluding its external pores. To overcome this drawback and to achieve full pores opening, samples obtained after the emulsion were subjected to a short (1min) ultrasound treatment at 40 kHz and RT that broken PCL particles aggregates and favoured their release into the media without damaging μ -scaffold architecture (Figure 2.3).

2.3.2. Modulation of micro-scaffold diameter and porous structure

In this work, we implemented a fluidic emulsion process (Figure 2.1) suitable for the fabrication of PCL μ -scaffold starting from PCL-PEO solutions in dichloromethane. Various types of fluidic devices were proposed to obtain particles with diverse morphologies and structures. The fluidic device of this work was obtained by assembling laboratory tubing, syringes and needles, similar

to the device described in previous works [19,39], that do not require complex and expensive configurations and equipment.

As shown in Figures 2.4 and 2.5, despite its simplification, this device allowed the fabrication of PCL μ -scaffold of controlled diameter distribution by simply modulating the composition of the starting polymeric solution and the fluidic conditions. We therefore studied the correlation among polymers concentration in the dispersed phase, in the 1-10 w% range, Q_{CP} of either 8 or 18 mL/min, and μ -scaffold diameter distribution and architecture, while fixing Q_{DP} to 90 μ L/min.

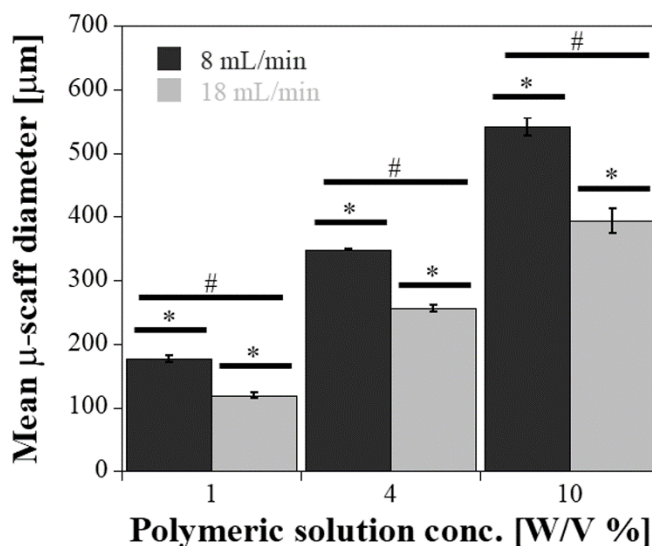


Figure 2.4: Mean μ -scaffold diameter as a function of polymers concentration and Q_{CP} . Samples were prepared by setting $Q_{DP} = 90 \mu$ L/min and by using 0.5 w/v% PVA solution as coagulation bath at RT for 3 hours.

In agreement with other studies, μ -scaffold diameter decreased with decreasing polymers concentration and with increasing Q_{CP} [19,40-42]. In particular, at $Q_{CP} = 8$ mL/min, μ -scaffold diameter varied from $176.6 \pm 5.1 \mu$ m for 1 w% solution, to $541.8 \pm 13.4 \mu$ m for 10 w% solution; at $Q_{CP} = 18$ mL/min, μ -scaffold diameter varied from $119.4 \pm 4.6 \mu$ m for 1 w% solution, to $393.5 \pm 20.0 \mu$ m for 10 w% solution.

The formation of droplets by means of fluidic emulsions is affected by several parameters, including the flow rate of each phase, solutions viscosity and surface tension as well as fluidic channel geometry [40]. Typically, in dripping regime the polymeric solution was in contact with the continuous water phase at the tip of the needle and grew over time until the shear stress imposed by the continuous phase break-up the fluid bed to form emulsion droplets [42]. The increase of

Q_{CP} led to the reduction in the size of the emulsion droplets, and therefore the size of the final beads, due to the increase in the shear stress imposed to the dispersed phase at the tip of the needle [19,42].

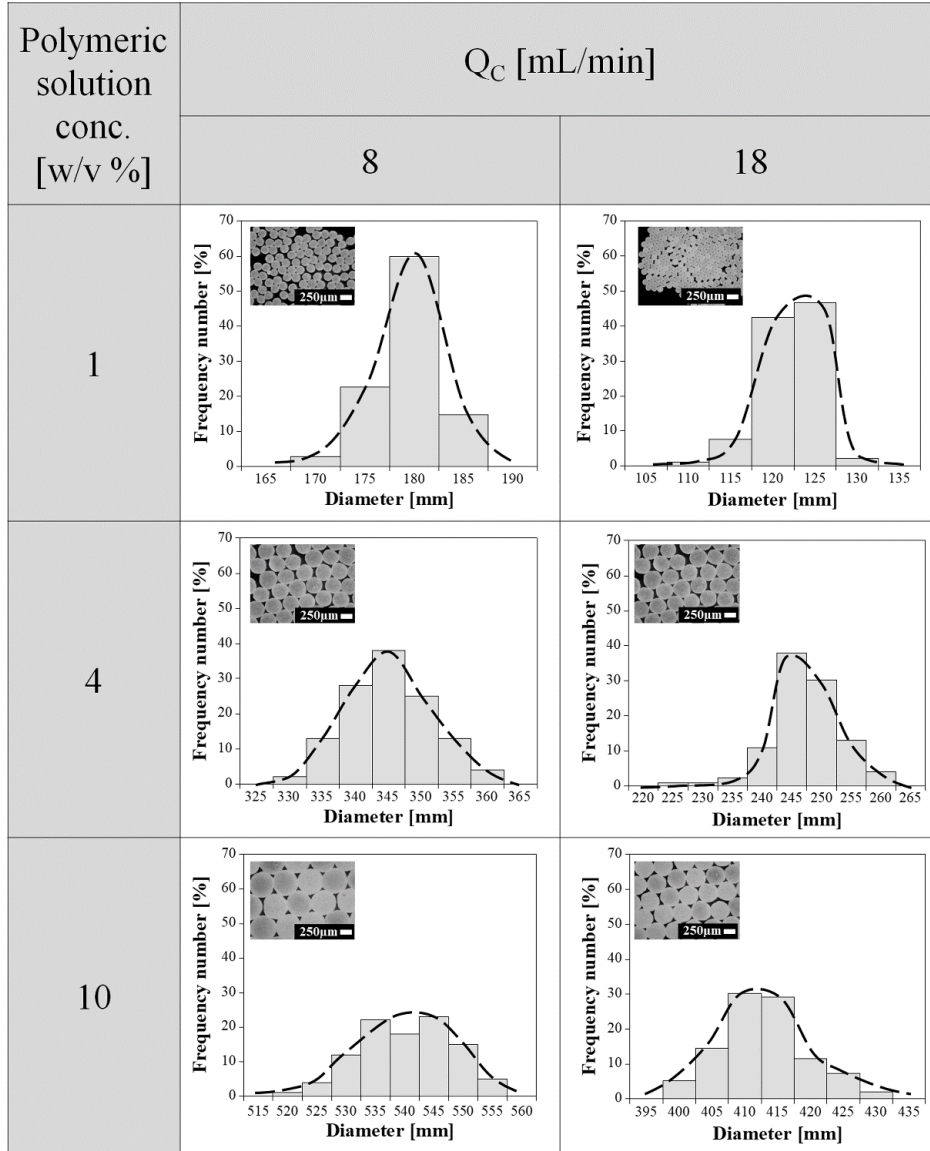


Figure 2.5: Stereomicroscope images and diameter distribution of μ -scaffold as a function of polymers concentration and Q_{CP} . Samples were prepared by setting $Q_{DP} = 90 \mu\text{L}/\text{min}$ and by using 0.5 w/v% PVA solution as coagulation bath at RT for 3 hours.

The effect of polymers concentration is more complex as polymeric solution concentration affects not only the viscosity of the solution but also its interfacial tension and phase separation mechanism. For example, as the solution concentration increased, the viscosity increased too,

finally leading to larger droplets. Concomitantly, higher polymer concentrations accelerate supersaturation and droplets solidification with the consequent decrease of droplets shrinkage and the formation of larger μ -scaffold.[41]. For the samples prepared at $Q_{CP} = 8$ mL/min and 10 w% polymers concentration, the diameter of the droplets generated at the needle tip was about twice the diameter of resulting μ -scaffold (1100 μ m approximately, not shown), therefore supporting the choice of a silicon tube with 2 mm ID for the fluidic device assembly. Optical images and diameter distributions of Figure 2.5 corroborated these considerations and also evidenced the uniform diameter of the different batches (the coefficient of variation, defined as the ratio between standard deviation and mean diameter, was less than 5%). In conclusion, our results suggested that the developed approach enabled to easily control the diameter of PCL μ -scaffold in the 100-600 μ m range, that is considered optimal for biomedical applications [9,11,12].

Figure 2.6 showed SEM micrographs of PCL μ -scaffold as a function of preparation conditions while Table 1 reported surface pore size obtained by Image J calculation.

Table 1.1: Mean size of the surface pores of PCL μ -scaffold as assessed by Image J analysis of SEM micrographs.

Q_{CP} [mL/min]	Polymeric solution concentration [w/v%]		
	<i>1</i>	<i>4</i>	<i>10</i>
8	9.3±3.1 (*)	19.4±5.1 (π)	33.4±7.1
18	7.4±1.7 (*)	9.4±2.3 (*)	22.1±4.6 (π)

All data are statistically significant at 0.05 level except those indicated by the symbols.

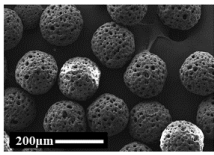
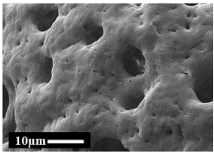
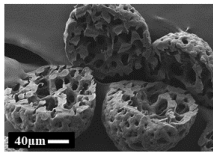
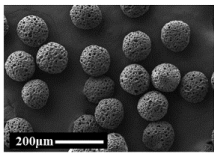
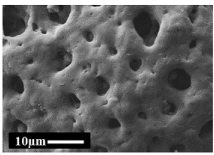
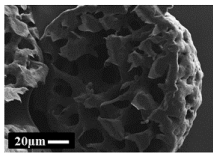
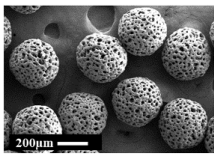
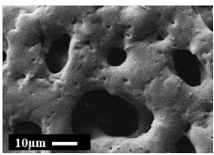
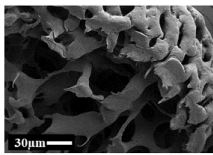
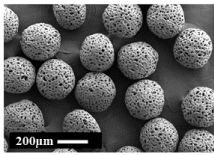
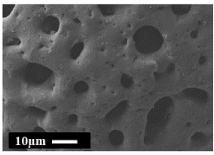
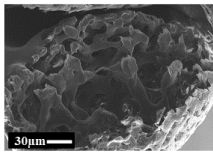
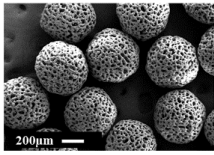
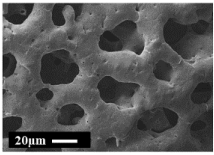
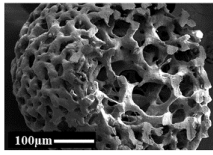
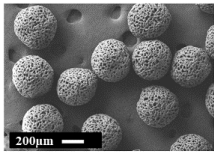
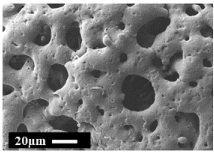
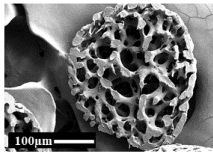
Polymeric solution conc. [w/v%]	Q_{CP} [mL/min]	Surface	Cross-section	
1	8			
	18			
4	8			
	18			
10	8			
	18			

Figure 2.6: Low and high magnification SEM images showing the morphology of the surface and cross-section of PCL μ -scaffold as a function of polymers concentration and Q_{CP} . Samples were prepared by setting $Q_{DP} = 90 \mu\text{L}/\text{min}$ and by using 0.5 w/v % PVA solution as coagulation bath at RT for 3 hours.

All samples have interconnected porosity on the surface and the core, while we observed the progressive decrease of surface porosity and pore size with the decrease of μ -scaffold diameter (Table 1). This effect may be explained considering that the smallest ($< 10 \mu\text{m}$) surface pores were obtained in the case of 4 w% sample prepared at $Q_{CP} = 18 \text{ mL}/\text{min}$ and 1 w% samples prepared at Q_{CP} equal to 8 and 18 mL/min. As the concentration of the polymers decreased, PCL crystallization and particle solidification were delayed and, therefore more PEO was leached out resulting in surface pores shrinkage. Nevertheless, samples prepared from 10 w% solution have surface pores

larger than 20 μm , suitable to promote 3D cell colonization. As shown in Table 2.2, Figure 2.7 and Figures S1-S3, MicroCT characterization provided additional important features of the μ -scaffold prepared. The samples have 3D porous architecture with a trabecular structure and high pores interconnectivity on both surface and core. Besides, μ -scaffold porosity increased from 64.3 ± 1.3 % for 1 w% sample prepared at 18 mL/min up to 79.8 ± 1.3 % for 10 w% sample prepared at 8 mL/min (Table 2.2).

Table 2.2: Total porosity, closed porosity, trabecular separation and trabecular thickness of the μ -scaffold as assessed by MicroCT analysis.

Polymeric solution concentration [w/v%]	Q_{CP} [mL/min]	Total porosity [%]	Closed porosity [%]	Mean pore size [μm]	Trabecular thickness [μm]
1	8	64.3 ± 1.3 (*, π)	/	22.6 ± 0.8 (π , *)	11.4 ± 0.3
	18	62.0 ± 3.0 (π)	10^{-2}	14.1 ± 0.8 (π)	8.8 ± 0.2
4	8	72.4 ± 2.2	/	35.8 ± 8.2 (#)	15.9 ± 0.9 (π)
	18	67.1 ± 1.2 (*)	/	24.6 ± 0.3 (*)	13.3 ± 0.1
10	8	79.8 ± 1.3 (#)	10^{-2}	46.8 ± 3.0	17.9 ± 0.2
	18	77.4 ± 0.5 (#)	10^{-3}	36.2 ± 0.7 (#)	15.1 ± 0.5 (π)

All data are statistically significant at 0.05 level except those indicated by the symbols.

In agreement with SEM analysis and considering the limit of MicroCT resolution, the percentage of closed pores was close to zero, while the mean pore size ranged from 14.1 ± 0.8 μm for 1 w% sample prepared at 18 mL/min up to 46.8 ± 3.0 μm for 10 w% sample prepared at 8 mL/min. These results, together with the pore size distributions of Figure S2 highlighted that μ -scaffold porosity and pore size are directly correlated with μ -scaffold diameter. The size distribution of the trabeculae progressively increased with the increase of μ -scaffold size (Figure S3).

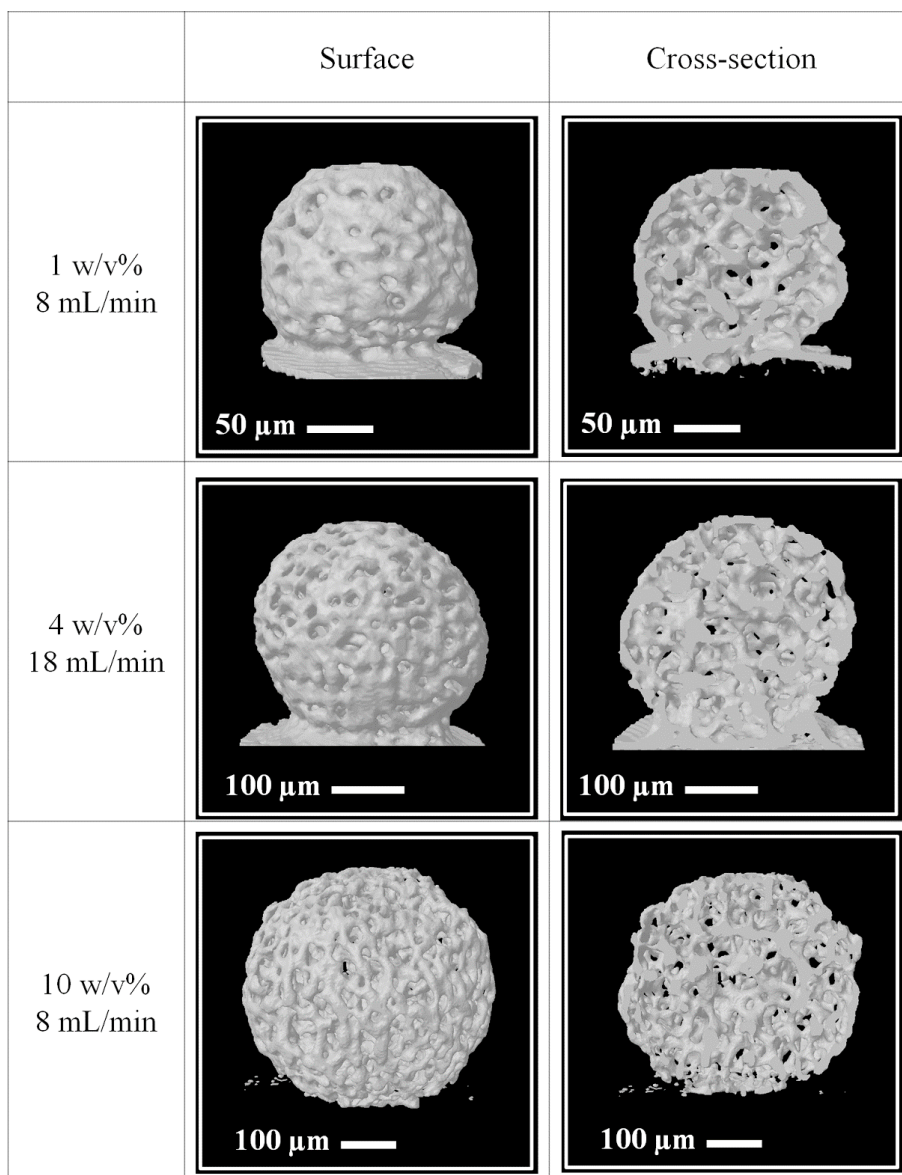


Figure 2.7: 3D reconstruction images of surface and cross-section of PCL μ -scaffold as a function of polymers concentration and Q_{CP} as obtained by MicroCT analysis. Samples were prepared by setting $Q_{DP} = 90 \mu\text{L}/\text{min}$ and by using 0.5 w/v% PVA solution as coagulation bath at RT for 3 hours.

Several methods are currently available to design and fabricate porous μ -scaffold with tailored diameter distribution and pore architecture by combining the advantages of particle leaching, emulsion templating, gas foaming, phase separation and freeze-drying, among others [12,23]. Lim and co-workers proposed a melt molding and particle (NaCl) leaching method to obtain porous PCL μ -scaffold for use as injectable cell carriers [9]. The prepared samples showed over 90% porosity, diameter in the 400-550 μm range and two variable pore sizes, 25-50 and 50-100 μm ,

respectively, achieved by selecting two NaCl size distributions. Double emulsion techniques were combined with either porogen leaching or gas foaming to obtain porous μ -scaffold from poly(lactide-co-glycolide) with high porosity and large surface pores [11,43,44]. Although all of these methods enabled the achievement of open porous μ -scaffold with controllable diameter and interconnected porosities, major difficulties may be related to the stability of the double emulsion and the achievement of highly interconnected pores even at lower total porosities [43]. Novel μ -scaffold designs strive to combine the established advantages of carriers for cells delivery with easy and reliable fabrication of uniform micrometric-sized particles that provide 100% open porosity with pores size larger than 20 μm for cells colonization and delivery [11]. The method proposed in this study addressed these important concerns as PCL μ -scaffold fabrication combined fluidic emulsion, for the control of samples shape and diameter distribution, with polymer (PEO) leaching, for the achievement of a highly opened trabecular architecture. The use of PEO as a polymeric porogen agent was extremely advantageous as the polymer was dissolved in dichloromethane together with PCL leaving a time-stable solution that can be loaded into a syringe and emulsified in the fluidic emulsion setup of Figure 2.1. Moreover, during the process of samples coagulation, PCL crystallization and PEO leaching timing scales were optimized to achieve porosity up to $79.8 \pm 1.3 \%$ and mean pore size up to $46.8 \pm 3.0 \mu\text{m}$. Most importantly, the use of fluidic emulsion technique could also open to the possible preparation of μ -scaffold with even complex shape and geometry by simply changing the features of the fluidic channels [20]. Taking into account all of these considerations and based on literature investigations, PCL μ -scaffold prepared from 10 w% solution at 8 mL/min were further used *in vitro* to test their degradation and biocompatibility.

2.3.3. In vitro degradation and biocompatibility

The effect of degradation on the weight loss and morphological change of the PCL μ -scaffold was evaluated by soaking the samples in PBS up to 40 days. As reported for other PCL scaffolds, the μ -scaffold did not undergo any significant weight loss or morphological change (data not shown) over time, which indicated that longer degradation times or more aggressive degradation media would be required to have an impact on the microstructural properties, as reported elsewhere [45,46].

The characterization of the biocompatibility properties of PCL μ -scaffold was an essential aspect of the proposed study and was carried out *in vitro* and by using HDFs towards collagenous

hybrid tissue building. Preliminary tests were carried out to establish cell seeding and culture conditions. In particular, the cell/ μ -scaffold was fixed to 200, while seeding conditions, culture media composition and frequency of agitation and incubation time were optimized depending on previous investigation [47]. The cell-seeded μ -scaffold were incubated for up to 25 days and the number of viable cells was assessed by Alamar blue assay, as shown in Figure 2.8A. Alamar blue is a metabolic assays nontoxic to cells that uses nonfluorescent resazurin as a primary constituent. Resazurin is transformed from blue colour to the highly fluorescent resorufin (pink) within a redox reaction process [48-50]. Resorufin, that is a redox indicator is used in assays for cell proliferation, cell viability, and mitochondrial respiratory activity by viable cells. Furthermore, even if it may be affected by limitations related to the reagents diffusion properties into the 3D TE constructs, this assay has some important advantages. First, measurements are non-invasive and may allow the real-time monitoring of cell viability on each specific sample during *in vitro* culture. Second, Alamar blue is a good fidelity assay as it has shown a good correlation with other metabolic activity assays such as the MTT assay [49]. Viable HDFs number increased significantly overtime on the μ -scaffold, from $3.04 \pm 0.59 \times 10^4$ cells at 6 hours to $1.10 \pm 1.49 \times 10^5$ cells on day 10, $1.52 \pm 1.49 \times 10^5$ cells on day 20 and $1.60 \pm 1.32 \times 10^5$ cells on day 25. These data followed previous works showing fibroblast proliferation until 10 days on porous μ -scaffold made from polylactic-co-glycolic acid [43,51], or chitosan [52]. The decrease of HDFs proliferation at longer culture times was already reported in the literature and ascribed to the complete cellular colonization of the μ -scaffold and the possible cellular necrosis which decreased viable cell number and growth [53]. Most importantly, optical microscope visualization of samples evolution over culture time indicated that cell/tissue growth induced inter- μ -scaffold assembly already at day 5 of culture (left-up inset of Figure A) while the formation of a single hybrid tissue was observed at day 10 (not shown). Further cell proliferation and ECM production resulted in enhanced inter-particles connection and higher tissue growth (right-down inset of Figure A). Literature studies indicated that HDF-seeded μ -scaffold aggregation depended on multiples factors, such as cells-scaffolds interaction and culture conditions used. For example, HDFs formed large conglomeration when cultured onto gelatin μ -scaffold in 12-well cell culture plates and continuous agitation [54], while HDF-seeded gelatin μ -scaffold fused already after 96 hours when cultured in dynamic spinner-flask conditions [55]. Actin cytoskeleton and nuclei staining were carried out on the HDFs-seeded μ -scaffold to visualize and assess cell morphology, adhesion and proliferation. As shown in

Figures 2.8B and H, the HDFs well attached to the μ -scaffold surface and displayed a flat and spread morphology already after 6 hours from seeding. These results indicated good cellular interaction with the supporting scaffold structure. Furthermore, cell proliferation resulted in significant increase of the cell population onto the surface of the scaffolds at day 5 (Figure 2.8C). Confocal images of the samples at longer culture times, from day 10 to day 25, showed the almost complete surface covering by the cells and the progressive formation of cell-ECM tissue between adjacent μ -scaffold characterized by densely packed cells aligned (day 20, Figure 2.8I).

Second harmonic generation pictures of the collagen fibres acquired by multiphoton microscopy test evidenced progressive collagen deposition by the HDFs from $49.8 \pm 1.4\%$ at day 5, to $71.7 \pm 4.0\%$ at day 14 and, finally, $86.6 \pm 3.6\%$ at day 25 (Figure 2.9A).

Figures 2.9B-D show the massive collagen deposition by the HDFs and the strong directionality of collagen fibres in the inter particles space from one particle towards the adjacent one. H&E stained cross-sections of the hybrid tissue were reported in Figure 2.10 to evaluate cells distribution and proliferation.

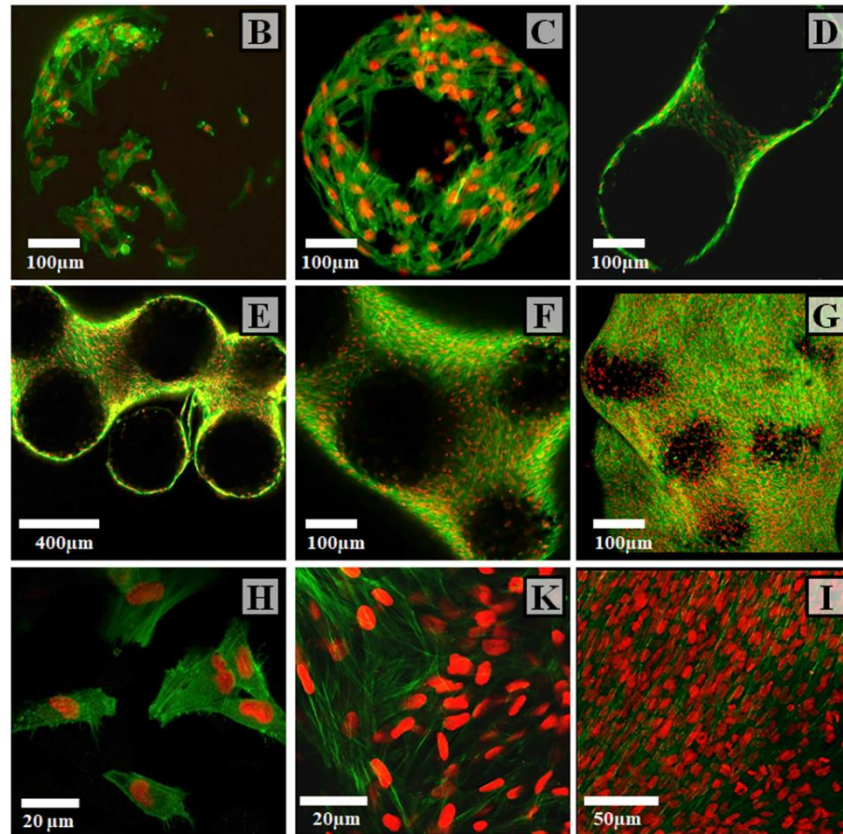
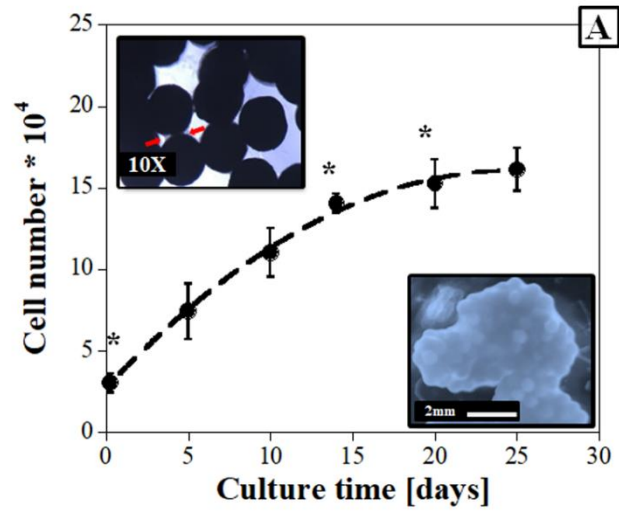


Figure 2.8: (A) Viability and proliferation of HDFs onto PCL μ -scaffold up to 25 days of *in vitro* culture as measured by Alamar blue assay. Data are presented as mean \pm SD (n=4). The insets of Figure A showed optical images of hybrid tissue at 5 days (left-up) and 25 days (right-down) of culture. The red arrows evidenced cell- and ECM-mediated linking of adjacent μ -scaffold. Figures 2.8B-I showed low and high magnification CLSM images showing the morphology and colonization of HDFs onto the surface of μ -scaffold and the inter-particles regions at different culturing time: 6 hours (B, H); 5 days (C), 10 days (D),

14 days (E,K), 20 days (F, I) and 25 days (G). Nuclei are marked in red (DRAQ5) and cytoskeleton in green (Phalloidin).

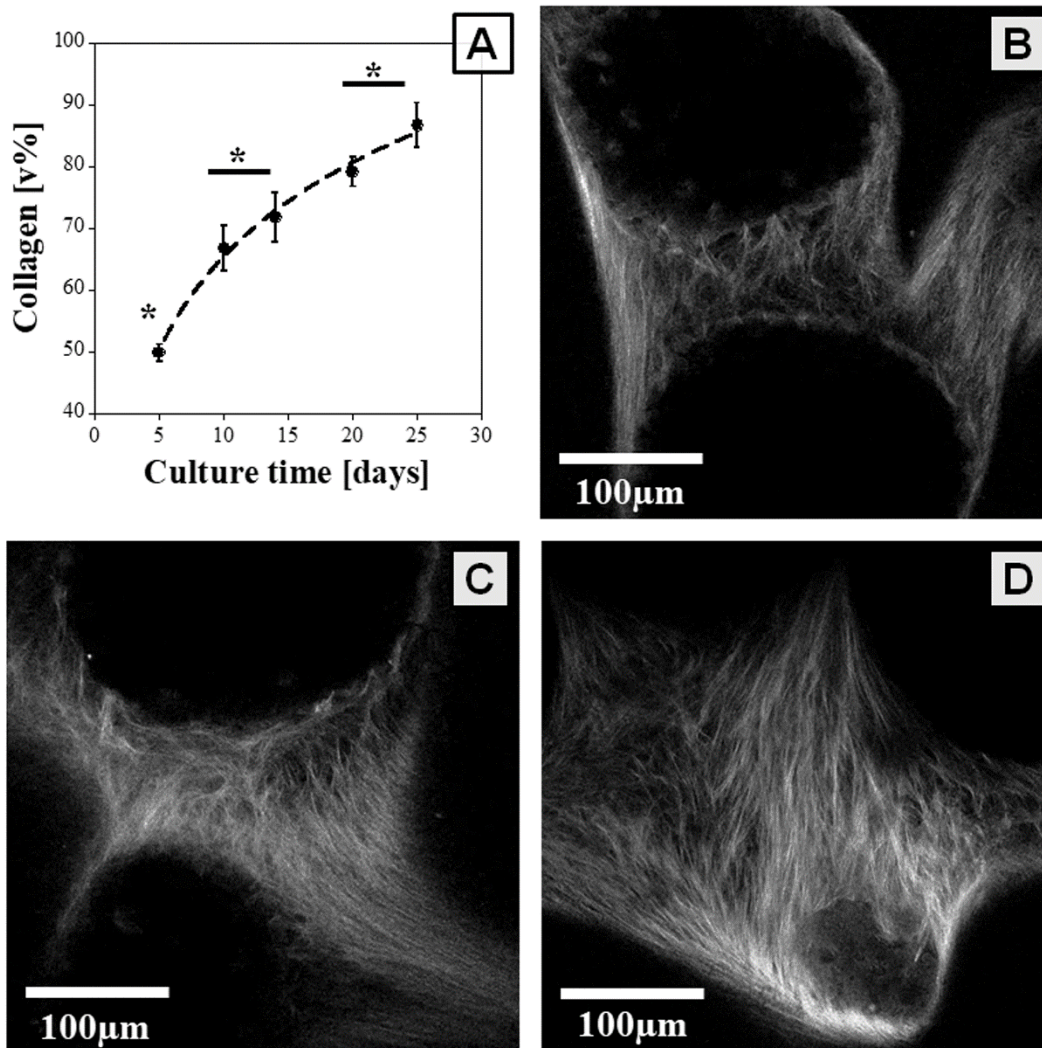


Figure 2.9: Multiphoton microscopy evaluation of collagen biosynthesis (A) and structure in the inter-particles regions at (B) 14 days, (C) 20 days and (D) 25 days of *in vitro* culture.

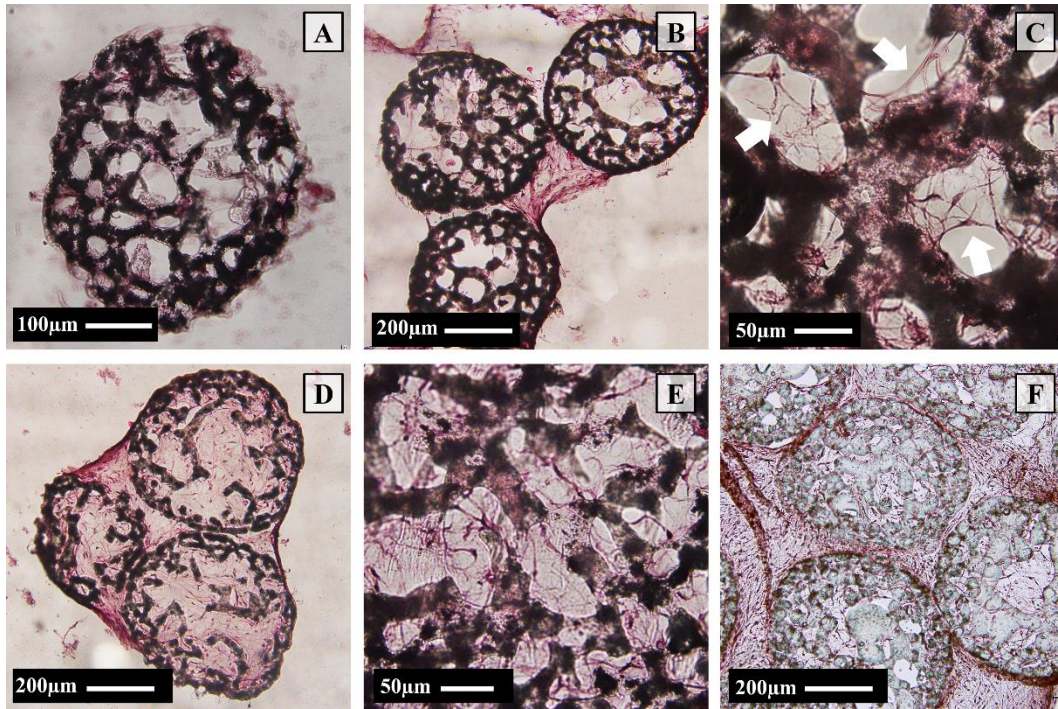


Figure 2.10: H&E staining of the cross-sections of cell/ μ -scaffold at (A) 6 h, (B, C) 14 days, (D, E) 20 days and (F) 25 days of *in vitro* culture. The white arrows of figure 2.10C evidenced HDFs creating bridges between the opposite pore walls of the inner μ -scaffold porosity.

As shown, HDFs adhered to the μ -scaffold surface and, after 14 days of culture, proliferated and colonized also the inner porosity (compare Figures 2.10A and 10C). The increase of culture time up to 20 and 25 days resulted in the almost full cell colonization (Figure 2.10E) and the formation of strong bonding between μ -scaffold (Figure 2.10F). Results of MicroCT analysis of hybrid tissue composition at different culture times are shown in Figure 2.11 together with a representative 3D reconstruction of the samples. The importance of scaffolds porosity on fibroblasts colonization, growth and migration is in agreement with previous works on synthetic and natural polymeric scaffolding materials [56-58].

In agreement with previous data, tissue growth increased from $1.7 \pm 2.4\%$ at day 10 to $19.6 \pm 6.2\%$ at day 14 up to $52.8 \pm 1.4\%$ at day 25 (Figure 2.11A). These data demonstrated that the final bio-hybrid was half composed by tissue, comprising of the cells and the collagenous matrix, and half by particles.

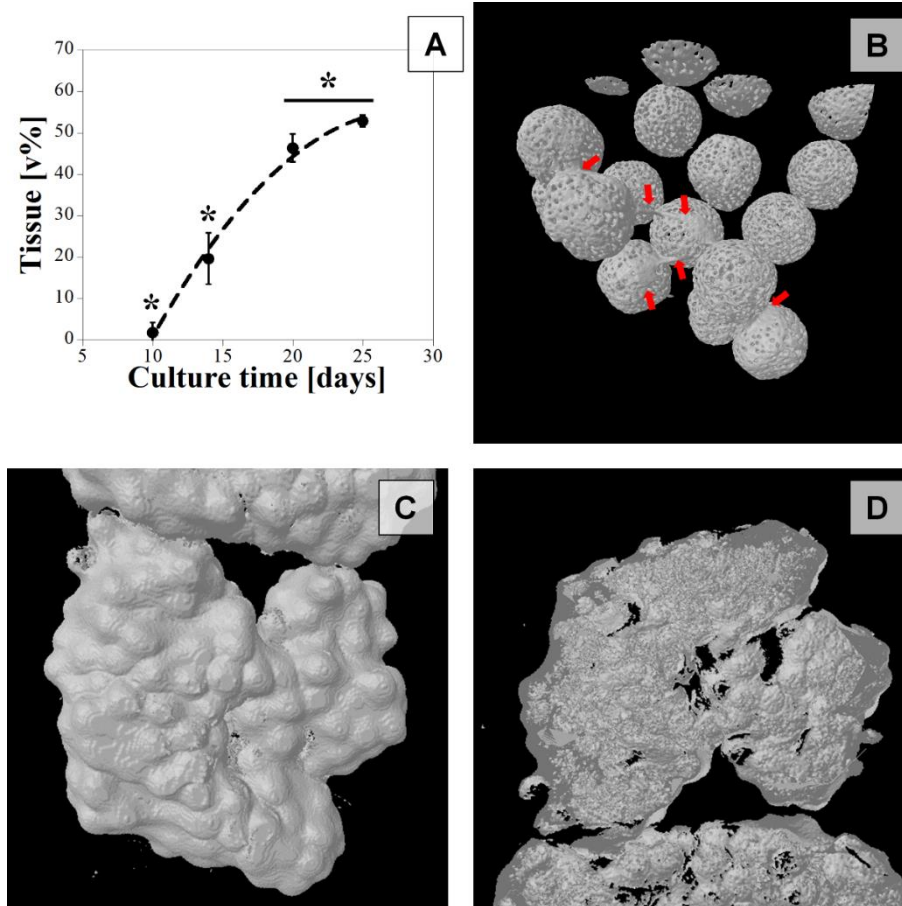


Figure 2.11: MicroCT evaluation of new tissue v% of the hybrid tissue at different time points (A) together with 3D reconstruction of the samples at (B) 10 days and (C, D) 20 days of *in vitro* culture. (C) Surface and (D) cross-section of the hybrid tissue.

Nowadays, biocompatible μ -scaffold are essential elements of modular TE approaches as they have to promote cells adhesion, proliferation and colonization in the entire porosity in order to guide cell-seeded modules assembly and hybrid tissue formation [5,59,60]. Porous μ -scaffold can be also used as carriers for *in vitro* cell expansion and proliferation and injectable filler for tissue defect repair/regeneration [9,51]. Gelatin is one of the most used μ -scaffold biomaterial for the regeneration of tissues such as the dermis [8], liver [61], vascular tissue ring [62], cardiovascular tissue [63], and bone [7], among others. Not so far, polysaccharide materials, such as chitosan, were used to produce μ -scaffold for 3D cultures of hepatocytes and neurons cells [64,65]. A major hurdle to the successful application of naturally derived μ -scaffold is the potential antigenic and immunogenic response that can be elicited from its *in vivo* use [66]. On the contrary, PCL is a slowly degradable synthetic biomedical polymer that received the US Food and Drug

Administration approval as a drug delivery system and in surgical sutures [26]. PCL fillers were also used for dermal and subcutaneous injection to study neo-collagenesis in human tissue for wrinkle improvement [27]. The results of this study demonstrated the biocompatibility of prepared PCL μ -scaffold and their potential use in modular TE applications, specifically for HDFs culture and collagenous tissue formation (Figures 2.8-2.10). Several published works reported the capability of PCL scaffolds to support HDFs growth, proliferation and biosynthesis. Recent works showed the potential of PCL scaffolds, prepared by electrospinning and gas foaming, to promote the growth and proliferation of HDFs up to 21 days *in vitro* [58,67]. PCL scaffolds were also blended with natural polymers, such as collagen [68], gelatin [69], or chitosan [70], as well as inorganic fillers to enhance scaffolds hydrophilicity and cellular interaction for wound healing purposes [67]. Further bioactivation strategies for PCL scaffolds involved surface functionalization by plasma treatment and addition of adhesive protein [71] either loading of bioactive molecules and therapeutic agents inside polymeric matrix [72,73]. Although there are several works about the fabrication of PCL microparticles for biomedical applications, literature regarding the manufacture of porous PCL μ -scaffold and their use as building blocks for HDFs culture and hybrid tissue manufacture is scarce. In recent work, Zhou and co-workers reported the fabrication of a series of PCL microspheres by combining emulsion/solvent evaporation and particle leaching techniques [74]. Microspheres with 57.4-75.5% range of porosity and 25.6-84.0 μm range of pores size were obtained by adjusting polymer/solvent and porogen (paraffin) amount. Further alkaline hydrolysis followed by hydroxyapatite surface coating was carried out to enhance the adhesion and growth of HDFs up to 7 days of *in vitro* culture. In agreement with our results, the PCL microspheres supported cell adhesion, proliferation and hybrid tissue formation at already 5 days of culture. Nevertheless, no information was provided about the effect of porosity architecture on 3D cell distribution as well as long-term hybrid tissue growth. The process herein described for the preparation of PCL μ -scaffold is valuable from both materials design and biomedical applications points of view. Indeed, we showed that μ -scaffold architectural features, mainly pore morphology and size, allowed fully cellular growth and colonization on both μ -scaffold surface and interior (Figures 2.8 and 2.10), overcoming limitations related to homogeneous cell distribution and nutrients transport in 3D tissue construct. Furthermore, PCL μ -scaffold diameter can be finely modulated by the choice of solution composition and Q_{CP} pair to meet the requirements of different tissues and regeneration therapies involving the application of

these samples. The use of a biocompatible and water-soluble porogen (PEO) for μ -scaffold fabrication may contribute to these positive biocompatibility results, as it limits the release of toxic residues from the polymeric matrix that may affect cell survival and viability.

2.4. Conclusion

Porous μ -scaffolds with a rounded shape, controllable size, and full pore interconnectivity were prepared in this work by combining fluidic emulsion, porogen leaching, and particle coagulation processes. The as-prepared μ -scaffolds have diameters in the range from 119.4 ± 4.6 to 541.8 ± 13.4 μm , porosity ranging from 64.3 ± 1.3 to $79.8 \pm 1.3\%$, and a mean pore size ranging from 14.1 ± 0.8 to 46.8 ± 3.0 μm . The μ -scaffold were tested *in vitro* for their capability to support HDF adhesion, proliferation, and biosynthesis. Cells adhered to the sample surface, proliferated up to five times over the entire culture time, and synthesized new collagenous ECM, which contributed to μ -scaffold aggregation even after 5 days of culture, as well as the formation of the hybrid tissue made of more than 50% of the new tissue. All of these results are promising for the future implementation of the as-prepared μ -scaffolds as building blocks for *in vitro* modular TE toward applications such as dermis and bone repair/regeneration. Challenging aspects of the proposed materials are (1) the possible integration of μ -scaffold bioactivation strategies (e.g., bioactive molecules/ceramic loading) within the fluidic emulsion process and (2) the control of the cell/ μ -scaffold composition and assembly process to regulate and guide ECM biosynthesis and vascularization.

2.5. References

- [1] Salerno, A.; Netti, P. A.; Di Maio, E.; Iannace, S. Engineering of foamed structures for biomedical application. *J. Cell. Plast.* **2009**, *45*, 103-117.
- [2] Chen, H.; de Botelho Ferreira Braga Malheiro, A.; van Blitterswijk, C.; Mota, C.; Wieringa, P. A.; Moroni, L. Direct writing electrospinning of scaffolds with multidimensional fiber architecture for hierarchical tissue engineering. *ACS Appl. Mater. Inter.* **2017**, *9*, 38187-38200.
- [3] Nichol, J. W. and Khademhosseini, A. modular tissue engineering: engineering biological tissues from the bottom Up. *Soft Matter* **2009**, *5*, 1312-1319.
- [4] Elbert, D. L. Bottom-up Tissue engineering. *Curr. Opin. Biotechnol.* **2011**, *22*, 674-680.
- [5] Salerno, A.; Cesarelli, G.; Pedram, P.; Netti, P. A. Modular strategies to build cell-Free and cell-laden scaffolds towards bioengineered tissues and organs. *J. Clin. Med.* **2019**, *8*, article n° 1816.
- [6] Scott, E. A; Nichols, M. D.; Kuntz-Willits, R.; Elbert, D. L. Modular scaffolds assembled around living cells using poly(ethylene glycol) microspheres with macroporation via a non-cytotoxic porogen. *Acta Biomater.* **2010**, *6*, 29-38.
- [7] Chen, M.; Wang, X.; Ye, Z.; Zhang, Y.; Zhou, Y.; Tan, W. A Modular approach to the engineering of a centimeter-sized bone tissue construct with human amniotic mesenchymal stem cells-laden microcarriers. *Biomaterials* **2011**, *32*, 7532-7542.
- [8] Imparato, G.; Urciuolo, F.; Casale, C.; Netti, P. A. The role of microscaffold properties in controlling the collagen assembly in 3D dermis equivalent using modular tissue engineering. *Biomaterials* **2013**, *34*, 7851-7861.
- [9] Lim, S. M.; Lee, H. J.; Oh, S. H.; Kim, J. M.; Lee, J. H. Novel fabrication of PCL porous beads for use as an injectable cell carrier system. *J. Biomed. Mater. Res. Part B: Appl. Biomater.* **2009**, *90*, 521-530.
- [10] Martin, Y.; Eldardiri, M.; Lawrence-Watt, D. J.; Sharpe, J. R. Microcarriers and their potential in tissue regeneration. *Tissue Eng. Part B* **2011**, *17*, 71-80.
- [11] Ambrosch, K.; Manhardt, M.; Loth, T.; Bernhardt, R.; Schulz-Siegmund, M.; Hacker, M.C. Open porous microscaffolds for cellular and tissue engineering by lipid templating. *Acta Biomater.* **2012**, *8*, 1303-1315.

- [12] Choi, S.; Zhang, Y.; Yeh, Y. C.; Wooten, A. L.; Xia, Y. Biodegradable porous beads and their potential applications in regenerative medicine. *J. Mater. Chem.* **2012**, *22*, 11442-11452.
- [13] Mazio, C.; Casale, C.; Imparato, G.; Urciuolo, F.; Attanasio, C.; Gregorioa, M. De.; Rescigno, F.; Netti, P. A. Pre-vascularized dermis model for fast and functional anastomosis with host vasculature. *Biomaterials* **2019**, *192*, 159-170.
- [14] Chau, D. Y. S.; Agashi, K.; Shakesheff, K. M. Microparticles as tissue engineering scaffolds: manufacture, modification and manipulation. *Mater. Sci. Tech.* **2008**, *24*, 1031-1044.
- [15] Zhang, Z.; Eyster, T. W.; Ma, P. X. Nanostructured Injectable Cell Microcarriers for Tissue Regeneration. *Nanomedicine* **2016**, *11*, 1611-1628.
- [16] John, J. V.; McCarthy, A.; Wang, H.; Chen, S.; Su, Y.; Davis, E.; Li, X.; Sung Park, J.; Reinhardt, R. A.; Xie, J. Engineering biomimetic nanofiber microspheres with tailored size, predesigned structure, and desired composition via gas bubble-mediated coaxial electrospray. *Small* **2020**, *16*, 1-9.
- [17] Oh, S. H.; Kim, I. G.; Lee, J. Y.; Lee, J. Y.; Lee, J. H. Bioactive porous beads as an injectable urethral bulking agent: their in Vitro evaluation on smooth muscle cell differentiation. *Tissue Eng. Part A* **2011**, *17*, 655-664.
- [18] Kemala, T.; Budianto, E.; Soegiyono, B. Preparation and characterization of microspheres based on blend of poly(lactic acid) and poly(ϵ -caprolactone) with poly(vinyl alcohol) as emulsifier. *Arab. J. Chem.* **2012**, *5*, 103-108.
- [19] Salerno, A.; Levato, R.; Mateos-Timoneda, M. A.; Engel, E.; Netti, P. A.; Planell, J. A. modular polylactic acid microparticle-based scaffolds prepared via microfluidic emulsion/solvent displacement process: fabrication, characterization, and in vitro mesenchymal stem cells interaction study. *J. Biomed. Mater. Res. Part A* **2012**, *101A*, 720-732.
- [20] Xu, S.; Nie, Z.; Seo, M.; Lewis, P.; Kumacheva, E.; Stone, H. A.; Garstecki, P.; Weibel, D. B.; Gitlin, I.; Whitesides, G. M. Generation of monodisperse particles by using microfluidics: control over size, shape, and composition. *Angew. Chem. Int. Ed.* **2005**, *44*, 724-728.

- [21] Fatnassi, M.; Jacquart, S.; Brouillet, F.; Rey, C.; Combes, C.; Fullana, S. G. Optimization of spray-dried hyaluronic acid microspheres to formulate drug-loaded bone substitute materials. *Powder Tech.* **2014**, *255*, 44-51.
- [22] Zeng, W.; Huang, J.; Hu, X.; Xiao, W.; Rong, M.; Yuan, Z.; Luo, Z. Ionically cross-linked chitosan microspheres for controlled release of bioactive nerve growth factor. *Int. J. Pharm.* **2011**, *421*, 283-290.
- [23] Totaro, A.; Salerno, A.; Imperato, G.; Domingo, C.; Urciuolo, F.; Netti, P. A. PCL–HA micro scaffolds for in vitro modular bone tissue engineering. *J. Tissue Eng. Regen. Med.* **2017**, *11*, 1865-1875.
- [24] Hong, S.; Yu, H.; Kim, H. Tissue engineering polymeric microcarriers with macroporous morphology and bone-bioactive surface. *Macromol. Biosci.* **2009**, *9*, 639-645.
- [25] Kim, T. K.; Yoon, J. J.; Lee, D. S.; Park, T. G. Gas foamed open porous biodegradable polymeric microspheres. *Biomaterials* **2006**, *27*, 152-159.
- [26] Kim, J.; In, C.; Park, N.; Kim, B.; Yoon, H. Comparative study of rheological properties and preclinical data of porous polycaprolactone microsphere dermal fillers. *J. Cosmet. Dermatol.* **2020**, *19*, 596-604.
- [27] Kim, J. A.; Abel, D. Van. Neocollagenesis in human tissue injected with a polycaprolactone-based dermal filler. *J. Cosmet. Laser. Ther.* **2015**, *17*, 99-101.
- [28] Leferink, A.; Schipper, D.; Arts, E.; Vrij, E.; Rivron, N.; Karperien, M.; Mittmann, K.; van Blitterswijk, C.; Moroni, L.; Truckenmüller, R. Engineered micro-objects as scaffolding elements in cellular building blocks for bottom-Up tissue engineering approaches. *Adv. Mater.* **2014**, *26*, 2592-2599.
- [29] Xiao, W.; Xi, H.; Li, J.; Wei, D.; Li, B.; Liao, X.; Fan, H. Fabrication and assembly of porous micropatterned scaffolds for modular tissue engineering. *Mater. Lett.* **2018**, *228*, 360-364.
- [30] Yuan, Z.; Favis, B. D. Macroporous poly(l-lactide) of controlled pore size derived from the annealing of co-continuous polystyrene/poly(l-lactide) blends. *Biomaterials* **2004**, *25*, 2161-2170.
- [31] Yin, H. M.; Li, X.; Xu, J. Z.; Zhao, B.; Li, J. H.; Li, Z. Highly aligned and interconnected porous poly(ϵ -caprolactone) scaffolds derived from co-continuous polymer blends. *Mater. Des.* **2017**, *128*, 112-118.

- [32] Salerno, A.; Oliviero, M.; Maio E. Di.; Iannace, S.; Netti, P. A. Design of porous polymeric scaffolds by gas foaming of heterogeneous blends. *J. Mater. Sci. Mater. Med.* **2009**, *20*, 2043-2051.
- [33] (29) Washburn, N.R.; Simon, C. G.; Tona, A.; Elgandy, H. M.; Karim, A.; Amis, E. J. Co-extrusion of biocompatible polymers for scaffolds with co-continuous morphology. *J. Biomed. Mater. Res.* **2001**, *60*, 20-29.
- [34] (30) Reignier, J.; Huneault, M. A. Preparation of interconnected poly(3-caprolactone) porous scaffolds by a combination of polymer and salt particulate leaching. *Polymer* **2006**, *47*, 4703-4717.
- [35] (31) Qiu, Z.; Ikehara, T.; Nishi, T. Miscibility and crystallization of poly(ethylene oxide) and poly(ϵ -caprolactone) blends. *Polymer* **2003**, *44*, 3101-3106.
- [36] Causa, A.; Filippone, G.; Domingo, C.; Salerno, A. Study of the morphology and texture of poly(3-caprolactone)/polyethylene oxide blend films as a function of composition and the addition of nanofillers with different functionalities. *RSC Adv.* **2015**, *5*, 59354-59363.
- [37] Sato, T.; Araki, S.; Morimoto, M.; Tanaka, R.; Yamamoto, H. Comparison of Hansen Solubility Parameter of Asphaltenes Extracted from Bitumen Produced in Different geographical regions. *Energy & Fuels* **2014**, *28*, 891-897.
- [38] Liu, T.; Ozisik, R.; Siegel, R. W. Phase Separation and surface morphology of spin-coated films of polyetherimide/polycaprolactone immiscible polymer blends. *Thin Solid Films* **2007**, *515*, 2965-2973.
- [39] Quevedo, E.; Steinbacher, J.; McQuade, D. T. Interfacial polymerization within a simplified microfluidic device: capturing capsules. *J. Am. Chem. Soc.* **2005**, *127*, 10498-10499.
- [40] Choi, S.; Cheong, I. W.; Kim, J.; Xia, Y. Preparation of uniform microspheres using a simple fluidic device and their crystallization into close-packed lattices. *Small* **2009**, *5*, 454-459.
- [41] Watanabe, T.; Ono, T.; Kimura, Y. Continuous fabrication of monodisperse polylactide microspheres by droplet-to-particle technology using microfluidic emulsification and emulsion-solvent diffusion. *Soft Matter* **2011**, *7*, 9894-9897.

- [42] Moon, S.; Cheong, I. W.; Choi, S. Effect of Flow Rates of the Continuous phase on droplet size in dripping and jetting regimes in a simple fluidic device for coaxial flow. *Colloids Surf. A Physicochem. Eng. Asp.* **2014**, *454*, 84-88.
- [43] Choi, S.; Yeh, Y.; Zhang, Y.; Sung, H.; Xia, Y. Uniform beads with controllable pore sizes for biomedical applications. *Small* **2010**, *6*, 1492-1498.
- [44] Qutachi, O.; Vetsch, J. R.; Gill, D.; Cox, H.; Scurr, D. J.; Hofmann, S.; Müller, R.; Quirk, R. A.; Shakesheff, K. M.; Rahman, C. V. Injectable and porous PLGA microspheres that form highly porous scaffolds at body temperature. *Acta Biomater.* **2014**, *10*, 5090-5098.
- [45] Salerno, A.; Zeppetelli, S.; Oliviero, M.; Battista, E.; Di Maio, E.; Iannace, S.; Netti, P. A. Microstructure, degradation and in vitro MG63 cells interactions of a new poly(ϵ -caprolactone), zein, and hydroxyapatite composite for bone tissue engineering. *J. Bioact. Compat. Polym.* **2012**, *27*, 210-226.
- [46] Rezwani, K.; Chen, Q. Z.; Blaker, J. J.; Boccaccini, A. R. Biodegradable and bioactive porous polymer/inorganic composite scaffolds for bone tissue engineering. *Biomaterials* **2006**, *27*, 3413-3431.
- [47] Mazio, C.; Casale, C.; Imperato, G.; Urciuolo, F.; Netti, P. A. Recapitulating spatiotemporal tumor heterogeneity in vitro through engineered breast cancer microtissues. *Acta Biomater.* **2018**, *73*, 236-249.
- [48] Pabbruwe, M. B.; Stewart, K.; Chaudhuri, J. B. A comparison of colorimetric and DNA quantification assays for the assessment of meniscal fibrochondrocyte proliferation in microcarrier culture. *Biotechnol. Lett.* **2005**, *27*, 1451-1455.
- [49] Zhou, X.; Holsbeeks, I.; Impens, S.; Sonnaert, M.; Bloemen, V.; Luyten, F.; Schrooten, J. Noninvasive real-time monitoring by alamarBlue during in vitro culture of three-dimensional tissue-engineered bone constructs. *Tissue Eng. Part C* **2013**, *19*, 720-729.
- [50] Quent, V. M. C.; Loessner, D.; Friis, T.; Reichert, J. C.; Hutmacher, D. W. Discrepancies between metabolic activity and DNA content as tool to assess cell proliferation in cancer research. *J. Cell. Mol. Med.* **2010**, *14*, 1003-1013.
- [51] Kim, S.; Gwak, S.; Choi, C. Y.; Kim, B. Skin regeneration using keratinocytes and dermal fibroblasts cultured on biodegradable microspherical polymer scaffolds. *J. Biomed. Mater. Res. Part B Appl. Biomater.* **2005**, *75B*, 369-377.

- [52] Chen, X.; Liu, C.; Liu, C.; Meng, X. H.; Lee, C. M.; Park, H. Preparation and biocompatibility of chitosan microcarriers as biomaterial. *Biochem. Eng. J.* **2006**, *27*, 269-274.
- [53] Puente, P. De.; Ludena, D.; Fernandez, A.; Aranda, J. L.; Varela, G.; Iglesias, J. Autologous fibrin scaffolds cultured dermal fibroblasts and enriched with encapsulated bFGF for tissue engineering. *J. Biomed. Mater. Res. Part A* **2011**, *99A*, 648-654.
- [54] Huang, S.; Fu, X. Naturally derived materials-based cell and drug delivery systems in skin regeneration. *J. Control. Release* **2010**, *142*, 149-159.
- [55] Palmiero, C.; Imparato, G.; Urciuolo, F.; Netti, P. Engineered dermal equivalent tissue in vitro by assembly of microtissue precursors. *Acta Biomater.* **2010**, *6*, 2548-2553.
- [56] Qi, X.; Su, T.; Zhang, M.; Tong, X.; Pan, W.; Zeng, Q.; Zhou, Z.; Shen, L.; He, X.; Shen, J. Macroporous Hydrogel scaffolds with tunable physicochemical properties for tissue engineering constructed using renewable polysaccharides. *ACS Appl. Mater. Inter.* **2020**, *12*, 13256-13264.
- [57] Qi, X.; Zhang, M.; Su, T.; Pan, W.; Tong, X.; Zeng, Xiong, W.; Jiang, N.; Quian, Y.; Li, Z.; He, X.; Shen, L.; Q.; Zhou, Z.; Shen, J. Biocompatible hydrogels based on food gums with tunable physicochemical properties as scaffolds for cell culture. *J. Agric. Food Chem.* **2020**, *68*, 3770-3778.
- [58] Salerno, A.; Leonardi, A. B.; Pedram, P.; Maio, E. Di.; Fanovich, M. A.; Netti, P. A. Tuning the three-dimensional architecture of supercritical CO₂ foamed PCL scaffolds by a novel mould patterning approach. *Mater. Sci. Eng. C* **2020**, *109*, article n° 110518.
- [59] Urciuolo, F.; Imparato, G.; Totaro, A.; Netti, P. A. Building a tissue in vitro from the bottom up: implications in regenerative medicine. *Methodist Debaquey Cardiovasc J.* **2013**, *4*, 213-217.
- [60] Schon, B. S.; Hooper, G. J.; Woodfield, T. B. F. Modular tissue assembly strategies for biofabrication of engineered cartilage. *Ann. Biomed. Eng.* **2017**, *45*, 100-114.
- [61] Corrado, B.; De Gregorio, V.; Imparato, G.; Attanasio, C.; Urciuolo, F.; Netti, P. A. A three-dimensional microfluidized liver system to assess hepatic drug metabolism and hepatotoxicity. *Biotechnol. Bioeng.* **2019**, *116*, 1152-1163.

- [62] Strobel, H. A.; Dikina, A. D.; Levi, K.; Solorio, L. D.; Alsberg, E.; Marsha, W. R. Cellular self-assembly with microsphere incorporation for growth factor delivery within engineered vascular tissue rings. *Tissue Eng. Part A* **2017**, *23*, 143-155.
- [63] Lee, B. W.; Liu, B.; Pluchinsky, A.; Kim, N.; Eng, G.; Vunjak-Novakovic, G. Modular assembly approach to engineer geometrically precise cardiovascular tissue. *Adv. Healthc. Mater.* **2016**, *5*, 900-906.
- [64] Huang, L.; Xiao, L.; Poudel, A. J.; Li, J.; Zhou, P.; Gauthier, M.; Liu, H.; Wu, Z.; Yang, G. Porous chitosan microspheres as microcarriers for 3D cell culture. *Carbohydr. Polym.* **2018**, *202*, 611-620.
- [65] Tedesco, M. T.; Di Lisa, D.; Massobrio, P.; Colistra, N.; Pesce, M.; Catelani, T.; Dellacasa, E.; Raiteri, R.; Martinoia, S.; Pastorino, L. Soft chitosan microbeads scaffold for 3D functional neuronal networks. *Biomaterials* **2018**, *156*, 159-171.
- [66] Rose, J. B.; Pacelli, S.; Haj, A. J. E.; Dua, H. S.; Hopkinson, A.; White, L. J.; Rose, F. R. A. J. Gelatin-based materials in ocular tissue engineering. *Materials* **2014**, *7*, 3106-3135.
- [67] Keivani, F.; Shokrollahi, P.; Zandi, M.; Irani, S.; Shokrollahi, F.; Khorasani, S. C. Engineered electrospun poly(caprolactone)/polycaprolactone-g-hydroxyapatite nanofibrous scaffold promotes human fibroblasts adhesion and proliferation. *Mater. Sci. Eng. C* **2016**, *68*, 78-88.
- [68] Zhang, Q.; Lv, S.; Lu, J.; Jiang, S.; Lin, L. Characterization of polycaprolactone/collagen fibrous scaffolds by electrospinning and their bioactivity. *Int. J. Biol. Macromol.* **2015**, *76*, 94-101.
- [69] Prado-Prone, G.; Bazzar, M.; Focarete, M. L.; García-Macedo, J. A.; Perez-Orive, J.; Ibarra, C.; Velasquillo, C.; Silva-Bermudez, P. Single-step, acid-based fabrication of homogeneous gelatin polycaprolactone fibrillar scaffolds intended for skin tissue engineering. *Biomed. Mater.* **2020**, *15*, article n° 035001.
- [70] Prasad, T.; Shabeena, E. A.; Vinod, D.; Kumary, T. V.; Anil Kumar, P. R. Characterization and in vitro evaluation of electrospun chitosan/polycaprolactone blend fibrous mat for skin tissue engineering. *J. Mater. Sci. Mater. Med.* **2015**, *26*, 28.
- [71] Siri, S.; Wadbua, P.; Amornkitbamrung, V.; Kampa, N.; Maensiri, S. Surface modification of electrospun PCL scaffolds by plasma treatment and addition of adhesive protein to promote fibroblast cell adhesion. *Mater. Sci. Tech.* **2010**, *26*, 1292-1297.

- [72] Joseph, B.; Augustine. R.; Kalarikkal, N.; Thomas, S.; Seantier, B.; Grohens, Y. Recent advances in electrospun polycaprolactone based scaffolds for wound healing and skin bioengineering applications. *Mater. Today Comm.* **2019**, *19*, 319-335.
- [73] Park, K. E.; Kim, B. S.; Kim, M. H.; You, H. K.; Lee, J.; Park, W. H. Basic fibroblast growth factor-encapsulated PCL nano/microfibrous composite scaffolds for bone regeneration. *Polymer* **2015**, *76*, 8-16.
- [74] Zhou, A.; Ye, Z.; Zhou, Y; Tan, W. Bioactive poly(ϵ -caprolactone) microspheres with tunable open pores as microcarriers for tissue regeneration. *J. Biomater. Appl.* **2019**, *33*, 1242-1251.

Figure S1: 3D reconstruction images of surface and cross-section of PCL μ -scaffold as a function of polymers concentration and Q_{CP} as obtained by MicroCT analysis. Samples were prepared by setting $Q_{DP} = 90 \mu\text{L}/\text{min}$ and by using 0.5 w/v % PVA solution as coagulation bath at 4 °C for 3h.

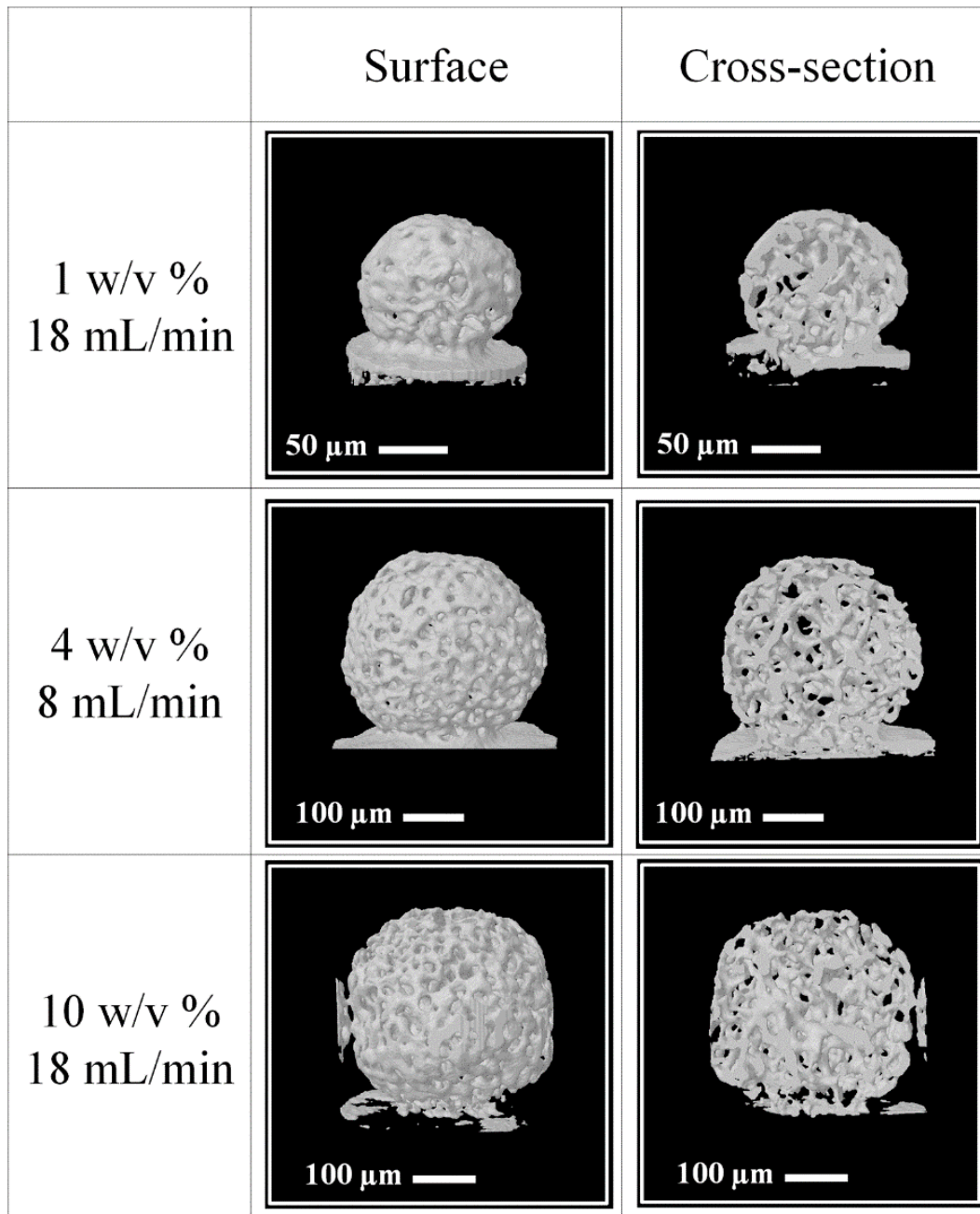


Figure S2: Pore size distributions of the μ -scaffold as a function of polymers concentration and Q_{CP} as obtained by MicroCT analysis. Samples were prepared by setting $Q_{DP} = 90 \mu\text{L}/\text{min}$ and by using 0.5 w/v % PVA solution as coagulation bath at 4 °C for 3h.

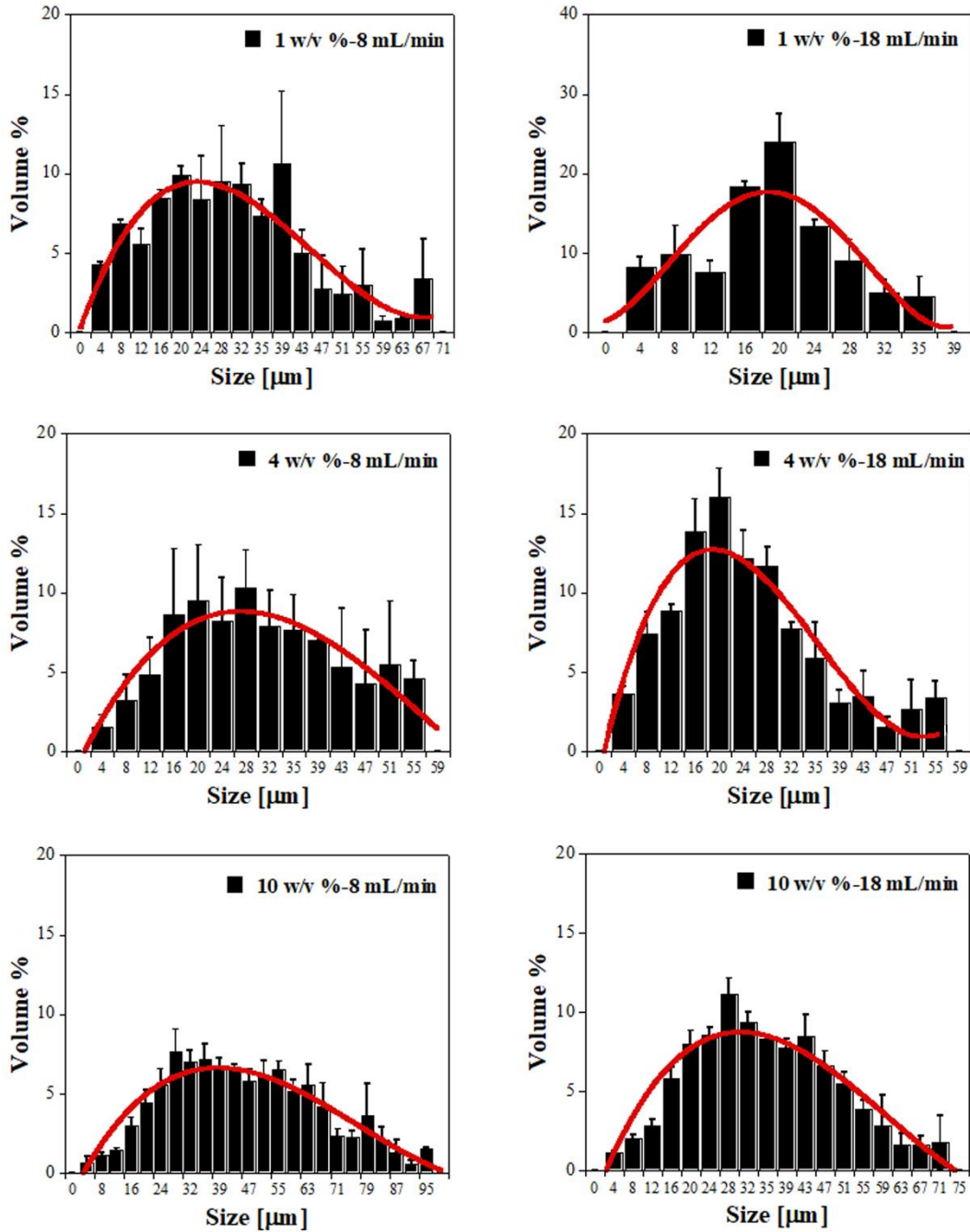
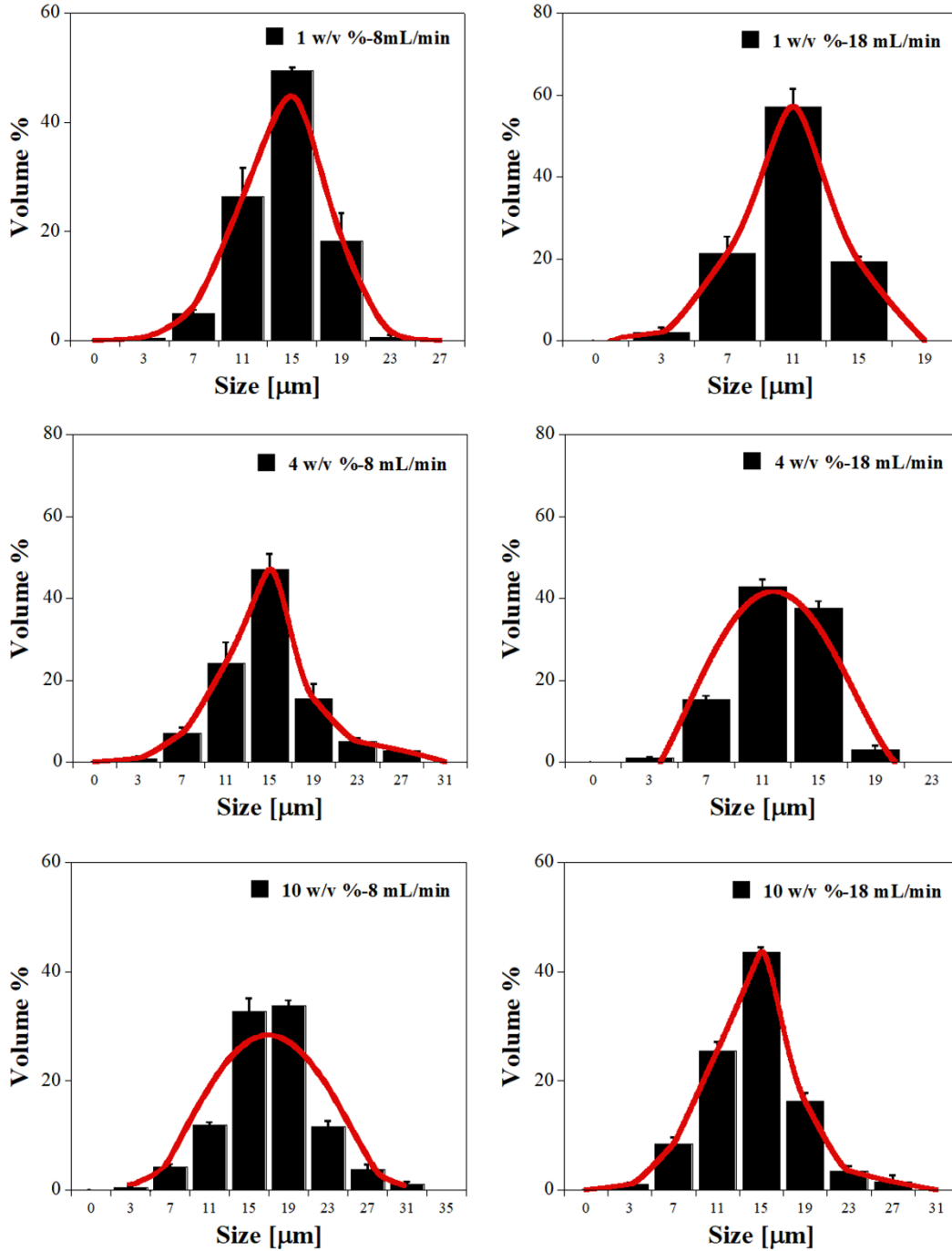


Figure S3: Trabecular thickness distributions of the μ -scaffold as a function of polymers concentration and Q_{CP} as obtained by MicroCT analysis. Samples were prepared by setting $Q_{DP} = 90 \mu\text{L}/\text{min}$ and by using 0.5 w/v % PVA solution as coagulation bath at 4 °C for 3h.



Chapter 3

In vitro microscale engineering of 3D vascularized hybrid tissues by micro-scaffolds patterning and co-culture of fibroblasts and endothelial cells

PCL μ -scaffolds were successfully fabricated as described in Chapter 2 by using PEO porogen agent and by a fluidic oil/water emulsion and particles coagulation process. These PCL μ -scaffolds have trabecular architecture with full pores interconnectivity and surface pores size suitable for HDFs growth and colonization and, as we will describe in this chapter have been used for the fabrication of vascularized hybrid tissue. It's important to point that these hybrid tissues are not engineered for towards specific vascularized tissues, but our aim is to demonstrate to developed strategy may allow to control the features of the vasculature of these hybrid tissues (distribution and organization of blood vessels) by tuning the design of the array of μ -scaffolds.

In this part of dissertation and following the μ -scaffolds preparation process in Chapter 2, PCL μ -scaffolds with diameter of 450 μm were produced by using 10 w/v% of PCL-PEO solution and by selecting Q_{CP} of 13 mL/min. Then, PCL μ -scaffolds were assembled onto the surface of PDMS moulds obtained by soft-lithography technique. These moulds were provided an array of the pillars to control the spatial assembly of PCL μ -scaffolds to form two different kinds of patterned monolayers, named ordered and disordered. These monolayers were used as platform for the *in vitro* co-culture of HDFs and HUVECs with the aim to access the effect of patterning on cells distribution, ECM biosynthesis and blood vessels formation. This was achieved by using characterization techniques such as, micro-CT, histological analysis, confocal and multiphoton analysis. Chapter 3 focuses also on the fabrication and characterization of millimetre thick vascularized hybrid constructs build by the controlled assembly of two ordered layered samples.

3.1. Introduction to micro-scaffolds patterning and modular tissue vascularization

There is significant clinical demand for de-novo engineered biomimetic tissue-analogues capable of substituting the large tissues and complex organs biochemical and biomechanical functions. A major obstacle in realizing this goal is the diffusion limit of oxygen and nutrients into the bulk of these newly synthesized tissues. In fact, there are several evidences that TE constructs exceeding dimensions beyond several hundred micrometers fail to fully integrate with host tissue due to lack of blood perfusion, resulting in loss of function and necrosis [1, 2]. Oxygen and nutrients are supplied to cells and tissues naturally by the microvasculature, which is composed of branching, variable diameter blood vessels. These blood vessels are made of a single layer of endothelial cells that mediate both passive and active transport across the vessel wall into the surrounding tissue [3]. The lack and/or inadequate growth of such microvasculature inside newly-engineered tissues lead to inhomogeneous concentration of oxygen and nutrients from the surface to the inner part of the tissue. The concomitant accumulation of metabolic wastes into the tissue core also lead to tissue necrosis and final cells death. Arguably, one of the greatest challenges in engineering clinically relevant tissue analogues, therefore, is the development of proper vascularized and viable constructs [4].

The mechanisms that control microvascular network assembly and nutrient delivery are complex and challenging to recreate *in vitro* [3]. Tubular vessels created by *in vitro* seeding autologous bone marrow-derived mononuclear cells (BM-MNC) onto biodegradable tubular scaffolds allowed to elucidate the roles of the microvasculature in health and disease tissue models [3]. Biologically derived or synthetic materials have been used to generate macrovessel tubes [5] and endothelialized microtubes [6]; cellular self-assembly has been used to generate random microvasculature [7]; microfabrication has been used to define complex geometries in hydrogels at the micro-scale [8]; and distributions of cells and biochemical factors within 3D scaffolds [9].

Several modular approaches have been studied towards the formation of microvascular networks in TE constructs. For instance, Kenar et al. fabricated a novel collagen/hyaluronic acid/poly(L-lactide-co- ϵ -caprolactone) microfibrinous scaffold by electrospinning that supports cell proliferation and angiogenesis for wound healing applications. Co-culture of HUVECs and MSCs induced the formation of interconnected vessels whose total length was 1.6 fold of the total vessel length on scaffold made of poly(L-lactide-co- ϵ -caprolactone) alone [10].

Co-culture of HUVECs and HDFs was also used in modular microspheres-based approaches to promote the formation of pre-vascularized dermis equivalent tissue. The endogenous matrix produced by HDFs provided the optimal 3D substrate for HUVECs to develop mature capillary-like-structures as demonstrated by both the inner lumen and the positivity for alpha-smooth muscle actin, laminin and collagen. The pre-vascularized dermis model so obtained had a human matrix populated by fibroblasts as well as a complex capillary network making the construct ready to be implanted [11]. In another work, Zhong et al: engineered bone-like constructs by self-assembly of osteon-like modules, obtained by seeding HUVECs onto collagen microspheres populated by MG63 osteoblasts and collagenase, and fast degradable gelatin microspheres [12]. Authors observed that the direct interaction of osteoblasts and HUVECs promoted the early vascularization while the presence of porosity induced by gelatin microspheres dissolution was pivotal for guide the later vascularization and osteogenesis of engineered tissue constructs. A similar approach was proposed by Liu et al. that prepared a bioinspired 3D Gel-MA hydrogel with dissolvable microspheres for the encapsulation and delivery of hMSCs and HUVECs. This 3D system was used to investigate whether HMSCs could play a pericytes-like role and enhance 3D vascularization [13].

The previously discussed works have demonstrated that *in vitro* strategies using modular approaches and HUVECS-based co-cultures may allow to improve the process of vascularization for newly-engineered tissues *in vitro*. However, these techniques usually result in the formation of randomly organized microvascular networks that may be unsuitable for the regeneration of hierarchical structured tissues, like bone. For these reasons, alternative methods to guide the growth and spatial development of blood vessels within viable cell/tissue constructs at micro-metric size scale are needed [4]. Great efforts in this direction have been done by taking advantage of advanced techniques, such as soft- and photo-lithography and 3D bioprinting, and cell-based approaches, where functional capillaries are engineered in cell-laden scaffolds prior to implantation. These strategies seek to engineer pre-vascularized tissues *in vitro*, allowing for improved anastomosis with the host vasculature upon implantation, while also improving cell viability and tissue development *in vitro* [4, 14].

Wray et al.: We report the fabrication of a silk-based TE scaffold that contains an embedded network of porous microchannels. The microchannels were fabricated with rectangular or half-moon profiles, and variable channel widths and heights were designed to mimic different levels of

capillary branching. This platform supports microvascular endothelial cell proliferation and lumen formation, a critical step toward development of the functional vascularization, while the porous scaffold surrounding the microchannels supports tissue growth by hMSCs. This approach for fabricating vascularized TE constructs evidenced again the importance of porosity and controlled biodegradability during new tissue formation [3].

Similar to the previous work, Zheng et al. engineered microvascular network by seeding HUVECs into microfluidic circuits formed via soft lithography in a type I collagen gel. The microvascular network provided appropriate endothelial morphology and barrier function over two weeks *in vitro* culture and allowed also to investigate angiogenic remodeling, interactions between HUVECs and perivascular cells, and interactions between blood components and endothelium with flow [15]. Raghavan et al. used microfabricated PDMS templates to spatially arrange endothelial cells within collagen gels to promote de novo endothelial cord formation. Authors reported that individual endothelial cells organized into capillary tubes after stimulation with VEGF and basic fibroblast growth factor (bFGF) over 24–48 h and demonstrated that tube diameter can be modulated by both channel width and collagen concentration. This method provided a novel tool to generate tubes with branched architecture by designing PDMS templates and to spatially organize endothelial cells for tissue engineering applications as well as to investigate the basic process of tubulogenesis [16].

Microfluidic technology has emerged as a promising tool also for tissue constructs perfusion and control of the vascular microenvironment cues *in vitro* [17-19]. For instance, Cuchiara et al. fabricated multilayer, microfluidic, PDMS-PEG hydrogel microdevice capable to spatiotemporally control microvascular network self-assembly and persistence. In addition, integration of self-assembled microvascular networks with microfabricated channels shifted the biomaterial transport regime to vessel-supported convective transport and subsequent extravascular diffusion [19].

All of previously reported studies involved the use of PDMS-based lithography techniques suitable to obtain nanometer features in the master structure through replica molding. In fact, the good moldability, biocompatibility, and optical transparency of the PDMS enable the widespread use of lithography-based microfabrication technology in a number of bioengineering fields including mechanobiology, microfluidics, and tissue engineering. However, due to its poor cellular

interaction and degradability, PDMS devices have limited utility in tissue regeneration and devices implantation [20].

3D bioprinting of vascular networks with hierarchical structures that resemble *in vivo* structures has allowed blood circulation within thick tissue constructs to accelerate vascularization and enhance tissue regeneration [21-23]. Bertassoni et al. reported a 3D micromolding technique combined with bioprinted agarose template fibers to fabricate microchannel networks with various architectural features within photo cross linkable hydrogel constructs. In particular, GelMA hydrogels were used as a scaffolding structure with pre-defined channels to enhance mass transport, cellular viability and differentiation within the construct core [24]. In another work, bioprinting technique was used to develop an *in vitro* engineered vascularized bone model to study crosstalk between blood vessel morphogenesis and osteogenesis during tissue development. To this end, the bone construct was made of a gelatin-nanohydroxyapatite 3D bioprinted scaffold with an interconnected pore network and seeded with hMSCs subjected to osteogenic differentiation. Furthermore, lentiviral-GFP transfected HUVECs loaded inside fibrin gel were added to the construct pores to stimulate the formation of a capillary- like network within the 3D bioprinted scaffold [25].

These efforts are progressing as new materials, assembly techniques and cell culture methods are developed. However, the research in this field is still at the beginning as new advanced approaches are required to create 3D tissue constructs with specific size and shape, tailor-made cellular composition and distribution as well as blood vessels branching. Furthermore, is a particular challenge the creation of these structures inside physiologically relevant extracellular matrix components [26]. In this context, this chapter describes a new approach to modularly engineer 3D bio-hybrids with specific design and precise cells/ECM organization and vascular network organization starting from the PCL μ -scaffolds previously prepared. To this aim, we fabricated hybrid vascularized 3D monolayers, in which PCL μ -scaffolds guided the formation and organization of an endothelial network within a collagenous matrix produced by HDFs and spatially distributed by using patterned moulds obtained by soft-lithography technique. Specifically, hybrid vascularized mono-layers constructs were fabricated by using two kinds of patterned moulds to obtain ordered and disordered configurations, both involving the co-culture of HDFs and HUVECs. Afterwards, thick 3D vascularized hybrid constructs with the approximately 1mm dimension were fabricated by the controlled assembly of two ordered layered

samples within a pre-designed bonding chamber able to provide the desired alignment of the samples and the correct tissue culture and growth *in vitro*.

3.2. Experimental part

3.2.1. Materials

The materials that we used for the experimental activity are the same that are described in the materials section of Chapter 2 (2.2.1).

3.2.2. Porous polycaprolactone micro-scaffolds fabrication and characterization

The same procedure and characterization methods were done for the preparation of PCL porous μ -scaffolds as reported in Chapter 2 (2.2.2 and 2.2.3). Briefly, PCL μ -scaffolds were fabricated by a fluidic oil/water emulsion and particles coagulation process and by using PEO as a biocompatible pore-generating material, by selecting PCL-PEO concentration in the 10 w/v% range and Q_{CP} of 13 mL/min. Therefore, μ -scaffolds morphology, pore architecture and diameter distribution were evaluated by SEM analysis, MicroCT technique and Image analysis.

3.2.3. Polydimethylsiloxane patterned moulds design and fabrication by soft lithography

PDMS moulds were fabricated through micromilling machine (Minitech Mini-Mill/GX, Minitech Machinery Corporation, USA) and soft-lithography. First, ordered and disordered patterns were designed by Draftsight (version 2018 SP1, Dassault Systems, France) and converted into machine G-codes by Deskam 2000 (version 5.1.5.11, Carlen Co. Ltd., USA) software. The as generated file was then used to prepare polymethylmethacrylate (PMMA, 4 mm ME303020, Goodfellow Cambridge Limited, England) master by micromilling machine. Thus, PMMA master moulds were replicated in PDMS. To this propose, PDMS 10:1 (precursor: curing agent ratio) mixture (Sylgard 184, Dow Corning, USA) was prepared and degassed for at least 20 minutes into a vacuum chamber to remove trapped air bubbles. Then, a certain volume of this mixture was poured onto the PMMA master and, subsequently, air bubbles were removed by vacuum-degassing cycles. PDMS mixture was added to completely fill the replica system hole and flattened by small glass slide (1 mm thickness) (10143562, Thermo Fisher Scientific, USA). This system was heated in an oven (VC 20, Salvis Lab, Switzerland) at 80°C for 2 hours to thermally cross-link PDMS. Consequently, ordered and disordered moulds were disassembled after 24 hours at RT. The 3D reconstructions of the as obtained PDMS moulds are shown in (Figure 3.1).

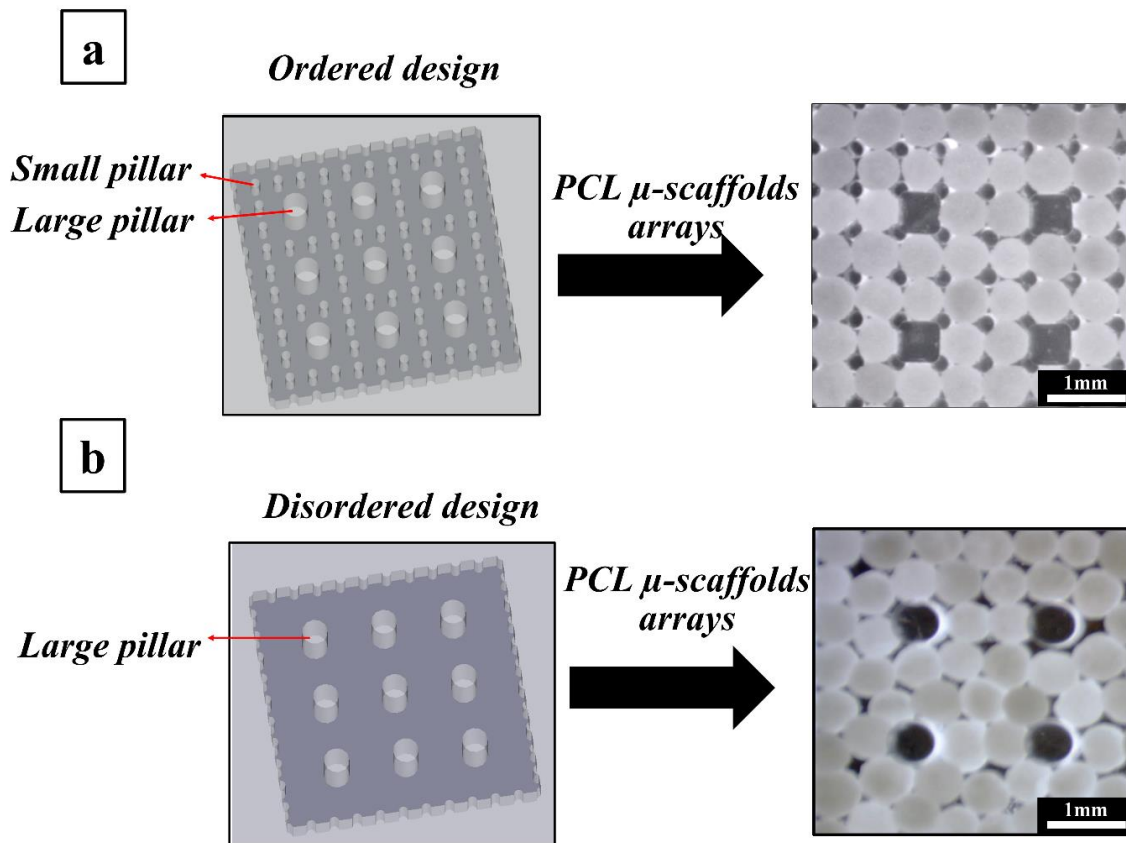


Figure 3.1: ordered and disordered assembly design and assembly. (a) ordered pattern and assembly of PCL μ -scaffolds by using predefined ordered assembly. (b) disordered design and assembly of PCL μ -scaffolds on disordered pattern.

The ordered pattern was provided of two types of pillars. Smaller pillars, with diameter of 200 μm , were used to control μ -scaffolds positioning as their size fit the hole created by four 450 μm adjacent spheres centred in the square configuration. Larger pillars, with diameter of 500 μm , were placed into nine controlled positions to create additional porosity without affecting μ -scaffolds alignment. The disordered pattern different from the ordered one for the absence of the smaller pillars. As shown in (Figure 3.1), the two moulds allowed the achievement of two PCL porous μ -scaffolds arrays named, for convenience ordered and disordered. In the ordered monolayers, μ -scaffolds were placed and maintained in the pre-defined positions by presence of the pillars that acted as physical confinement structures as well as by the careful manipulation of materials and fluids during *in vitro* experiments. The correct positioning of the μ -scaffolds was also assayed by visual inspection with a stereomicroscope. Regarding the possible effect of PDMS pillars on tissue grow and vascularization in the space between μ -scaffolds, we expect that the cylindrical shape of

the pillars together with the shape of μ -scaffolds may ensure sufficient space for correct tissue development between and/ or around of the PCL μ -scaffolds.

3.2.4. Fibroblast and endothelial cell culture and expansion

Biological model was built up by using of HDFs to produce collagen matrix and with co-culture of HUVECs to produce a vascular network into the hybrid constructs. HDFs expansion and culture were carried out following the same protocols detailed in Chapter 2 (2.2.5).

HUVECs (GIBCO C0035C) were grown in 150 cm² polystyrene tissue culture flasks (Corning Inc., Corning, NY) after coating with 1% w/v gelatin type A (Porcine Skin (G-2500 sigma)) for 20 minutes at 37 °C and 5% CO₂. VasculLife VEGF medium and Complete Kit (CELLSYSTEM LL-0003) was used for the culture of the cells until passage 4. The medium was changed every two days until reaching 90 % confluence. Cells were washed three times with Dulbecco's Phosphate Buffered Saline (PBS, Sigma Aldrich, Milano, Italy), and incubated with trypsin-ethylenediaminetetraacetic acid (EDTA) (0.25% trypsin, 1 mM EDTA; Microtech, Naples, Italy) for 5 minutes at 37°C to detach the cells [11].

3.2.5. Vascularized hybrid mono-layer constructs fabrication by micro-scaffolds patterning onto polydimethylsiloxane moulds and co-culture of fibroblasts and endothelial cells

μ -scaffolds were sterilized in absolute ethanol for 12 hours at RT and washed three times with sterile PBS for 20 minutes. Thus, μ -scaffolds were assembled into ordered and disordered PDMS autoclaved moulds. Specifically, μ -scaffolds were precisely placed onto the ordered mould by using of stereomicroscope (Olympus SZX16) (Figure 3.1a) in the sterile condition. μ -scaffolds were also assembled on the disordered mould (Figure 3.1b). Then, layers with μ -scaffolds were washed three times with the pen/strep (1% v/v) solution and subsequently exposed to UV light for 1 hour. Therefore, pen/strep (1% v/v) solution was removed, and the layers were covered with enriched MEM medium for 48 hours at 5 % CO₂ and 37°C. For cell seeding, the layers were moved to the 6 multiwell and loaded with 22×10^3 fibroblasts cells, suspended in 200 μ L of enriched MEM. Cell adhesion occurred after 2 hours and enriched MEM was added up to 1ml. Culture medium was changed at day 1 after seeding and then every other day. From the 3th day of culture, the culture medium was supplemented with Ascorbic Acid (2-O-a DGlucopyranosyl-L-Ascorbic-Acid TCI; Cf: 0.5 mM) to stimulate collagen biosynthesis by HDFs.

10 days after HDFs seeding, HUVECs were added for the co-culture. By this way, we expect that HDFs grow and biosynthesis resulted in a collagenous matrix almost uniformly distributed onto the samples that can act as a supporting natural substrate for HUVECs adhesion, proliferation and colonization. To this end, samples were moved into a new 6 multiwell and dried under biological hood. Each layer was loaded with 22×10^3 HUVECs, suspended in 200 μ L of Vasculife, and placed into the incubator at 5 % CO₂ and 37°C. After 2 hours, samples were covered with Vasculife up to 1ml of final volume. The day after the seeding the medium was replaced with a with co-culture medium containing enriched MEM and Vasculife in 2:1 ratio and changed every 24 hours for 10 days.

3.2.6. Analysis of monolayer morphology and growth by MicroCT and histology

Protocol used for the characterization of MicroCt and histology were the same described in Chapter 2 (2.2.7), with minor differences. Please refer to this part for experimental details.

3.2.7. Characterization of cells growth and tissue vascularization by confocal and multiphoton analyses

Ordered and disordered hybrid monolayer were fixed in 4% Paraformaldehyde (P61148-500 g Sigma Aldrich) for 30 minutes at RT and washed in PBS. They were then permeabilized using 0,1% Triton (Triton® X-100 T9284- 100 ML Sigma) in PBS for 5 minutes at RT, washed in PBS and blocked in 3% BSA and 3% FBS blocking buffer in PBS for 1 hour at RT. Afterwards, samples were stained with Rhodamine Ulex Europaeus Agglutinin I (UEAI Vector Laboratories RL-1062) at a final concentration of 20 μ g/ml in blocking solution, overnight at 4 °C in the dark, in order to mark the human endothelium. The morning after, samples were washed with PBS1X and the actin cytoskeleton of all the cells was stained with Phalloidin-488 (Invitrogen, 1:200 diluted in blocking buffer) for 40 minutes at RT. Samples were washed with PBS three times and the nuclei were stained with HOECHST (Sigma Aldrich, 1:1000 diluted in PBS) for 20 minutes at RT. The samples were finally washed three times with PBS and characterized by CLSM (Carl Zeiss, Germany) using 10x objective to assess HDFs and HUVECs morphology and distribution. Multiphoton microscope was used to assay collagen biosynthesis over time. Samples were analysed by two-photon excited fluorescence (Leica TCS SP5 II coupled with a Multiphoton Microscope stage Chamaleon Compact OPO-Vis, Coherent) to induce second harmonic generation and obtain high-resolution images of unstained collagen structures. Samples were observed by using $\lambda_{ex} = 840$ nm

(two photons) and $\lambda_{em} = 415-425$ nm and a 25x water immersion objective (HCX IRAPO L 25.0, 0.95 Water, n.a. 0.95). Besides, Image analysis was used to quantify the density of collagen matrix in the hybrid mono-layers regions. The Collagen density was defined as the percentage of the ratio between bright pixels to total pixels in the selected regions.

Volume fraction of blood vessels was calculated in as percentage of the ratio between the thresholded red volume of the endothelium marked by Rhodamine-UEAI and the total volume of the sample acquired for each stack. The volume values were obtained applying the ImageJ plugin Measure Stack to the red thresholded channel and to the total volume of tissue acquired [11].

$$\text{Blood vessel volume fraction} = \frac{\text{acquired blood vessel volume}}{\text{acquired sample volume}} \times 100$$

3.2.8. Collagen biosynthesis evaluation by second harmonic generation test

The orientations of collagen biosynthesis were measured by using the plugin OrientationJ of ImageJ. The local orientation and isotropic properties (coherency and energy) of every pixel of the image evaluated by the plugin. The following parameters defined: Gaussian window r 1 pixel, Min Coherency 20%, Min Energy 2%. The plugin also outputs a distribution of the collagen alignment directions and blood vessels. These distributions were normalized to attain a normal distribution and compare collagen alignment in different point of the hybrid monolayers [11].

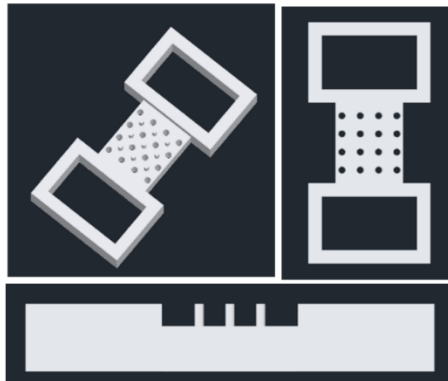
3.2.9. Fabrication of vascularized hybrid bilayer constructs by monolayers assembly and bonding into de-novo designed culturing chamber

After 10 days of co-culture, two hybrid ordered monolayers were removed from PDMS moulds and hybrid bilayer constructs were fabricated by using the bonding chamber. In the first stage, bonding chamber is made by two parts: PDMS-based and polytetrafluoroethylene (PTFE)-locks. PDMS-based with external cornering and two large pillars were designed for layers alignment and fabricated following the process of (3.2.3) (Figure 8a-c). PTFE-locks were designed and fabricated by μ -milling machine of PTFE to guarantee large pores preservation during the assembly of the contacting layers and consequently maintain open porosity in the bilayer constructs (Figure 3.2). PTFE is a good choose to fabricate the top portion of device has it is stiff enough to fabricate pillars with length/diameter higher than 2 and to limit possible cells and ECM adhesion.

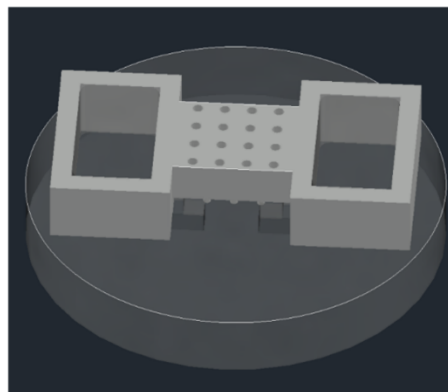
Monolayers were then assembled into the PDMS support mould with precisely controlling the assembly of each monolayer with PTFE-locks for layer contacting and preserve open porosity (Figure 3.3). Thus, Hybrid bilayers were removed from assembly system and some of these samples were fixed after 5 days bonding and others were leave 7 days more to investigate the evolution of the endothelial network and hybrid construct structure (Figure 3.3).



***PDMS support for
layers alignment***



***PTFE top for
layers contacting
and large pores
preservation***



Closed device

Figure 3.2. PDMS and PTFE moulds for fabrication of bilayers. PDMS-based for controlling the assembly of monolayers and layers contacting to form hybrid bilayer construct. PTFE-locks for closing the system and maintain the open porosity for fabrication of the hybrid bilayer.

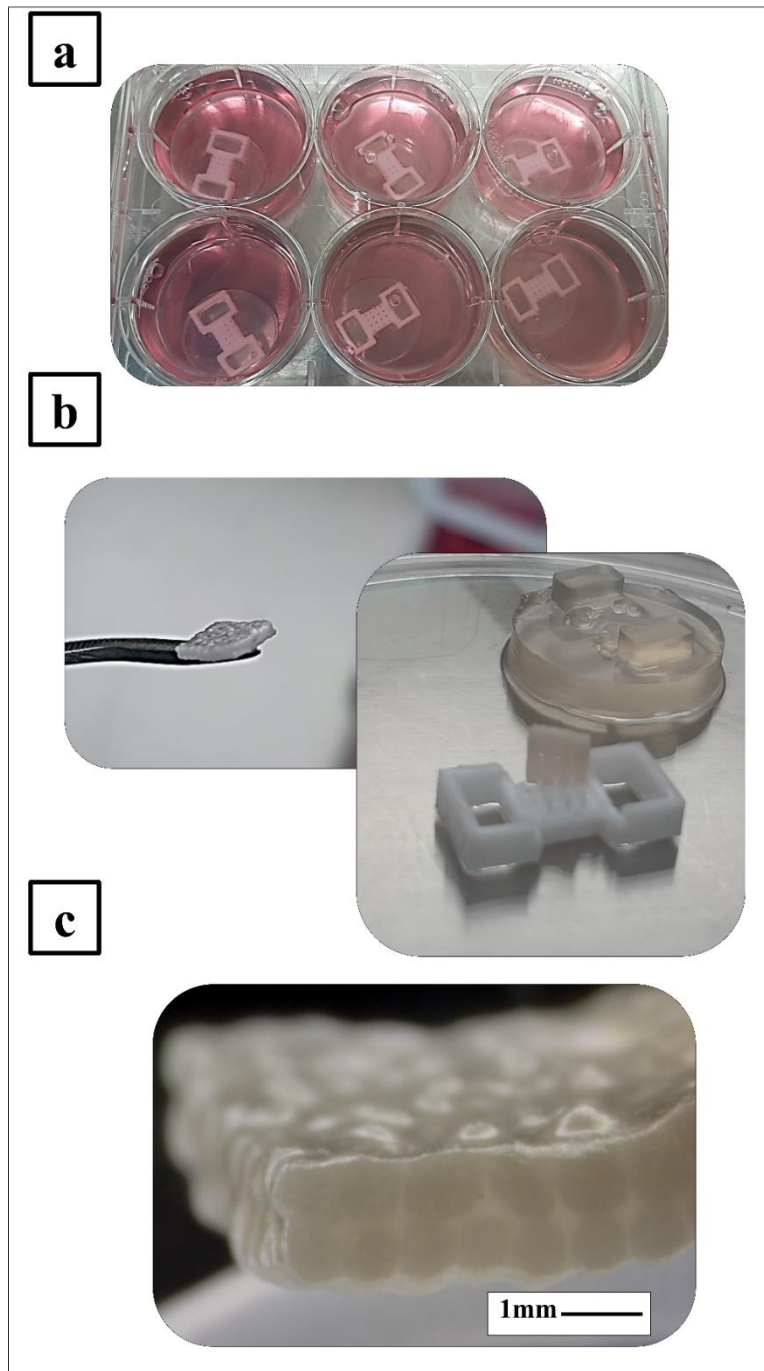


Figure3.3: Fabrication of hybrid bilayers. (a), hybrid bilayer with closed system and supported PDMS modules during the culturing time. (b), hybrid bilayer after removing from fabrication devices. (c), lateral side of hybrid bilayer.

3.2.10. *Analysis of bilayer constructs morphology and growth by MicroCT and histology*

Protocol used for the characterization of MicroCt and histology were the same described in Chapter 2 (2.2.7), with minor differences. Please refer to this part for experimental details.

3.2.11. *Characterization of cells growth, and tissue vascularization by confocal and multiphoton analyses*

Hybrid bilayers were fixed in 4% Paraformaldehyde (P61148-500 g Sigma Aldrich) for 30 minutes at RT and washed in PBS. They were then permeabilized using 0,1% Triton (Triton® X-100 T9284- 100 ML Sigma) in PBS for 5 minutes at RT, washed in PBS and blocked in 3% BSA and 3%FBS blocking buffer in PBS1X for 1 hour at RT. Afterwards, samples were stained with Rhodamine Ulex Europaeus Agglutinin I (UEAI Vector Laboratories RL-1062) at a final concentration of 20 µg/ml in blocking solution, overnight at 4 °C in the dark, in order to mark the human endothelium. The morning after, samples were washed with PBS1X and the actin cytoskeleton of all the cells was stained with Phalloidin-488 (Invitrogen, 1:200 diluted in blocking buffer) for 40 minutes at RT. Samples were washed with PBS three times and the nuclei were stained with HOECHST (Sigma Aldrich, 1:1000 diluted in PBS) for 20 minutes at RT. The samples were finally washed three times with PBS and characterized by CLSM (Leica TCS SP5 II, Wetzlar, Germany) using 4x and 10x objectives to assess HDFs and HUVECs morphology and distribution. Multi-photon microscope was used to assay collagen biosynthesis over time. Samples were analysed by two-photon excited fluorescence (Leica TCS SP5 II coupled with a Multiphoton Microscope stage Chamaleon Compact OPO-Vis, Coherent) to induce second harmonic generation and obtain high-resolution images of unstained collagen structures. Samples were observed by using $\lambda_{ex} = 840$ nm (two photons) and $\lambda_{em} = 415-425$ nm and a 25x water immersion objective (HCX IRAPO L 25.0, 0.95 Water, n.a. 0.95). Besides, Image analysis was used to quantify the collagen fraction in the inter-µ-scaffolds regions. The Collagen Fraction (v%) was defined as the percentage of the ratio between bright pixels to total pixels in the selected regions. The volume fraction of blood vessels for bilayers were calculated with the same method as reported for monolayers (3.2.7).

3.2.12. *Collagen biosynthesis evaluation by second harmonic generation test*

The collagen biosynthesis of the bilayers was evaluated following the same procedures used for the monolayers. Please refer to the (3.2.8) part for technical details.

3.2.13. *Statistical analysis of data*

The statistical significance of the results was assessed by one-way analysis of variance (ANOVA) and Tukey post-hoc test at the significance level $p < 0.05$.

3.3. Results and discussion

- *Monolayers*

3.3.1. *Micro-scaffolds morphology and pore structure features*

In the first part of this chapter, PCL porous μ -scaffolds with the diameter of 450 μm were fabricated by optimizing the fluidic emulsion conditions, namely 10% PCL-PEO solution, Q_{DP} and Q_{CP} set to 90 $\mu\text{l}/\text{min}$ and 13 mL/min (Chapter 2). Figure 3.4 shows the morphology of the surface and cross-section of the μ -scaffolds as assessed by SEM analysis, together with 3D reconstruction of the μ -scaffolds structure and the inner pore size and trabecular size distributions obtained by Micro-Ct analysis. As shown in (Figures 3.4a and 3.4b), obtained μ -scaffolds SEM have spherical shape and full pores opening (Figure 3.4c, high magnification). Besides, the cross-section image of (Figure 3.4d) evidenced that PCL μ -scaffolds were characterized by highly interconnected trabecular architectures, similar to the results reported in the previous chapter (Chapter 2). MicroCt analysis confirmed the SEM results (Figures 3.4e and 3.4f) and also show that the mean pore size and pore wall thickness were $45 \pm 20 \mu\text{m}$ and $19.3 \pm 5.4 \mu\text{m}$, respectively (Figures 3.4g, h). Based on the previous results, we expect that these samples are suitable to promote and guide cell adhesion, colonization, and ECM biosynthesis towards functional hybrid tissue development.

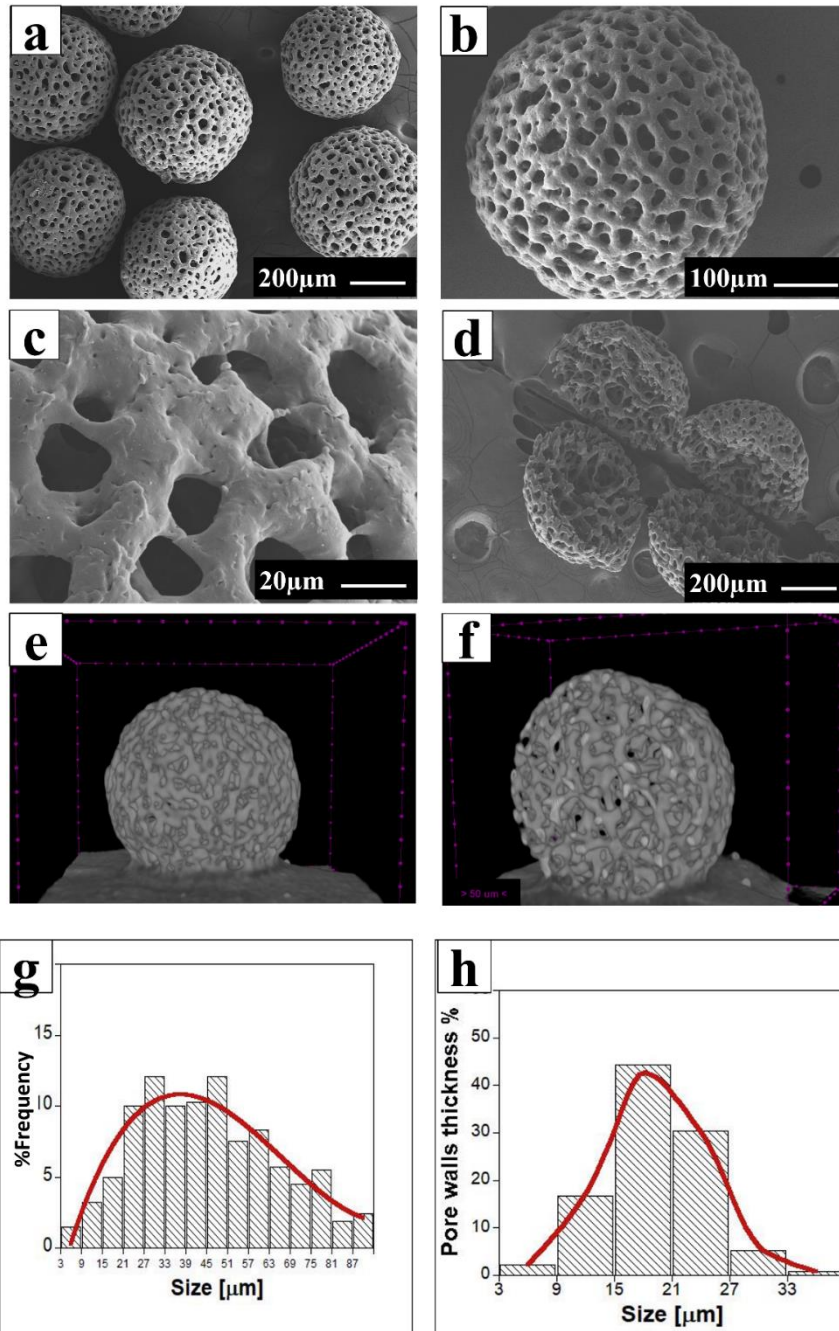


Figure 3.4: SEM of the surface of PCL/PEO 40/60 (% v/v) sample (after the dissolution of the PEO phase, the presence of small droplets of PEO, which are entrapped inside the PCL phase. Magnifications (scale bar: 20 μm) (A), SEM image of PCL/PEO porous micro-beads after ultrasound exposure showing a porous structure with enhanced porosity, magnifications (scale bar: 100 μm) (B), high magnification SEM images of the cross section of PCL μ -scaffolds (C). MicroCT reconstruction and pore size distribution of PCL μ -scaffolds (D).

3.3.2. Monolayer constructs morphology, composition and vascularization

In this chapter we fabricated hybrid monolayers by assembly of μ -scaffolds into ordered and disordered PDMS moulds and by seeding HDFs and HUVECs on the top of monolayer arrays. The evolution of tissue formation into the ordered and disordered hybrid monolayers were monitored by MicroCt analysis. Figure 3.5 shows the MicroCt analysis of hybrid monolayers after 10 days of HDFs and HUVECs co-culture, with a representative 3D reconstruction and cross-section of ordered and disordered hybrid layers. 3D reconstruction of upper- and lower-part of the ordered monolayer are shown in Figures 3.5a, and b, respectively. Instead, Figures 3.5c, d show the upper- and lower-part of the disordered monolayer. In both conditions, cells were able to assemble and develop a unique and compact tissue. In spite of this, the tissue grew regularly according to the ordered design and around the porosity of structure compare to disordered layer (Figures 3.5b, d). More importantly, in the case of ordered array, the position of the μ -scaffolds describes highly aligned and straight pores. On the contrary the random configuration was characterized by high tortuosity and variable pore size, finally resulting in heterogeneous vascularization. Furthermore, the cross-section images of the ordered and disordered layers (Figure 3.5e, f), revealed the formation of strong bonding between μ -scaffolds into the tissue layer thanks to the presence of growing cells producing ECM. Most importantly, the comparison between two monolayers evidenced that the ordered array produced a uniform square sample (Figure 3.5a). Conversely, the disordered array resulted in a deformed and irregular shape. This effect is dependent to the presence of zones with wide μ -scaffolds spacing (Figures 3.1b) and due to the absence of small pillars.

Figure 3.6 shows the percentage of tissue growth (cells and matrix) of ordered and disordered monolayers evaluated by MicroCt analysis. These data demonstrated that the ordered monolayer was composed by a tissue percentage of $57\pm 0.5\%$ and the disordered monolayer of $54\pm 2.5\%$, without statistically relevant differences.

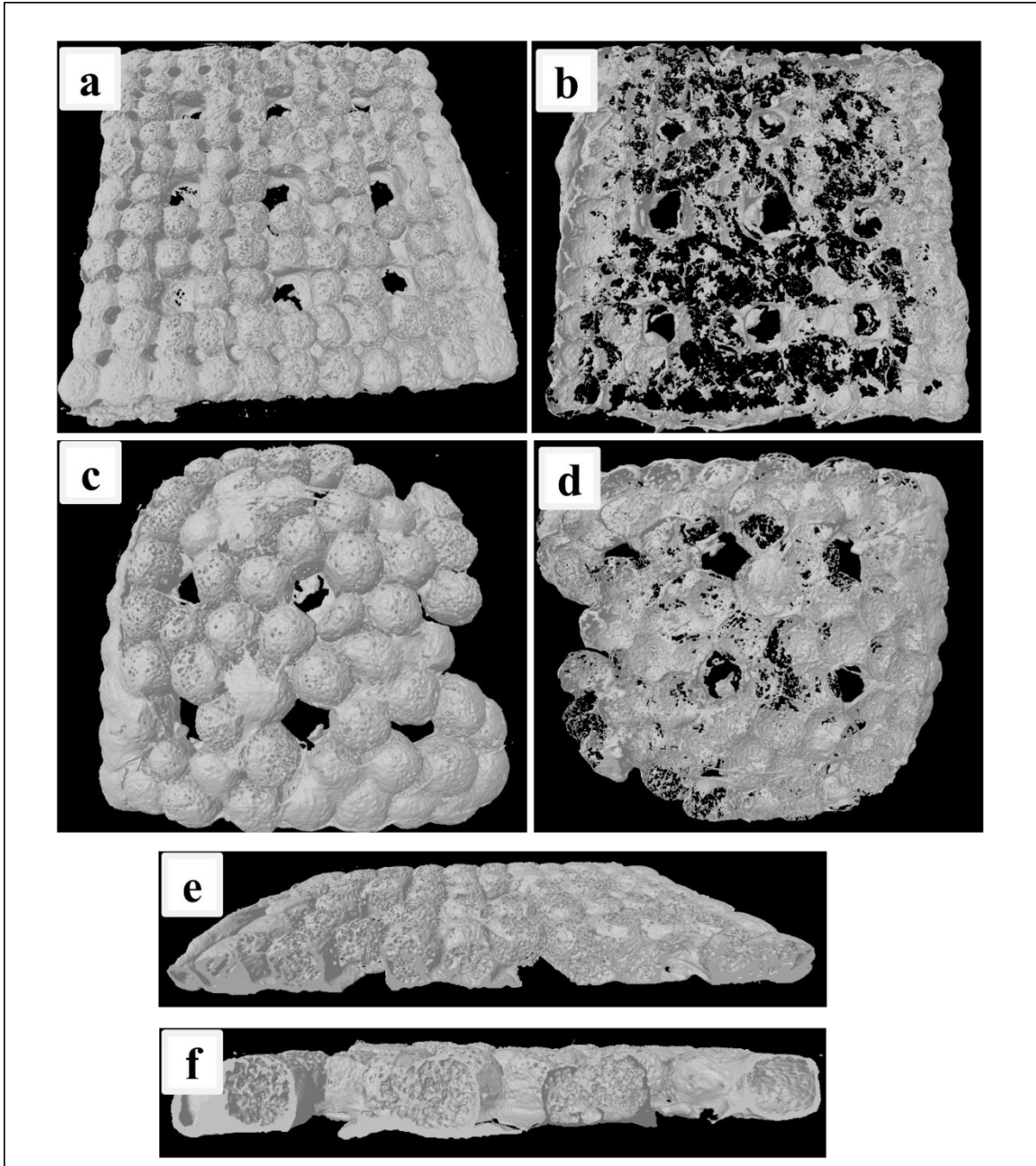


Figure 3.5: MicroCT analysis of new tissue of the hybrid monolayers. 3D reconstruction of the ordered sample: upper side (a), and lower side (b). 3D reconstruction of the disordered sample: upper side (c), and lower side (d). Cross-section of the hybrid monolayer: ordered (e) and disordered (f).

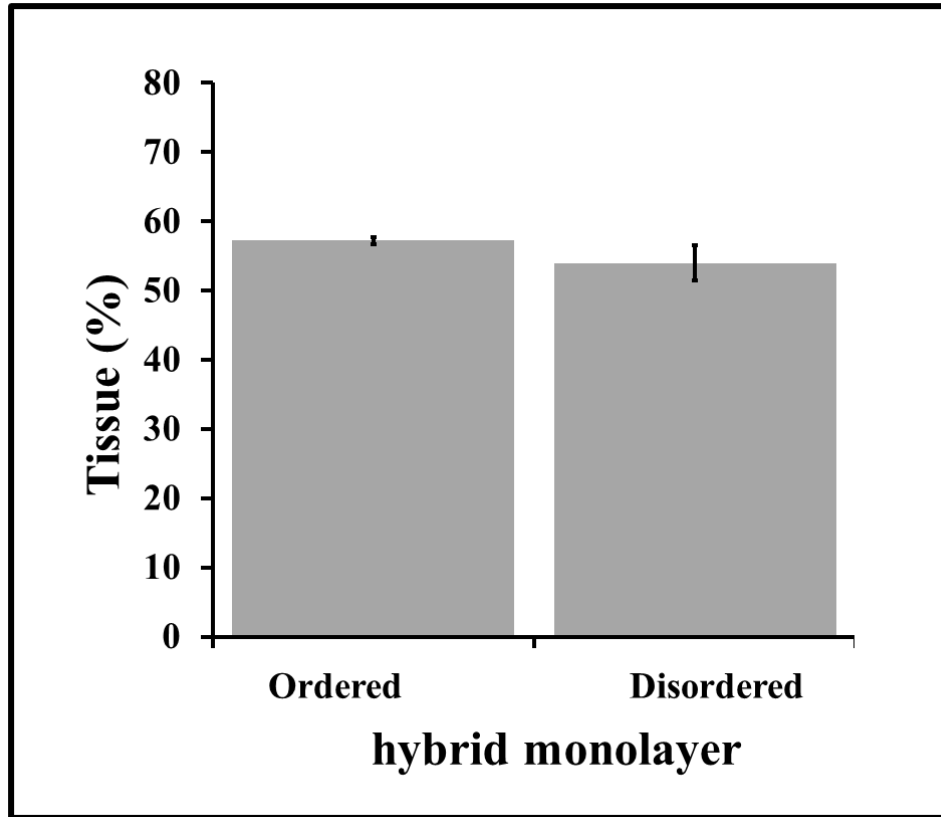


Figure3.6: MicroCT evaluation of new tissue v % of the ordered and disordered hybrid monolayers.

In agreement with previous results, cell colonization into the hybrid monolayers was assessed by histology analysis. Figure 3.7 shows the histology analysis of hybrid monolayers. Cells adhered to the μ -scaffolds surface and porosity, proliferated, and colonized the inner part of μ -scaffolds to form hybrid layers. These results clearly demonstrated the presence of cells and matrix into and around the μ -scaffolds in the ordered (Figures 3.7a, b), and disordered (Figures 3.7c) monolayers, used to guide cell-seeded modules assembly and hybrid tissue formation. However, the more regular spacing among the μ -scaffolds in the ordered array may allow the formation of a more uniform cells and tissue in the sample.

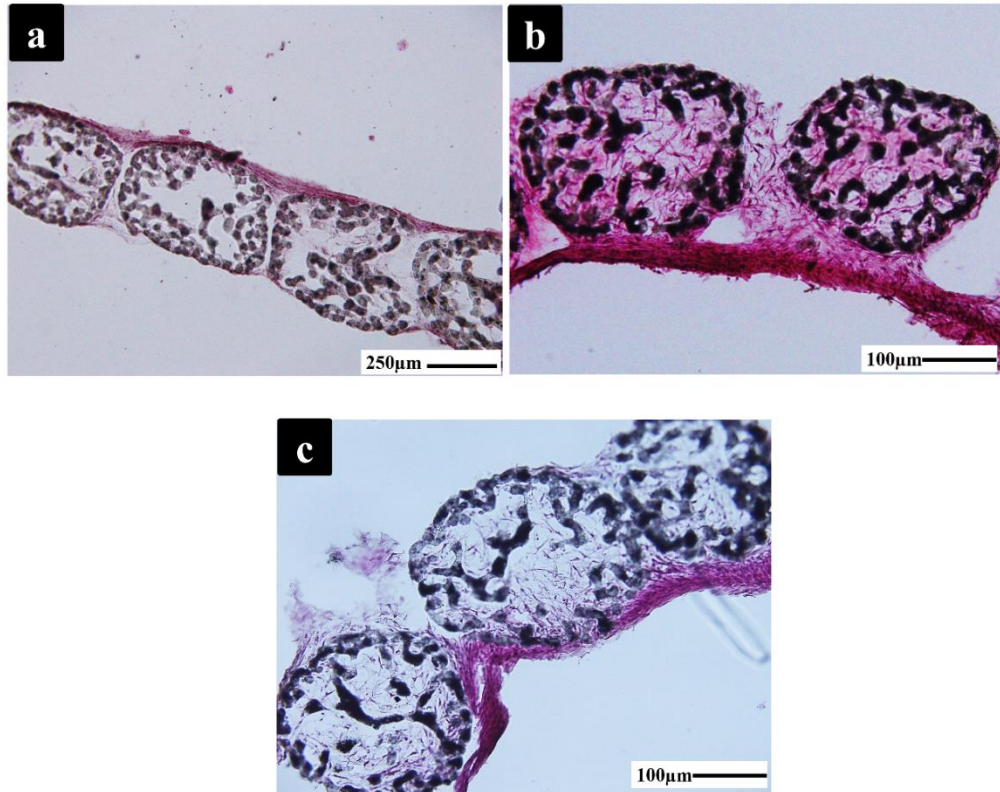


Figure 3.7: H&E staining of the cross-sections of hybrid monolayers. (a, b), ordered. (c), disordered.

The evolution of the cell distribution and endothelial network onto the hybrid monolayers were monitored by confocal imaging (Figures 3.8 and 3.9). In these figures, cytoskeleton, blood vessels and nuclei were highlighted by green, red, and blue colours respectively. These results revealed that HUVECs were able to form capillary like structures onto the monolayers. As shown in (Figures 3.8 a-d), lower side and upper side (Figure 3.8e-h) of ordered monolayers, cells distributed homogeneously onto the ordered design. More importantly, blood vessels were almost confined around the large pillars and between μ -scaffolds (Figure 3.8b). These results demonstrated that blood vessels grew more on the upper side than the lower side. However, the organization of blood vessels was more regular on the lower side comparing to upper side.

As shown in (Figures 3.9 a-d), onto the lower side of disordered monolayer, cells distributed heterogeneously and consequently, blood vessels formed randomly according to the design. Similarly, blood vessels observed in the lower side of the disordered layer were less organized than the upper.

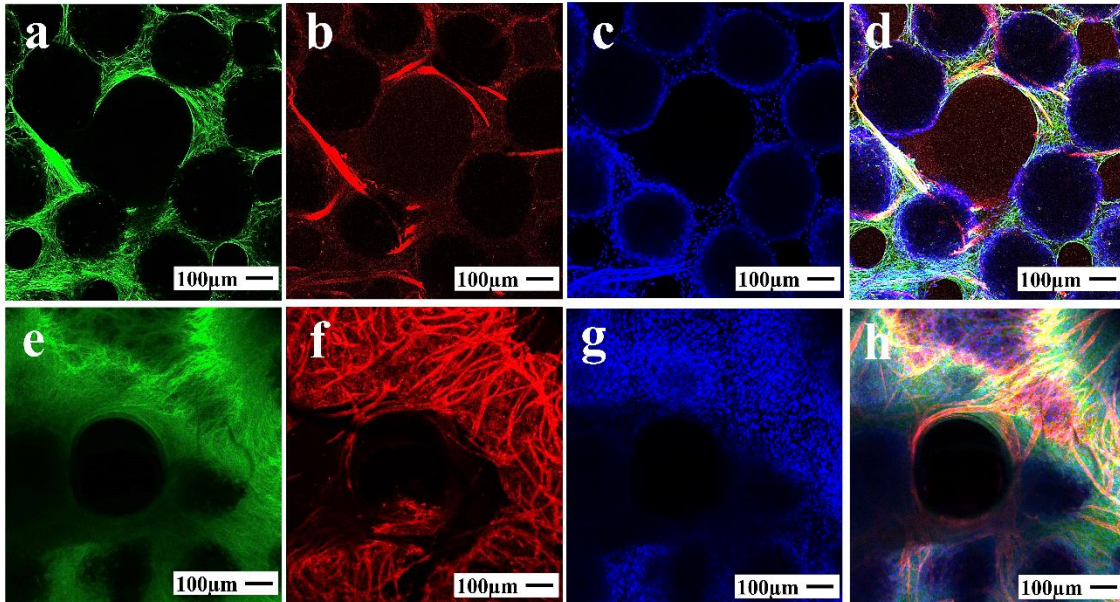


Figure3.8: CLSM images showing the morphology and colonization of HDFs and HUVECs into the ordered monolayers. (a-d), lower side. (e-h), upper side. The actin cytoskeleton is marked in green (Phalloidin-488), Nuclei are marked in blue (HOECHST), and blood vessels in red (UEAI).

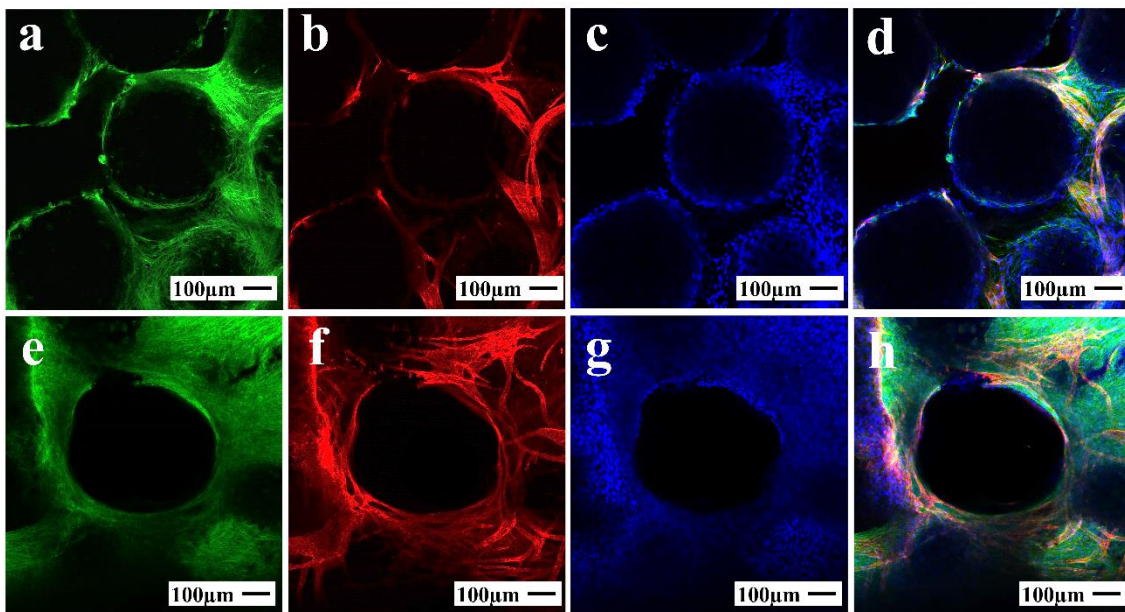


Figure3.9: CLSM images showing the morphology and colonization of HDFs and HUVECs into the disordered monolayers. (a-d), lower side. (e-h), upper side. The actin cytoskeleton is marked in green (Phalloidin-488), Nuclei are marked in blue (HOECHST), and blood vessels in red (UEAI).

Moreover, the volume fraction of blood vessels of the monolayers was evaluated (Figure 3.10). Specifically, these data were obtained by means of quantitative z-stacks analysis and the results indicated the blood vessels on the upper side were more than lower side on the both monolayers. Most probably, this result was related to the side of cell seeding and therefore, can be overcome by performing cell seeding before μ -scaffolds arrangement in the layers. Besides, the lower side of monolayers were contacting to the PDMS moulds and the diffusion of nutrients and oxygen were less than upper side of monolayers. Therefore, cells distribution and blood vessels formation were less than upper side. Indeed, cells mainly formed capillary-like structures on the side of cell seeding and then sprouted into the layer coming up to the opposite side of the sample. Furthermore, we observed that the upper side of ordered layer was significantly more vascularized than the disordered monolayer. Considering that monolayers thickness was about 500 μm and CLSM depth analysis was about 200 μm , the measure values of (Figure 3.10), referred to about half of the samples thickness.

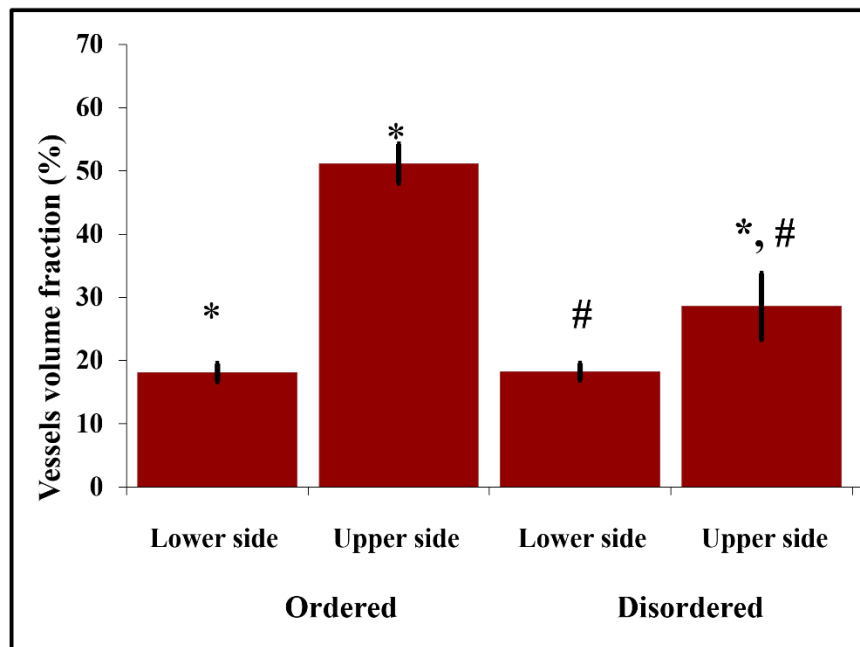


Figure 3.10: Image analysis of vessels volume fraction (%) on the monolayers.

To better visualize blood vessels, we took advantage of 3D sample view obtained by confocal analysis. The images in (Figure 3.11) show pieces of the forming of 3D blood vessel network into the monolayers. Results demonstrated that the upper side of both the ordered and disordered monolayers was fully vascularized (Figures 3.11a, c). However, the distribution of blood vessels

into the disordered layer was less homogenous than the ordered monolayer. In agreement with CLSM analysis, these results confirmed that in the lower side of the ordered design the blood vessels were homogeneously distributed in the space between μ -scaffolds and around the pillars (Figure 3.11b). However, no regular blood vessels patterning was observed in the case of the lower side of disordered monolayer (Figure 3.11d).

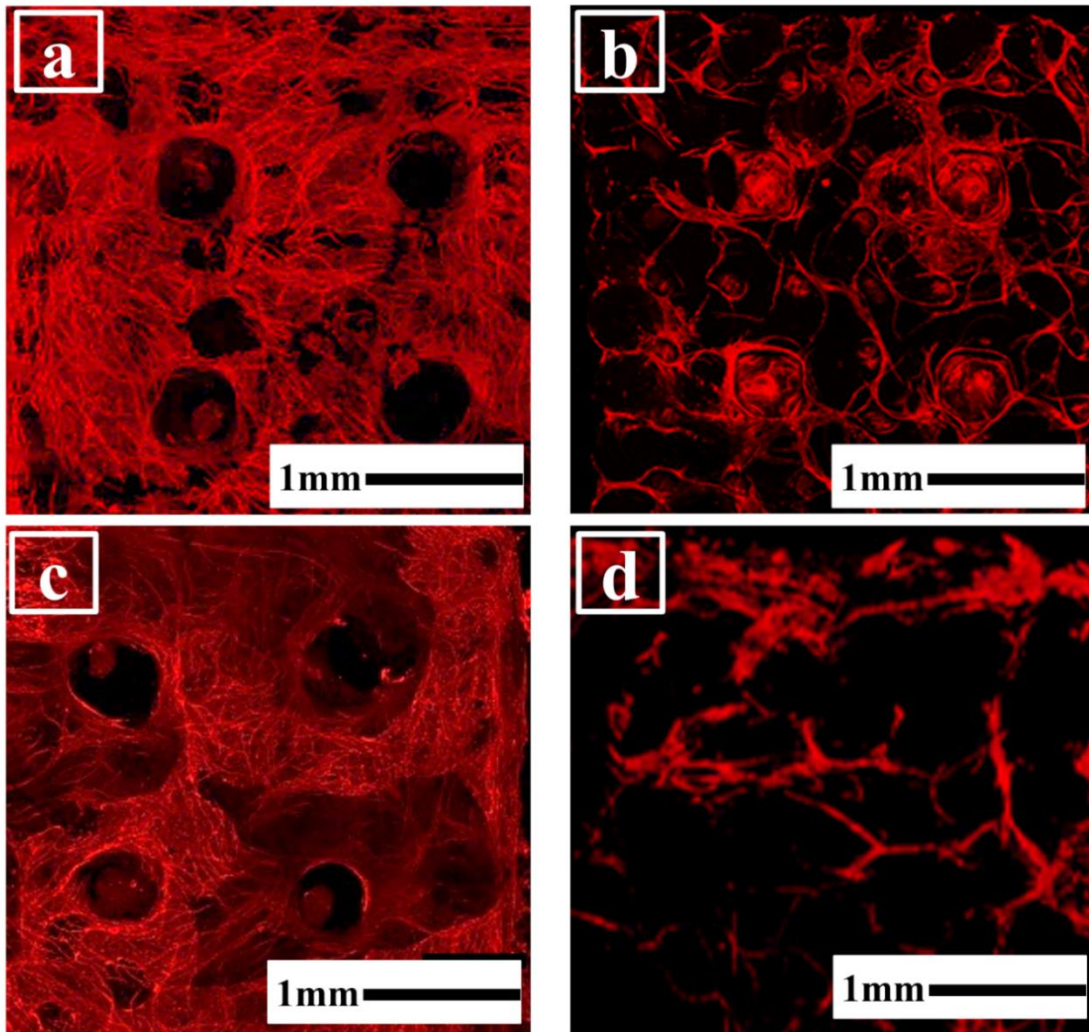


Figure 3.11: Confocal analysis show the pieces of 3D views of blood vessels formation on monolayers. (a, b), upper and lower side of the ordered layer, respectively. (c, d), upper and lower side of disordered layer, respectively. HUVECs are marked in red by Rho-UEAI.

Cell distribution and blood vessels formation in the inner part of monolayers were obtained by fluorescence analysis of the monolayer sections (Figure 3.12). These results revealed that blood vessels were able to grow into both ordered (Figure 3.12b) and disordered (Figure 3.12f)

monolayers. However, blood vessels better penetrated the inner part of the μ -scaffold onto the ordered than disordered monolayers. The blood vessel volume fraction was evaluated by ImageJ analysis (Figure 3.12i). These data confirmed that the volume fraction of blood vessels in the ordered monolayer section was higher (6.3 ± 1.2 %) than the disordered monolayer (5.3 ± 0.5 %), even if this difference was not statistically significant. Most probably, the absence of statistical difference may be related to the presence of abundant capillary structures in the external part of the scaffolds in both conditions.

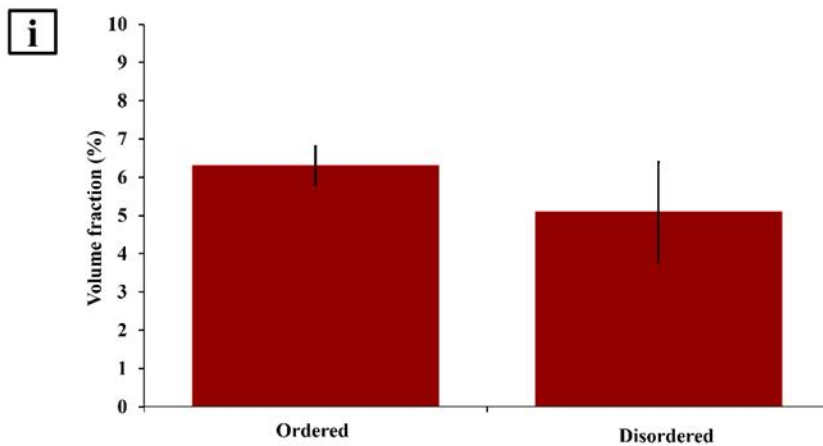
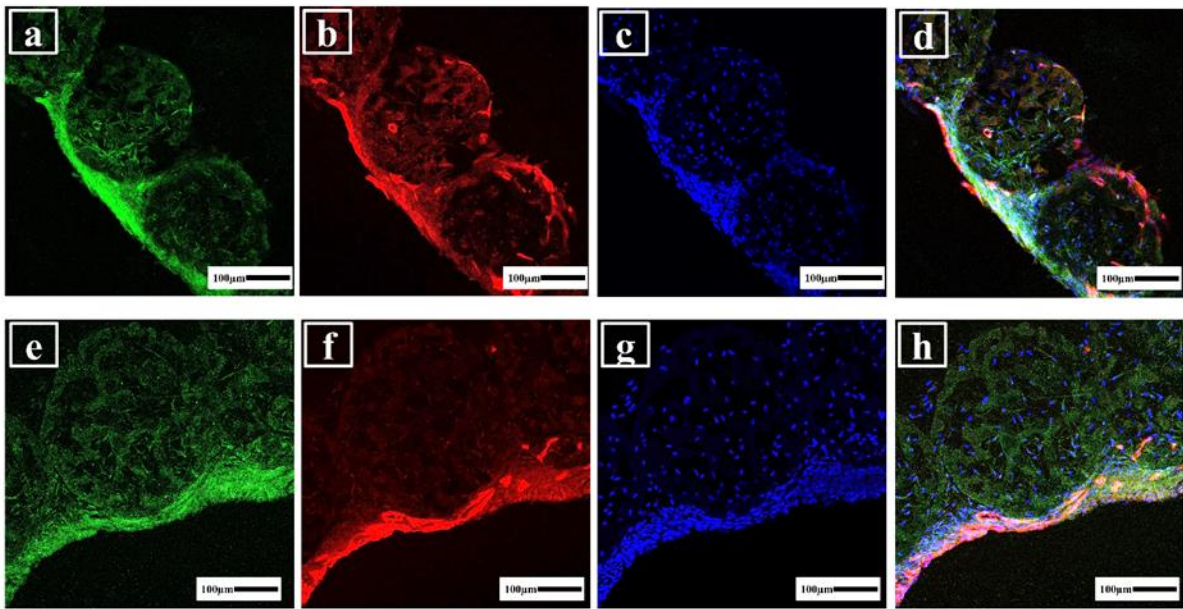


Figure3.12: Fluorescence analysis showing the blood vessels formation in the inner part of monolayers obtained by CLSM. (a-d), ordered monolayers (e-h), disordered monolayers (i), volume fraction of blood

vessels on monolayer sections. The actin cytoskeleton is marked in green (Phalloidin-488) (a, e), blood vessels in red (UEAI) (b, f) and nuclei are marked in blue (HOECHST) (c, g), merge (d, h).

3.3.3. Collagen amount and density of monolayer constructs

To correlate the role of ECM on blood vessels growth, we evaluated collagen and blood vessels organization in the monolayers (Figures 3.13 and 3.14) by SHG and confocal imaging. The images in (Figures 3.13a, b) of lower side and upper of the ordered monolayers, respectively showed that blood vessels were totally embedded into the ECM rich in collagen produced by HDFs (gray). More importantly, the graphs (red), showed that blood vessels have the same orientation of collagen (black), indicating the guidance role of collagen fibres on blood vessels growth, following the geometric design of the layer. As shown in (Figures 3.14a, b), similar results were found for disordered monolayers. Indeed, both the ordered and disordered design contained large pillars around which the cells developed an oriented tissue. Herein, fibroblasts organized themselves and produced the matrix around the large pillars that entirely crossed monolayers thickness. It is therefore evidenced that the circular section of the pillars acted as a physical guidance for cells and ECM orientation and therefore also the blood vessels grew following this pattern.

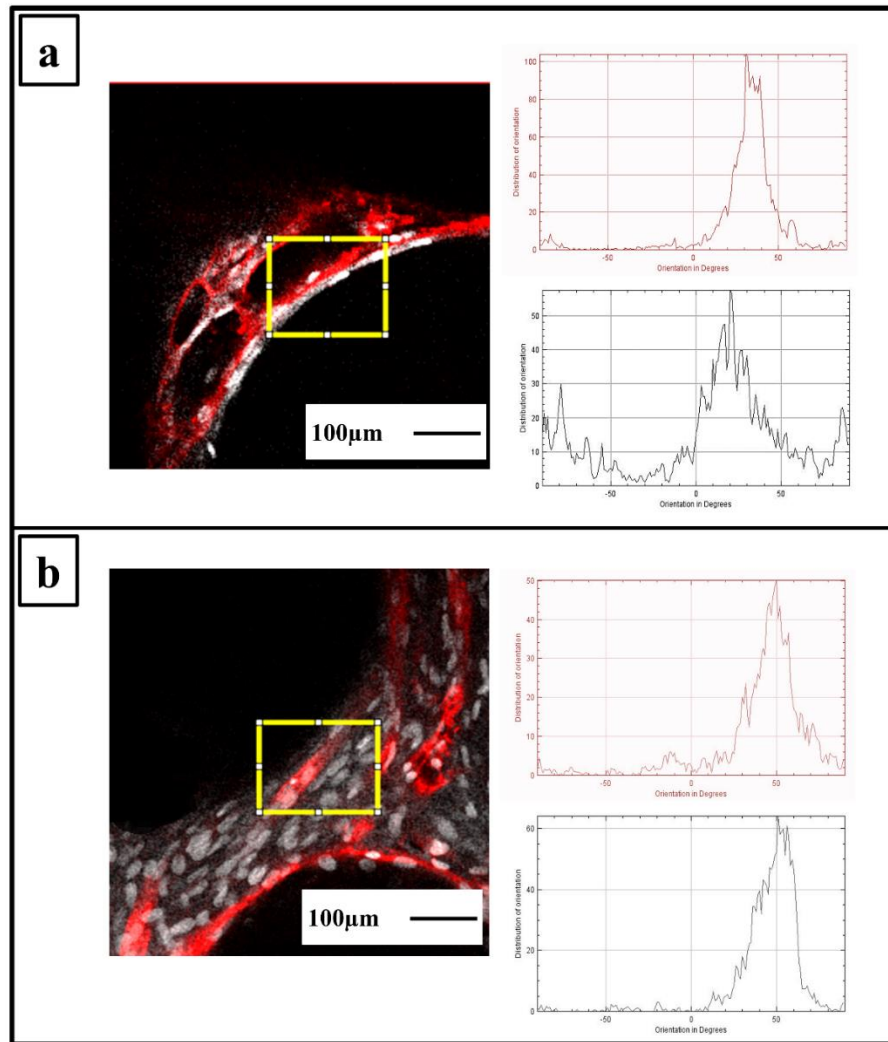


Figure 3.13: SHG signal of collagen in gray and blood vessels in red of the ordered monolayer. The graphics of the orientation of blood vessels (red) and ECM (black) were obtained by OrientationJ. (a), lower side. (b), upper side. (The dashed yellow rectangles indicate the analysed region, such as the pieces of big hole in the ordered monolayer).

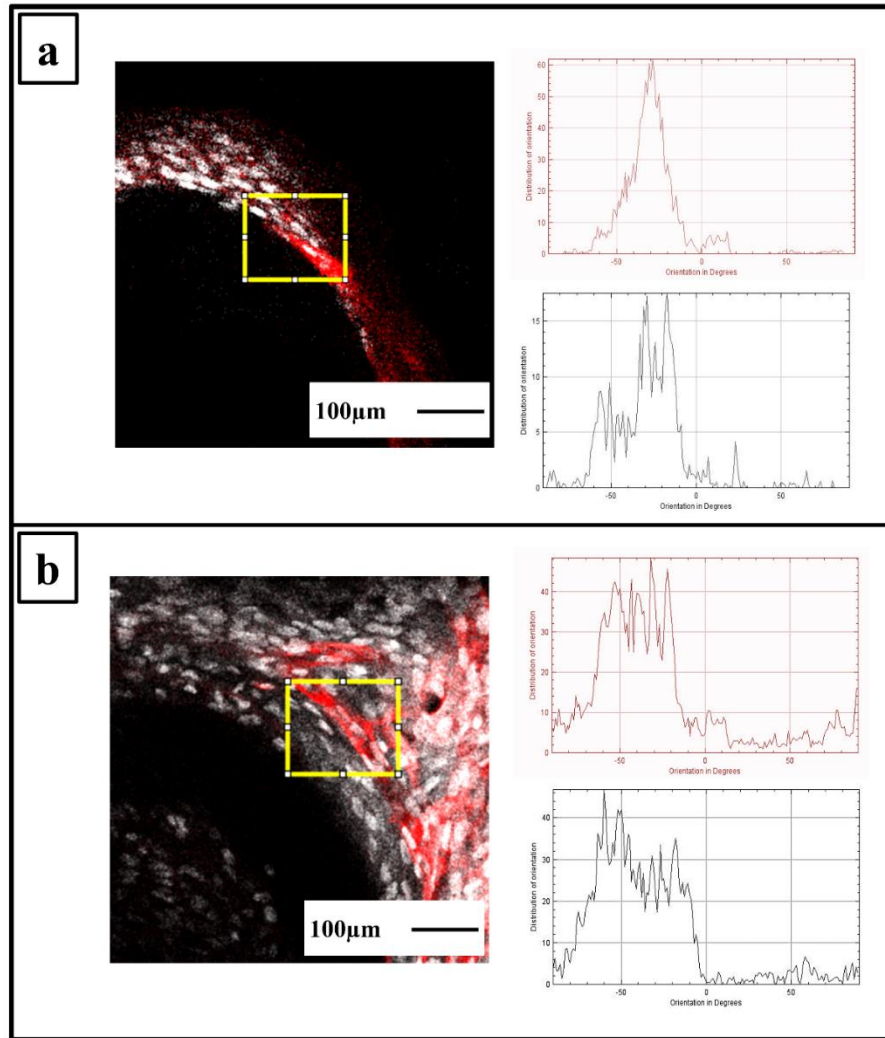


Figure 3.14: SHG signal of collagen in gray and blood vessels in red of the disordered monolayer. The graphics of the orientation of blood vessels (red) and ECM (black) were obtained by OrientationJ. (a), lower side. (b), upper side. (The dashed yellow rectangles indicate the analysed region, such as the pieces of big hole in the disordered monolayer).

Second harmonic generation analysis of the collagen fibres into the monolayers acquired by multiphoton microscopy evidenced that the percentage of collagen density deposited by HDFs (Figure 3.15). These data showed that the density of collagen matrix was almost the same in all the condition and side of the sample without statistically relevant differences.

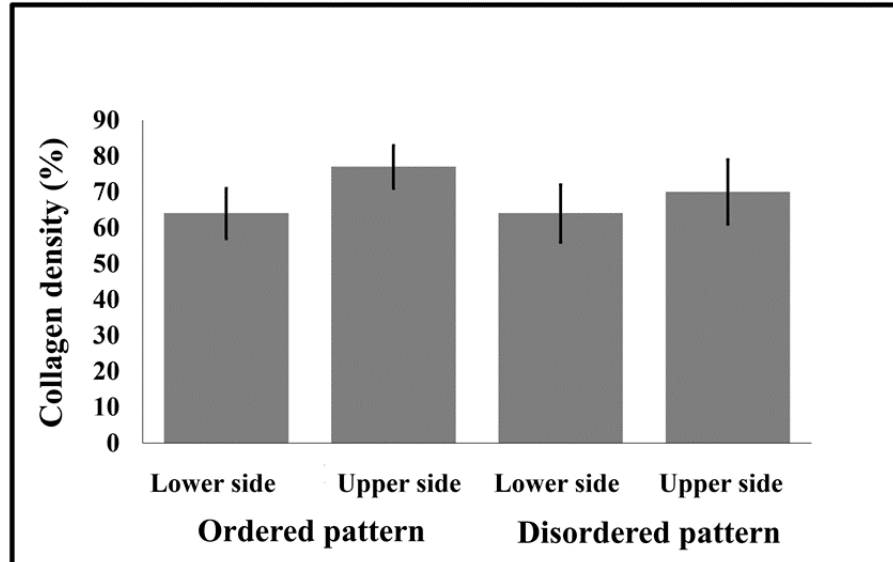


Figure3.15: Multiphoton microscopy evaluation of collagen density (%) into the monolayers.

3.3.4. Monolayers discussion

In the first part of this study, we developed a new strategy to evaluate ECM and vascularization inside the hybrid monolayer with ordered assembly of μ -scaffolds and compare to disordered monolayer. We utilize spatially arranged of the two micropillars to control the assembly of μ -scaffolds and fabrication of vasculature hybrid monolayers. Micropillars play two roles in the patterns: providing a specific position for each μ -scaffolds with controllable geometry and preventing the cells and matrix from shrinking (small pillars) and providing the additional porosity (large pillars). Pervious literature results showed that PCL scaffolds preprepared with nonporous microspheres following an ordered pattern improved blood vessel penetration and vasculature if compare to random scaffolds after *in vivo* implantation [27]. In our study, disordered monolayers, cells, and blood vessels were heterogeneously distributed onto the lower and upper side of the hybrid tissue. In contrast, ordered pattern provide a preformed, definite space between each μ -scaffolds that regulated cells and blood vessels growth homogenously onto the upper and lower sides of the samples. These results correspond with previous studies in which randomly distributed blood vessels into the disordered assembly of μ -scaffolds hybrid tissues [11-13], vs organization of blood vessels into the ordered design [28-31]. Following the previous literature work, ANOVA statistical tests showed no significant statistical difference between ordered and disordered hybrid tissue in the case of vascularization [27]. However, the ordered implants showed better internal

vascularization compare to the disordered ones and statistical significance [27]. This finding is in correspond to the response of our architectural of ordered and disordered arrays. In this study we used HUVECs since their ability to form blood vessels in co-culture with fibroblasts has been well documented in the literatures [32, 33], they have been used in co-culture in several in-vitro models. The optimal process of co-culture with HDFs and HUVECs allowed the production of strong bonding into 3D hybrid tissue is widely described in literatures [34, 35]. In this context, 20 days of co-culture could be sufficient for formation of bonding into hybrid tissues. In this optimal condition, HUVECs were sprouted and growth without observing any regression [11]. For both ordered and disordered arrays we found that tissue (cell, ECM and blood vessels) growth was enhanced on the upper side compared to the lower side. This effect is related to the fact that in the lower side the tissue growth in contact with PDMS, having less free space to grow and reduced nutrients and oxygen availability. However, the planar geometry of the samples with reduced thickness (500 μm approximately) resulted in the absence of any visible necrotic zone in the samples. Previous literature works highlighted the significant biochemical and biomechanical role of ECM components on blood vessels growth, development, and stability [36, 37]. In our samples μ -scaffolds spatial distribution and porosity guided the distribution and grow of cells collagen and vasculature. Furthermore, in agreement with previous studies, we found that the organization of collagen fibres controlled cellular alignment and blood vessels orientation [11, 20, 28-29].

- ***Bilayers***

3.3.5. Bilayer constructs morphology, composition, proliferation and vascularization

Hybrid bilayer were fabricated by assembling two ordered monolayers onto the PDMS mould closed by the PTFE-locks. These samples were then investigated in two different time points: 5 days and 7days of assembly. The evolution of tissue formation into the bilayers was monitored by MicroCt analysis. Figure 3.16 shows the MicroCt analysis of bilayer after 5 days bonding, with a representative 3D reconstruction, lateral side, and cross-section of bilayers. 3D reconstruction of upper- and lower-part of 5 days bonding is shown in Figures 3.16a, and b, respectively. These results demonstrated that cells were able to assemble and develop a unique and compact tissue to form bilayers. In addition, the lateral side and cross-section images of the bilayers (Figures 3.16c, d), revealed the formation of strong bonding between two monolayers into the tissue bilayers thanks to the presence of growing cells producing ECM. In addition, the linkage between two

monolayers shows that layers connected each other after 5 days of bonding (Figure 3.16d). However, the linkage of these two layers was not complete after 5 days of bonding and there was some open space between layers.

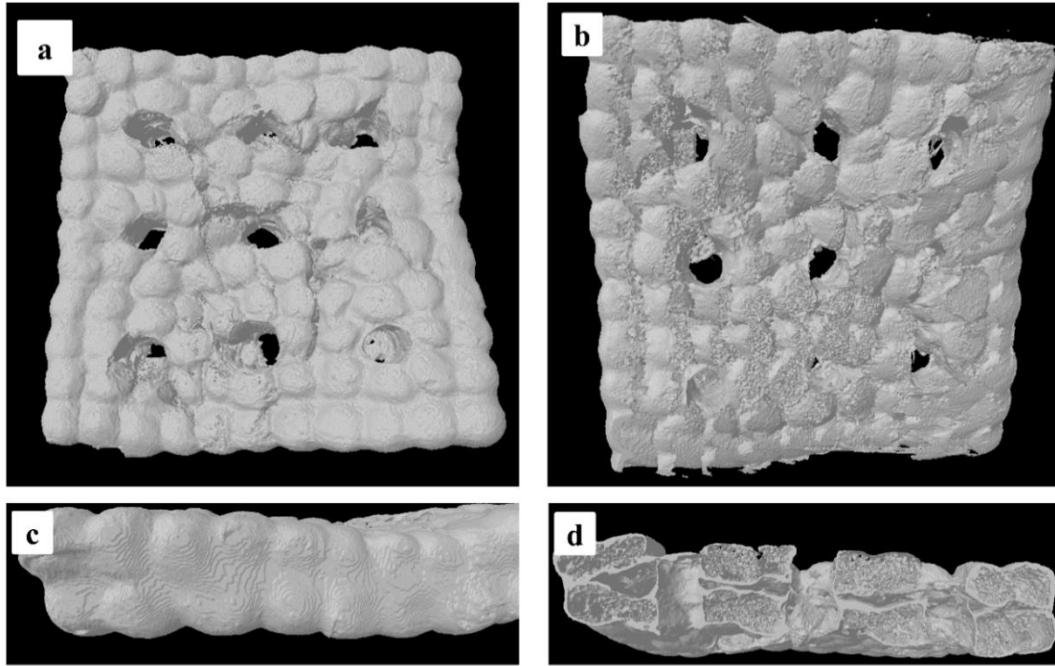


Figure 3.16: MicroCT analysis of the bilayer after 5 days bonding. 3D reconstruction of the bilayer: upper side (a), and lower side (b). lateral side (c). Cross-section (d).

Figure 3.17 shows the MicroCt analysis of bilayer after 7 days growth, with a representative 3D reconstruction, lateral side, and cross-section. 3D reconstruction of upper- and lower-part of 7 days growth are shown in Figures 3.17a, and b, respectively. These results demonstrated that cells were able to assemble and develop a unique and compact tissue to form bilayers., similarly as seen after 5 days. In addition, the lateral side and cross-section images of the bilayers (Figures 3.17c, d), revealed the formation of strong bonding between two monolayers into the tissue bilayers thanks to the presence of growing cells producing ECM. Moreover, the linkage between two monolayers shows that they were almost completely fused after 7 days of growth (Figure 3.16d).

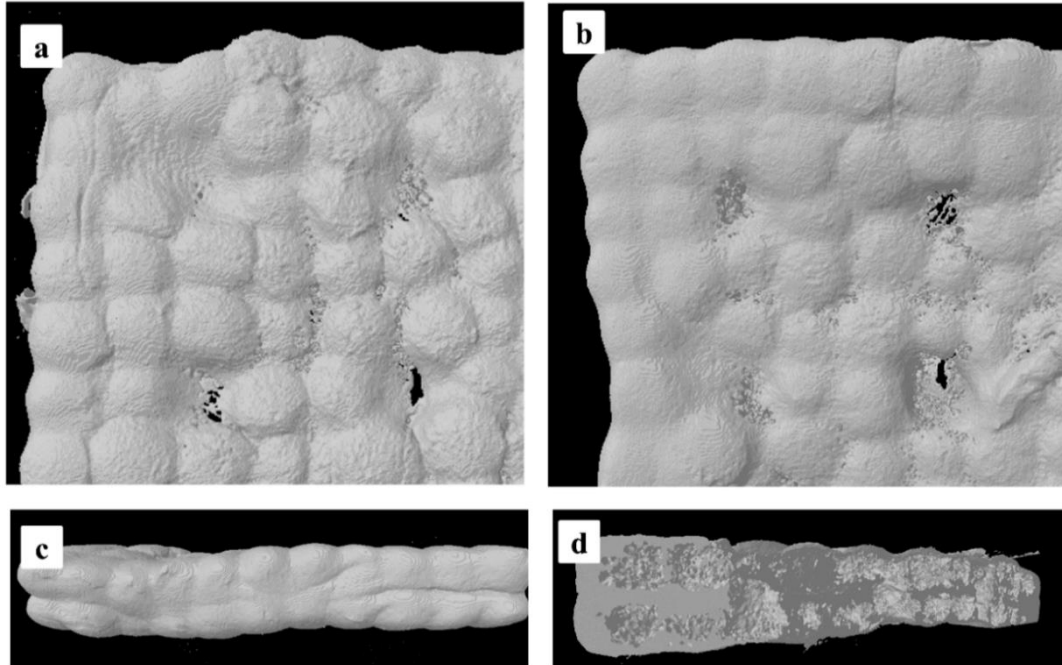


Figure 3.17: MicroCT analysis of new tissue of the bilayers after 7 days bonding. 3D reconstruction of the bilayer: upper side (a), and lower side (b). lateral side (c). Cross-section (d).

Figure 3.18 shows the percentage of tissue growth (cells and matrix) of bilayers after 5 days bonding and 7 days growth, evaluated by MicroCt analysis. These data demonstrated that the bilayers at 5 days bonding were composed by a tissue percentage of $63 \pm 1.9\%$ and at 7 days growth of $72 \pm 2.5\%$, with a statistically relevant increase over time.

In agreement with previous results, cell colonization into the bilayers were assessed by histology analysis. Figure 3.19 shows the histology analysis of bilayers at 5 days bonding and 7 days growth (low and high magnification). Cells grew up and colonized in the inner part of the bilayer obtained by assembling two ordered monolayers. These results clearly demonstrated the presence of cells and matrix into the bilayer at both 5 days of bonding (Figures 3.19a-c), and 7 days growth (Figures 3.19d-f). In addition, cell-cell and cell-ECM interactions at 7 days growth were more enhanced than 5 days bonding. These results confirmed the MicroCt analysis (Figure 3.16d and 3.17d) that showed the formation of strong bonding between two monolayers into the bilayers at day 7 growth.

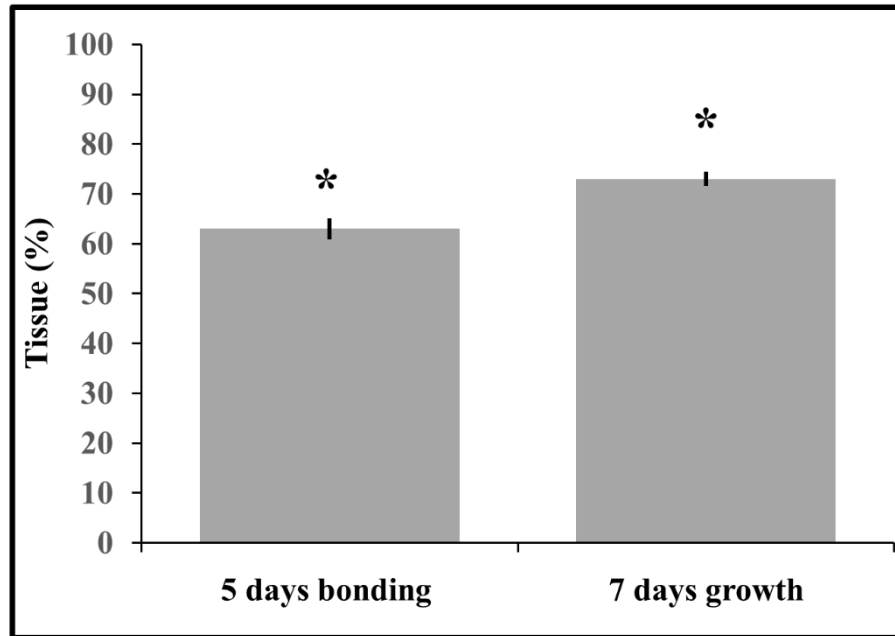


Figure3.18: MicroCT evaluation of the tissue volume fraction v % of the hybrid layers at 5 days bonding and 7 days growth.

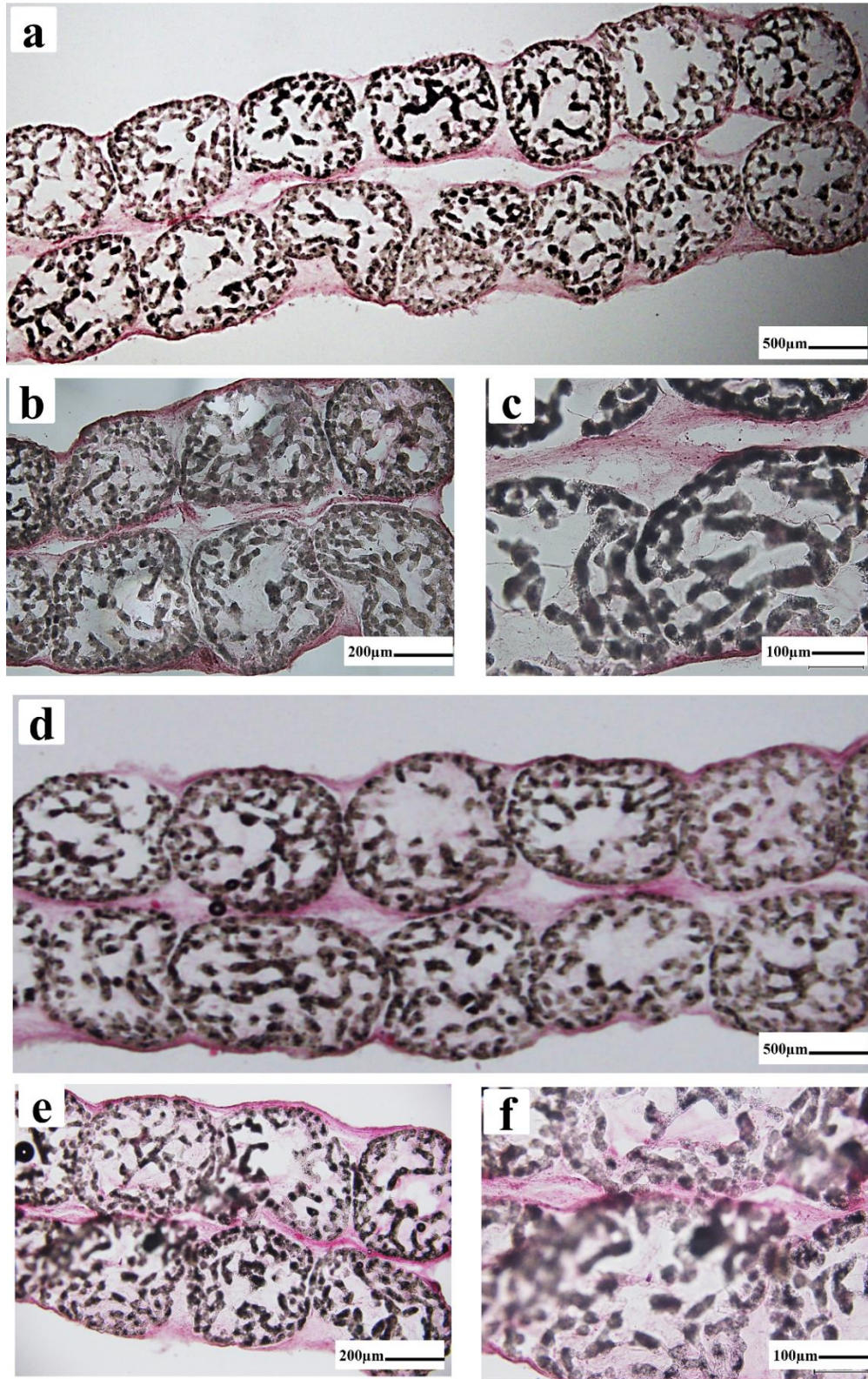


Figure 3.19: H&E staining of the cross-sections of the bilayers. (a-c), 5 days bonding. (d-f), 7 days bonding. Low and high magnification.

The evolution of the cell distribution and endothelial network formation onto the bilayer were monitored by confocal imaging (Figures 3.20 and 3.21). In these figures, the actin cytoskeleton, blood vessels and nuclei were highlighted by green, red, and blue colours respectively. These results revealed that HUVECs were able to form capillary like structures onto the bilayers. As shown in (Figures 3.20a-d), lower side and upper side (Figure 3.20e-h) of bilayers at 5 days bonding, cells distributed onto the entire surfaces of the bilayer. More importantly, blood vessels specifically organize themselves around the large pillars and μ -scaffolds (Figure 3.20b). These results demonstrated that blood vessels grew up more on the upper than the lower side, similarly, as observed for the monolayers.

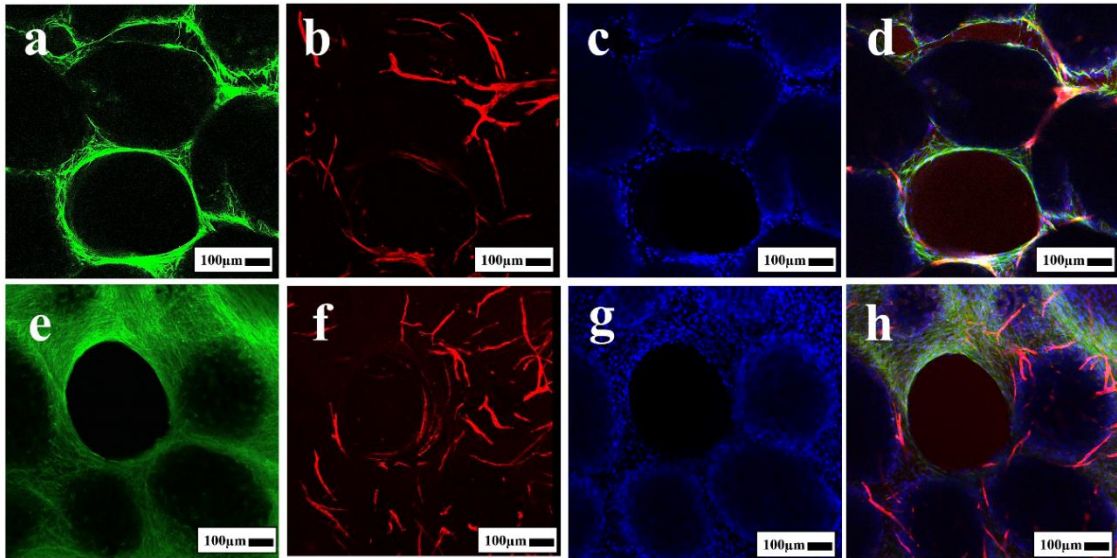


Figure3.20: CLSM images showing the morphology and colonization of HDFs and HUVECs co-culture cells on the bilayers at 5 days bonding. (a-d), lower side. (e-h), upper side. The actin cytoskeleton is marked in green (Phalloidin-488), Nuclei are marked in blue (HOECHST), and blood vessels in red (UEAI) and merge.

Figures 3.21a-d shows the lower side of bilayer at 7 days growth. Images demonstrate that after 7 days the cells occupied the space left by the large pillars and visible as a hole at the previous time point. In addition, lower side show less than blood vessels comparing with the upper side of bilayer at 7 days growth, similarly as observed for the monolayer.

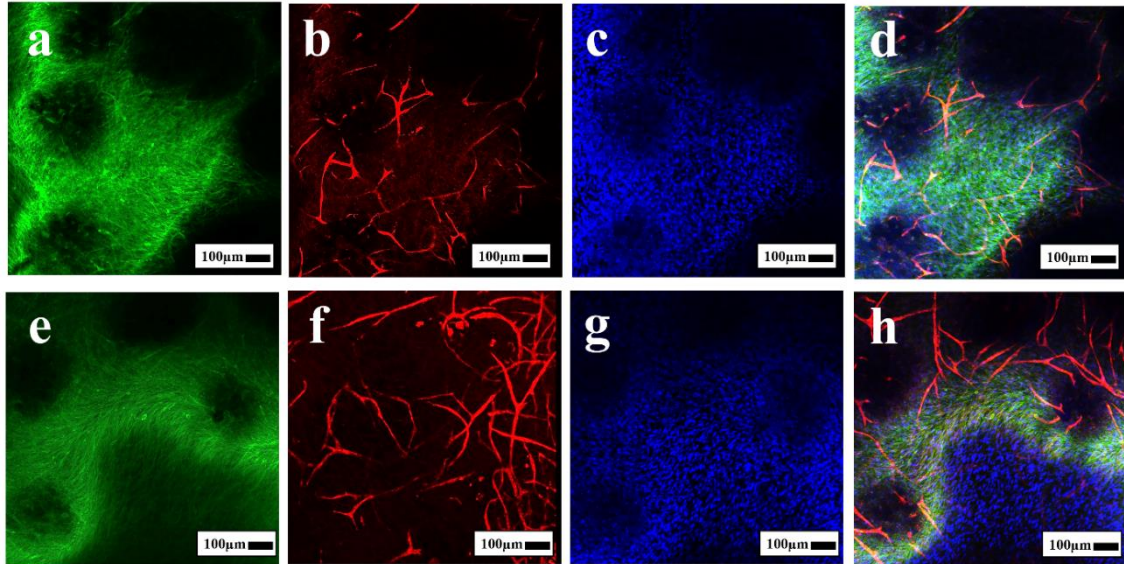


Figure 3.21: CLSM images showing the morphology and colonization of HDFs and HUVECs co-culture cells on the bilayers at 7 days bonding. (a-d), lower side. (e-h), upper side. The actin cytoskeleton is marked in green (Phalloidin-488), Nuclei are marked in blue (HOECHST), and blood vessels in red (UEAI) and merge.

Moreover, the volume fraction of blood vessels of the bilayers was evaluated (Figure 3.22). Specifically, these data were obtained by means of quantitative z-stacks analysis and the results indicated the blood vessels on the upper side were more abundant than lower side both after 5 days bonding and 7 days growth. As expected, the upper side at 7 days growth was more vascularized than 5 days bonding and they are significantly different.

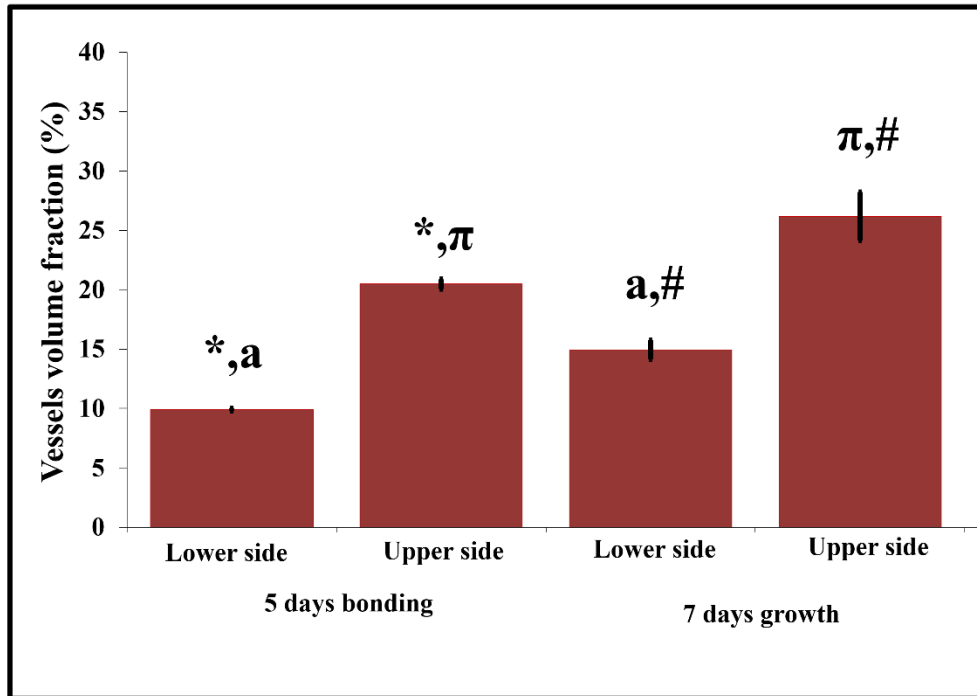


Figure 3.22: Image analysis of vessels volume fraction (%) on the bilayers at 5- and 7-days bonding.

Cell distribution and blood vessels formation in the inner part of bilayers were obtained as shown by confocal analysis of 20 μm thick bilayer sections (Figure 3.23). These results revealed that blood vessels were able to grow up into the 5 days bonding (Figure 3.23b) and 7 days growth (Figure 3.23f). In addition, blood vessels were more abundant at 7 days growth than 5 days bonding. The blood vessels volume fraction was evaluated by ImageJ analysis (Figure 3.23i). These data confirm that the volume fraction of blood vessels in the inner part of bilayers were enhanced with increasing the culture time. As discussed for the monolayers, also in the case of bilayers CLSM results have to be analysed taking into the account the 200 μm depth of the technique. In fact, the higher thickness of the bilayers (1 mm ca.), do not allowed the calculation of vascularization in the entire sample thickness but limit this measurement to the surfaces.

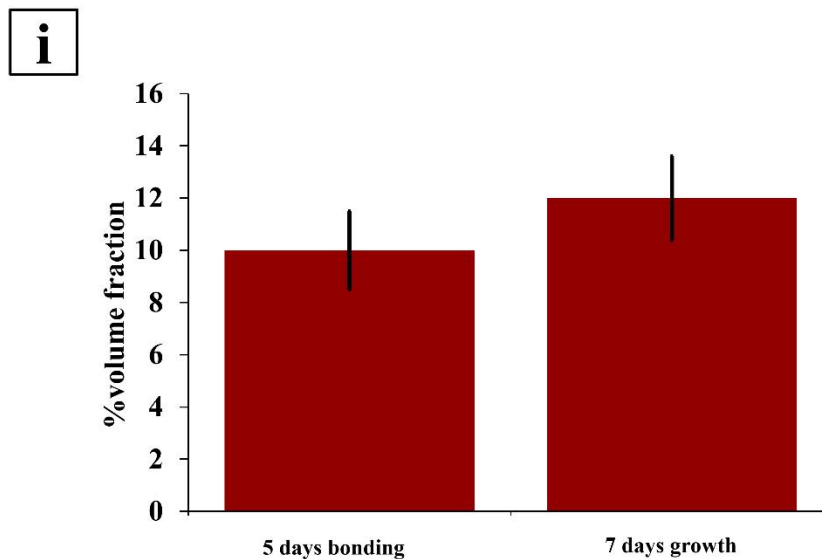
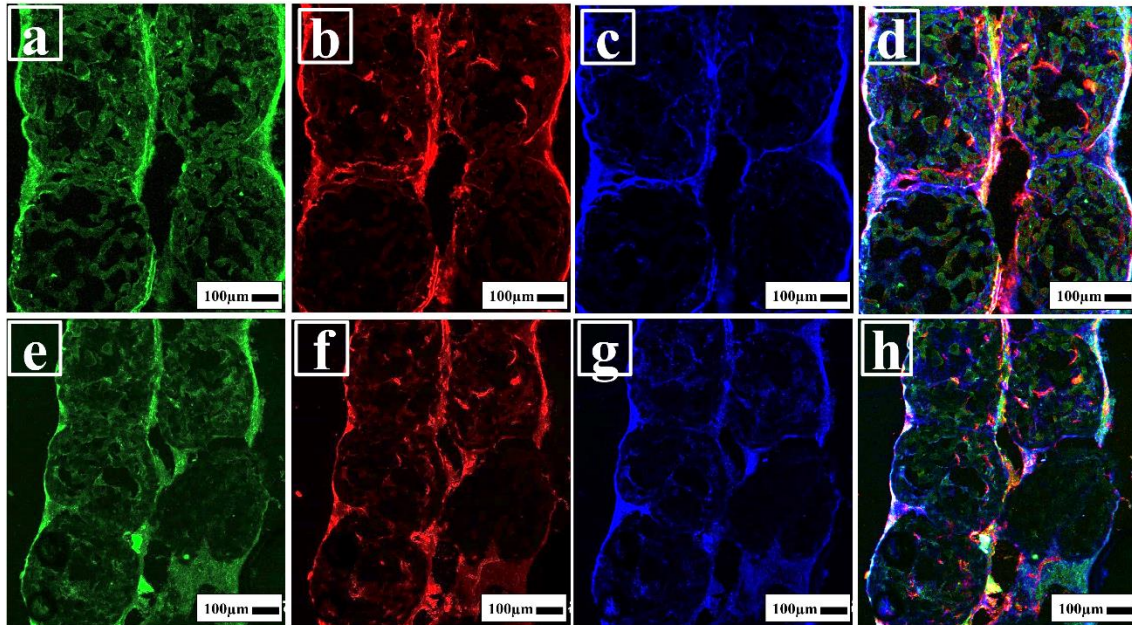


Figure3.23: CLSM analysis showing blood vessels formation in the inner part of bilayers. (a-d),5 days bonding. (e-h),7 days bonding. (i), volume fraction of blood vessels in the inner part of bilayers. for the actin cytoskeleton is marked in green (Phalloidin-488), Nuclei are marked in blue (HOECHST), and blood vessels in red (Rho-UEAI). nuclei (DAPI), merge.

3.3.6 Collagen amount and density into bilayer constructs

To correlate the role of ECM on blood vessels growth, we evaluated collagen organization and blood vessels in the bilayers (Figures 3.24 and 3.25) by SHG imaging. The images in (Figures

3.24a, b) of lower side and upper of the bilayers at 5 days bonding, respectively showed that blood vessels were totally embedded into the ECM rich in collagen produced by HDFs (gray). More importantly, the results showed that blood vessels (red) and collagen (black) followed similar orientation, indicating the guidance role of collagen fibres on blood vessels growth, both following the geometry of the original design of the mould used for the assembly.

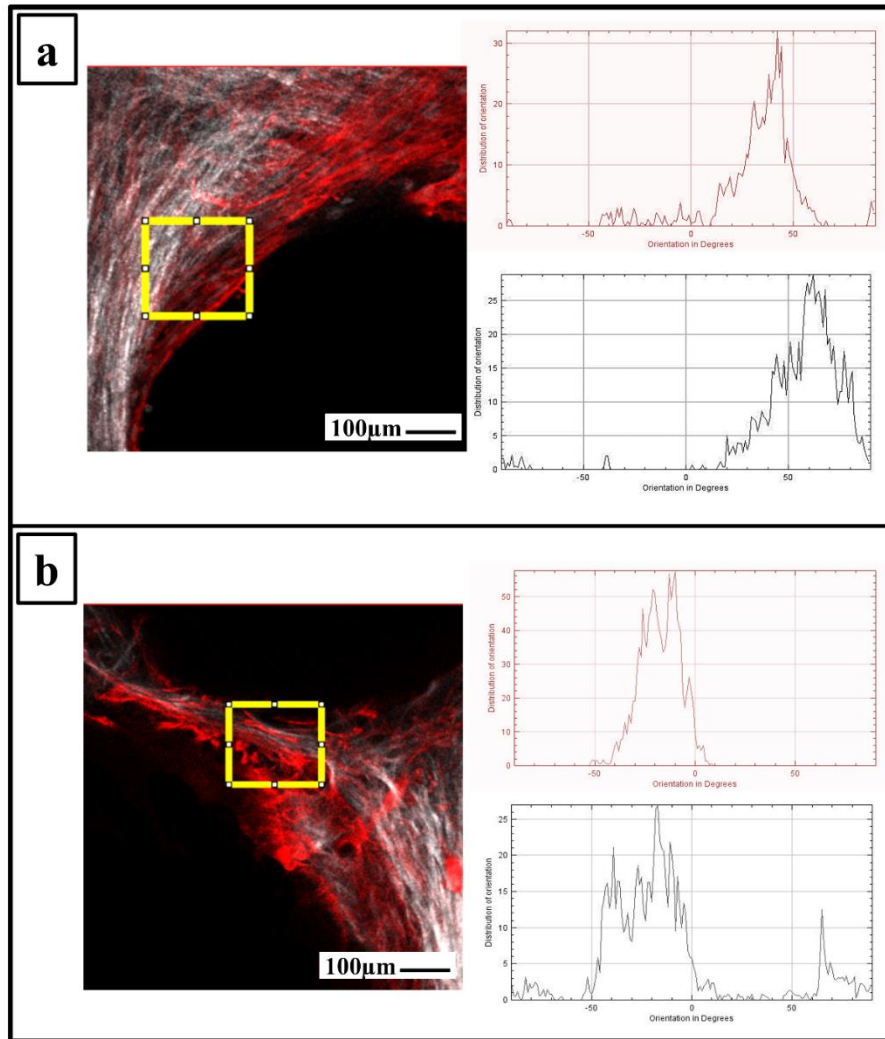


Figure3.24: SHG signal of collagen in gray and blood vessels in red of the bilayers at 5 days bonding. The graphics of the orientation of blood vessels (red) and ECM (black) were obtained by OrientationJ. (a), lower side. (b), upper side. (The dashed yellow rectangles indicate the region of interest analysed with OrientationJ).

As shown in (Figures 3.25a, b), similar results were found for bilayers at 7 days growth, despite cell colonization and closure of the big hole left by the pillars into the tissue.

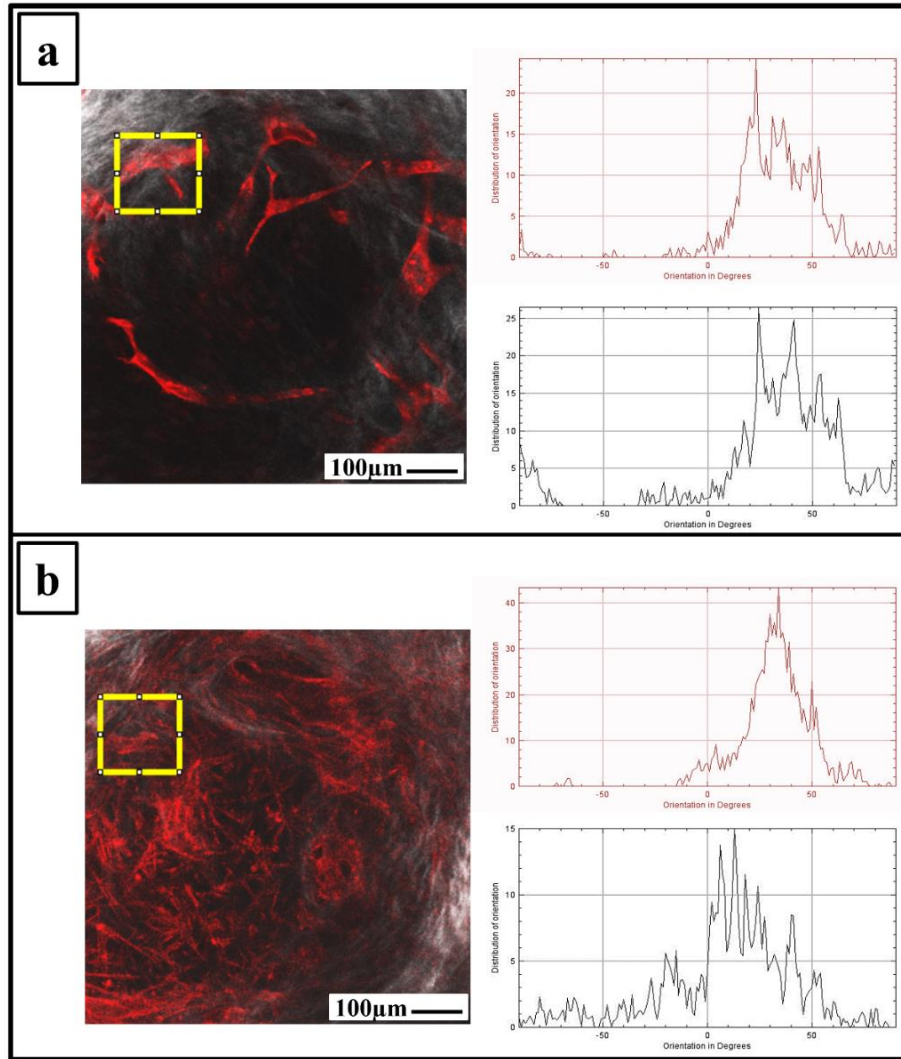


Figure 3.25: SHG signal of collagen in gray and blood vessels in red of the bilayers at 7 days bonding. The graphics of the orientation of blood vessels (red) and ECM (black) were obtained by OrientationJ (a), lower side. (b), upper side. (The dashed yellow rectangles indicate the region of interest analysed by OrientationJ).

Second harmonic generation pictures of the collagen fibres of the bilayer acquired by multiphoton microscopy analysis evidenced the percentage of collagen density deposition by the HDFs (Figure 3.26). These data showed that the density of collagen matrix was very similar in all the conditions.

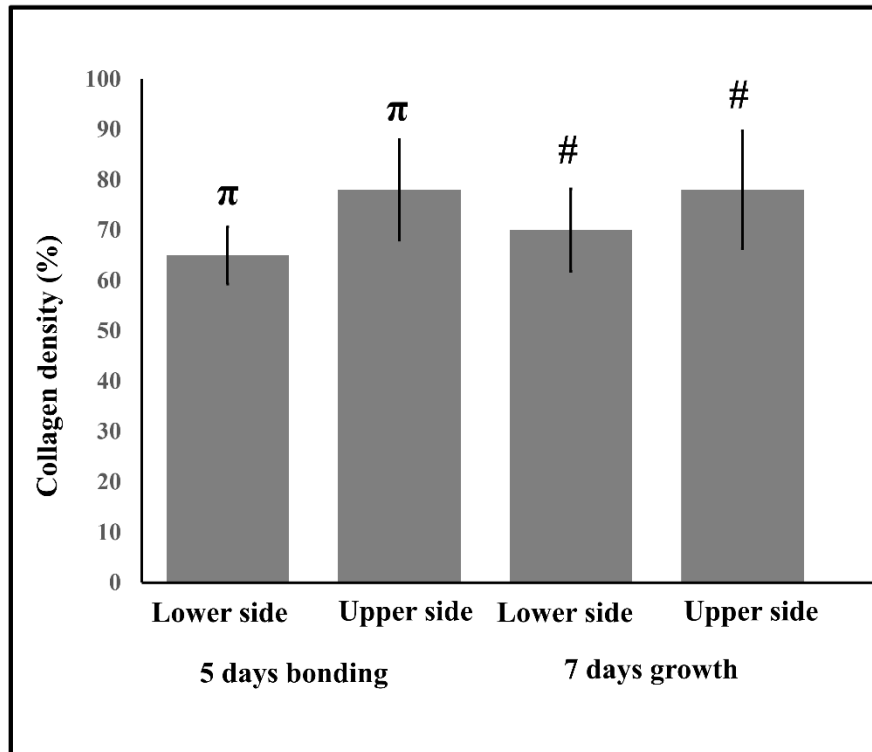


Figure3.26: Multiphoton microscopy evaluation of collagen biosynthesis of the monolayers

3.3.7 Bilayer discussion

In the second part of this study, thick vascularized bilayer constructs were built by the controlled assembly of two ordered monolayers. This was obtained by designing a bonding chamber is made of a PDMS-base suitable for monolayers alignment and PTFE-locks to maintain open porosity in the bilayer constructs. To achieve the final goal, the effect of culture time on the ECM and blood vessels growth onto the surface and inner part of the bilayers, were examined. There are recently reported works aiming to develop highly organized blood vessels *in vitro* engineered tissues [38-41]. For instance, mathematical modelling was used to demonstrate the importance of aligned channels on oxygen and nutrients transportation along the length of scaffold and finally on blood vessels formation and cell viability [42]. This virtual design was confirmed by another work where different regularly oriented micro-channels were produced by electrochemical replica deposition inside chitosan scaffolds to stimulate vascularization [40]. In our study, we used previous prepared ordered monolayers to build up to 1mm thick viable vascularized tissue constructs. Furthermore, the constructs were provided of nine aligned pores passing through the entire section for oxygen and nutrient transportation and metabolic wastes into the bilayer core. The results of formation

tissue of the bilayers characterization correspond with previous studies in which thick prevascularized tissues with highly organized in-built microvascular networks were fabricated [38-42]. In addition, the quantitative analysis of tissues formation was increased with increasing of culture time.

Here we showed the quantitative analysis of vessels volume fraction were increased of the upper and lower side of bilayers from 5 days bonding to 7 days growth and they were always higher into the upper side than lower side. Previous papers reported a similar behavior of co-culture with HDFs and HUVECs [11, 43]. Recent study was developed a multiple-micropillar system and designed micropillar array patterns to creation lung microtissues. They found that cells compact ECM freely along the micropillar height but such compaction in the horizontal plane is restricted by micropillar-defined boundary conditions, leading to the formation of thin, membranous microtissues [20]. Similar to that result and regardless of increasing culture time, we showed that the formation of tissue and blood vessels, at 5 days of bonding were less than 7 days growth, probably due to the present of the chamber device at 5 days bonding. We observed that dense collagen network formed onto the bilayers and onto the large hole of the hybrid tissue after 7 days growth. On the other hand, histology analysis showed that cells and ECM grew also at the interface between the monolayers creating a strong bonding between them. Furthermore, SHG imaging characterization of collagen showed the increase of collagen density over culture time and confirmed blood vessels grow along fibre direction. These results correspond with previous studies in which, collagen fraction and collagen assembly degree were significantly increased with increasing of culture time and were resembled with organization of blood vessels [11, 43].

3.4. Conclusion

The present work fabricated the complex vascularized hybrid tissues obtained *in vitro* by a new strategy in TE bottom-up approach. For this purpose, in the first step, the monolayers were fabricated by controlling the assembly of μ -scaffolds by using the soft-lithography techniques and HDFs-HUVECs co-culture system. In particular, we fabricated two monolayers named ordered and disordered to evaluate tissue, blood vessels, ECM formation, and cell distribution onto these monolayers. The results for assessing the utility of geometric control demonstrated that in contrast to the ordered monolayers, disordered monolayers were randomly organized blood vessels, especially onto the lower sides. Secondly, we successfully engineered the thick hybrid tissue by controlling the assembly of two ordered monolayers. Thus, further investigations on bilayers were

performed to assess constructs morphology, composition, and blood vessels. These findings demonstrate the importance of controlling the assembly of building blocks on vascular architecture. Moreover, our approach provides a unique strategy to control the assembly of monolayers and, consequently, engineer vascular architecture. The future perspective will focus on developing the cell seeding methods for forming more homogenous cell distribution and blood vessels in both sides of layers. The other possibility would be to investigate the 3D blood vessel network formation of the entire bilayers' inner part by confocal analysis.

3.5. References

- [1]. Lokmic, Z.; Mitchell, G.M. Engineering the microcirculation. *Tissue Eng, Part B*. **2008**, *14*, 87–103.
- [2]. Rouwkema, J.; Rivron, N.C.; van Blitterswijk, C.A. Vascularization in tissue engineering. *Trends Biotechnol*. **2008**, *26*, 434–441.
- [3]. Wray, L.S.; Tsioris, K.; Gi, E.S.; Omenetto, F.G.; Kaplan, D.L. Slowly degradable porous silk microfabricated scaffolds for vascularized tissue formation. *Adv Funct Mater*. **2013**, *23*, 3404-3412.
- [4]. Barabaschi, G.D.G.; Manoharan, V.; Li, Q.; Bertassoni, L.E. Engineering pre-vascularized scaffolds for bone regeneration, engineering mineralized and load bearing tissues advances in experimental medicine and biology. *Engineering Mineralized and Load Bearing Tissues*. **2015**, *881*, 79-94.
- [5]. Naito, Y.; Shinoka, T.; Duncan, D.; Hibino, N.; Solomon, D.; Cleary, M.; Rathore, A.; Fein, C.; Church, S.; Breuer, C. Vascular tissue engineering: Towards the next generation vascular grafts. *Advanced Drug Delivery*. **2011**, *63*, 312-323.
- [6]. Chrobak, K.M.; Potter, D.R.; Tien, J. Formation of perfused, functional microvascular tubes in vitro. *Microvascular Research*. **2006**, *71*, 185-196.
- [7]. Koike, N.; Fukumura, D.; Gralla, O.; Au, P.; Schechner, J.S.; Jain, R.K. Creation of long-lasting blood vessels. *Nature*. **2004**, *428*, 138-139.
- [8]. Choi, N.W.; Cabodi, M.; Held, B.; Gleghorn, J.P.; Bonassar, L.J.; Stroock, A.D. Microfluidic scaffolds for tissue engineering. *Nature Materials*. **2007**, *6*, 908-915.
- [9]. Harley, B.A.C.; Kim, H.D.; Zaman, M.H.; Yannas, L.V.; Lauffenburger, D.A.; Gibson, L.J. Microarchitecture of three-dimensional scaffolds influences cell migration behavior via junction interactions. *Biophysical Journal*. **2008**, *95*, 4013-4024.
- [10]. Kenara, H.; Ozdogan, C.Y.; Dumlu, C.; Doger, E.; Kose, G.T.; Hasirci, V. Microfibrous scaffolds from poly(L-lactide-co- ϵ -caprolactone) blended with xeno-free collagen/hyaluronic acid for improvement of vascularization in tissue engineering applications. *Mater Sci Eng C*. **2019**, *97*, 31-44.
- [11]. Mazio, C.; Casale, C.; Imperato, G.; Urciuolo, F.; Attanasio, C.; Gregorio, M. De.; Rescigno, F.; Netti, P.A. Pre-vascularized dermis model for fast and functional anastomosis with host vasculature. *Biomaterials*, **2019**, *192*, 159-170.

- [12]. Zhong, M.; Wei, D.; Yang, Y.; Sun, J.; Chen, X.; Guo, L.; Wei, Q.; Wan, Y.; Fan, H.; Zhang, X. Vascularization in engineered tissue construct by assembly of cellular patterned micro-modules and degradable microspheres. *ACS Appl. Mater. Interfaces*. **2017**, *9*, 3524-3534.
- [13]. Liu, J.; Chuah, Y.J.; Fu, J.; Zhu, W.; Wang, D.A. Co-culture of human umbilical vein endothelial cells and human bone marrow stromal cells into a micro-cavitary gelatin-methacrylate hydrogel system to enhance angiogenesis. *Mater Sci Eng C*. **2019**, *102*, 906-916.
- [14]. Sharma, D.; Ross, D.; Wang, G.; Jia, W.; Kirkpatrick, S.J.; Zhao, F. Upgrading prevascularization in tissue engineering: A review of strategies for promoting highly organized microvascular network formation. *Acta. Biomater*. **2019**, *95*, 112-130.
- [15]. Zheng, Y.; Chen, J.; Craven, M.; Choi, N.W.; Totorica, S.; Diaz-Santana, A.; Kermani, P; et al. In vitro microvessels for the study of angiogenesis and thrombosis. *PNAS*. **2012**, *109*, 9342-9347.
- [16]. Raghavan, S.; Nelson, C.M.; Baranski, J.D.; Lim, E.; Chen, C.S. Geometrically controlled endothelial tubulogenesis in micropatterned gels. *Tissue. Eng. Part A*. **2010**, *16*, 2255-63.
- [17]. Koroleva, A.; Deiwick, A.; Nguyen, A.; Narayan, R.; Shpichka, A. Hydrogel-based microfluidics for vascular tissue engineering. *BioNanoMat*. **2016**, *17*, 19-32.
- [18]. Tan, S.Y.; Leung, Z.; Wu, A.R. Recreating physiological environments in vitro: design rules for microfluidic-based vascularized tissue constructs. *Small*. **2020**, *16*, article n° 1905055.
- [19]. Cuchiara, M.P.; Gould, D.J.; McHale, M.K.; Dickinson, M.E.; West, J.L. Integration of self-assembled microvascular networks with microfabricated PEG-based hydrogels. *Adv. Funct. Mater*. **2012**, *22*, 4511-4518.
- [20]. Chen, Z.; Zhao, R. Engineered tissue development in biofabricated 3D geometrical confinement—A review. *ACS. Biomater. Sci. Eng*. **2019**, *5*, 3688-3702.
- [21]. Tomasina, C.; Bodet, T.; Mota, C.; Moroni, L.; Camarero-Espinosa, S. Bioprinting vasculature: materials, cells and emergent techniques. *Materials*. **2019**, *12*, article n° 2701.
- [22]. Miri, A.K.; Khalilpour, A.; Cecen, B.; Maharjan, S.; Shin, S.R.; Khademhosseini, A. Multiscale bioprinting of vascularized models. *Biomaterials*. **2019**, *198*, 204-216.

- [23]. Grebenyuk, S.; Ranga, A. Engineering organoid vascularization. *Front. Bioeng. Biotechnol.* **2019**, *7*, article n° 39.
- [24]. Bertassoni, L.E.; Cecconi, M.; Manoharan, V.; Nikkhah, M.; et al. Hydrogel bioprinted microchannel networks for vascularization of tissue engineering constructs. *Lab Chip.* **2014**, *14*, 2202-2211.
- [25]. Chiesa, I.; De-Maria, C.; Lapomarda, A.; Fortunato, G.M.; et al. Endothelial cells support osteogenesis in an in vitro vascularized bone model developed by 3D bioprinting. *Biofabrication.* **2020**, *12*, article n° 025013.
- [26]. Caldwell, D.J.; Rao, R.R.; Stegemann, J.P. Assembly of discrete collagen–chitosan microenvironments into multiphase tissue constructs. *Adv. Healthcare Mater.* **2013**, *2*, 673-677.
- [27]. Rossi, L.; Attanasio, C.; Vilaridi, E.; De Gregorio, M.; Netti, P.A. Vasculogenic potential evaluation of bottom-up, PCL scaffolds guiding early angiogenesis in tissue regeneration. *J. Mater. Sci: Mater. Med.* **2016**, *27*, article n° 107.
- [28]. Redd, M.A.; Zeinstra, N.; Qin, W.; Martinson, A. Patterned human microvascular grafts enable rapid vascularization and increase perfusion in infarcted rat hearts. *Nat Commun.* **2019**, *10*, article n° 584.
- [29]. Baranski, J.D.; Chaturvedi, R.R.; Stevens, K.R.; Eyckmans, J. Geometric control of vascular networks to enhance engineered tissue integration and function. *Proc. Natl. Acad. Sci. U S A.* **2013**, *110*, 7586-91.
- [30]. Song, W.; Chiu, A.; Wang, L.; Schwartz, R.E. Engineering transferrable microvascular meshes for subcutaneous islet transplantation. *Nat. Commun.* **2019**, *10*, article n° 4602.
- [31]. Cheng, G.; Liao, S.; Wong, H.K.; Lacorre, D.A. Engineered blood vessel networks connect to host vasculature via wrapping-and-tapping anastomosis. *Blood.* **2011**, *118*, article n° 17.
- [32]. Berthod, N.F.; Germain, L.; Tremblay, N.; Auger, F.A. Extracellular matrix deposition by fibroblasts is necessary to promote capillary-like tube formation in vitro. *J. Cell. Physiol.* **2006**, *207*, 12-22.
- [33]. Auger, F.A.; Gibot, L.; Lacroix, D. The pivotal role of vascularization in tissue engineering. *Annu. Rev. Biomed. Eng.* **2013**, *15*, 177-200.
- [34]. Yang, F.; Cohen, R.N.; Brey, E.M. Optimization of co-culture conditions for a human vascularized adipose tissue model. *Bioengineering.* **2020**, *7*, article n° 114.

- [35]. Costa-Almeida, R.; Gomez-Lazaro, M.; Ramalho, C.; Granja, P.L.; et al. Fibroblast-endothelial partners for vascularization strategies in tissue engineering. *Tissue Eng. Part A*. **2015**, *21*, 5-6.
- [36]. Rhodes, J.M.; Simon, M. The extracellular matrix and blood vessel formation: not just a scaffold. *J. Cell. Mol. Med.* **2007**, *11*, 176-205.
- [37]. Kusindarta, D.L.; Wihadmadyatami, H. The role of extracellular matrix in tissue regeneration, tissue regeneration. *Tissue Regeneration*. **2018**, 65-73.
- [38]. Andersson, H.; Van Den Berg, A. Microfabrication and microfluidics for tissue engineering: state of the art and future opportunities. *Lab Chip*. **2004**, *4*, 98-103.
- [39]. Varoni, E.M.; Altomare, L.; Cochis, A.; GhalayaniEsfahani, A.; et al. Hierarchic micro-patterned porous scaffolds via electrochemical replica-deposition enhance neo-vascularization, *Biomed. Mater.* **2016**, *11*, article n° 025018.
- [40]. Zhang, W.; Wray, L.S.; Rnjak-Kovacina, J.; Xu, L.; Zou, D.; Wang, S. Vascularization of hollow channel-modified porous silk scaffolds with endothelial cells for tissue regeneration, *Biomaterials*. **2015**, *56*, 68-77.
- [41]. Thomson, K.S.; Korte, F.S.; Giachelli, C.M.; Ratner, B.D.; Regnier, M.; Scatena, M. Prevascularized microtemplated fibrin scaffolds for cardiac tissue engineering applications. *Tissue Eng. Part A*. **2013**, *19*, 967-977.
- [42]. Mofrad, A.Z.; Mashayekhan, S.; Bastani, D. Simulation of the effects of oxygen carriers and scaffold geometry on oxygen distribution and cell growth in a channeled scaffold for engineering myocardium. *Math. Biosci.* **2017**, *294*, 160-171.
- [43]. Mazio, C.; Imperato, G.; Urciuolo, F.; Netti, P.A. Recapitulating spatiotemporal tumor heterogeneity in vitro through engineered breast cancer microtissues. *Acta Biomater.* **2018**, *73*, 236–249.

Chapter 4

Conclusions

Over the last decade, there has been an impressive advancement on μ -scaffolds and strategies for bioengineer functional tissues and organs *in vitro* and *in vivo*. In this regard, bottom-up approaches based on the assembly of modular building blocks are, nowadays, the most promising and used approaches. However, controlling the assembly of modular unit into ordered predefined geometry is still challenging and require technological advancement and innovation.

In this work we demonstrated that porous μ -scaffolds can be designed having a biomimetic trabecular architecture and, modularly assembled into predefined pattern to guide the spatial composition and organization of the de-novo synthesized cell/ECM construct.

In the first stage of this study, PCL porous μ -scaffolds with new morphology were successfully fabricated by a fluidic oil/water emulsion and particles coagulation process and by using PEO as a biocompatible pore-generating agent. The as obtained μ -scaffolds have spherical shape, complete pore interconnectivity, narrow diameter distribution and mean diameter easily controllable by adjusting the composition of the polymeric solution and the flow rate of the continuous phase. For the purpose of investigating the biocompatibility of PCL μ -scaffolds, HDFs were statically seeded and cultured *in vitro* for 25 days onto the μ -scaffolds. These results demonstrated that PCL μ -scaffolds with a trabecular architecture, full pores interconnectivity, and pores size suitable to promote and guide *in vitro* HDFs adhesion, colonization, and ECM biosynthesis towards functional hybrid tissue development.

In the second part of this work, a novel strategy is presented to precisely control the assembly of μ -scaffolds to fabricate vascularized complex hybrid tissue. First, monolayers were fabricated by patterning PCL μ -scaffolds following two different arrays, ordered and disordered, and using soft-lithography technique. The co-culture of HDFs and HUVECs was optimized to stimulate tissue grow and blood vessels formation. The results of this study demonstrated that tissue grow, and vascularization strictly depended on μ -scaffolds porosity and spatial distribution and, that an ordered design provide provided better results than a disordered one.

To achieve the final goal of fabricating thick hybrid viable vascularized tissues we assembled two ordered monolayers with the aid of specially designed chamber, and we evaluated the characteristics of the final tissues after 5 days monolayers bonding and 7 days growth. The results of bilayers construct morphology, composition and vascularization showed that the develop approach enabled the achievement of viable hybrid tissues provided of homogenous vascularization onto the surface and into the inner part. In the context of the biomimetic design of

the structure and vasculature of hybrid tissues the computer aided approach develop in this work may allow to adapt this design to specific tissue that we want to regenerate. In fact, by simply changing the design of patterned mold, it is possible to modulate the porosity and morphology of the layered structure to match those of other connective tissues, like bone. Furthermore, mold design can take into the account other biological constrains such as the development of anisotropic vasculature as well as cells population heterogeneity.

Chapter 5

Future perspectives

5.1. Control of hybrid tissue composition and growth by the modulation of micro-scaffolds degradation

The degradation of micro-scaffolds plays a crucial role in successful tissue regeneration. Therefore, the following recommendations for future work are worth considering for the sake of simplicity and to earn the basic knowledge about improving the degradation of μ -scaffolds in our strategy. In this regard, PLGA has been one of the most studied biopolymers in the literature as a popular and important biodegradable polyester owing to its tunable degradation rates, good mechanical properties, and processibility [1, 2]. Hence, to improve μ -scaffolds degradability, we replaced PLGA with a degradation rate of about 3-6 months with PCL. However, this system needs further investigation which can be consider as a future perspective of this project.

In summary, PLGA μ -scaffolds were fabricated by fluidic oil/water emulsion and particle coagulation process (chapter 2), and by using Pluronic F-127 as an excellent biocompatible pore-generating agent, similar to the process reported [3]. Through this process, we obtained PLGA μ -scaffolds provided of spherical shape, narrow diameter distribution of the μ -scaffolds size that was about 500 μm , and mean diameter easily controllable by adjusting the composition of the polymeric solution and the flow rate of the continuous phase. Here is showing the morphology of the porous PLGA μ -scaffolds with higher porosity in the surface and cross-section, (Figure 5.1a-d).

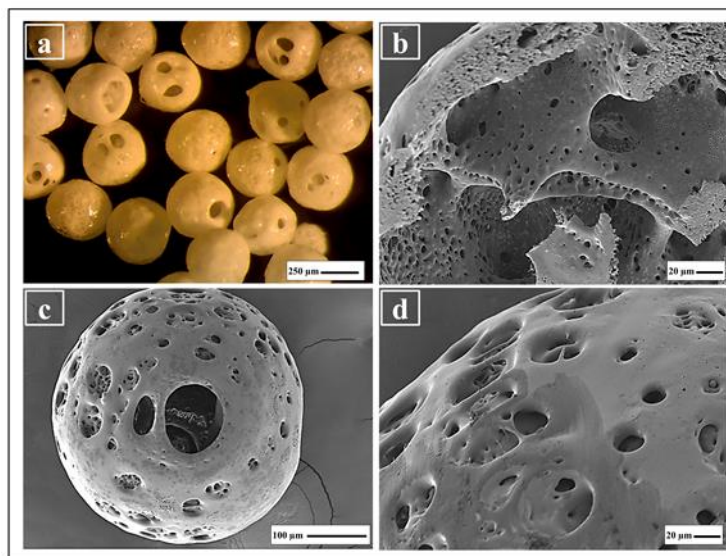


Figure5.1: Stereomicroscope and SEM images of the morphology of the surface and cross-section of PLGA μ -scaffolds obtained from 10 w/v % polymers concentration and Pluronic F-127 concentration in the 40

w/w %. Fluidic emulsion was carried out by setting $Q_{DP} = 90 \mu\text{L}/\text{min}$ and by using 0.5 w/v % PVA solution as coagulation bath at RT for 3h.

Therefore, there might be a possibility of forming a uniform morphology and highly open surface porosity of the PLGA μ -scaffolds. However, considering the different architecture between this PLGA μ -scaffolds and PCL μ -scaffolds previously characterized, the feasibility of using these newly faster degradable samples in our approach has to be validated.

5.2. Control of hybrid tissue vascularization by the incorporation of growth factors delivering micro-scaffolds

Designed drug delivery systems aim to provide control over the localization, time, and kinetics of the release pattern of signaling molecules such as growth factors according to the drug chemical properties and specific biological mechanisms. In this case, PLGA μ Ps encapsulating VEGF were prepared by water-in-oil-in-water emulsion procedure. As obtained μ Ps, measuring $25\mu\text{m}$ mean diameter approximately, were packed and sintered into a preformed pristine gelatin micro-holder to prepare $500\mu\text{m}$ sample suitable to be located inside the pores of the monolayers and bilayers samples (Figure 5.2).

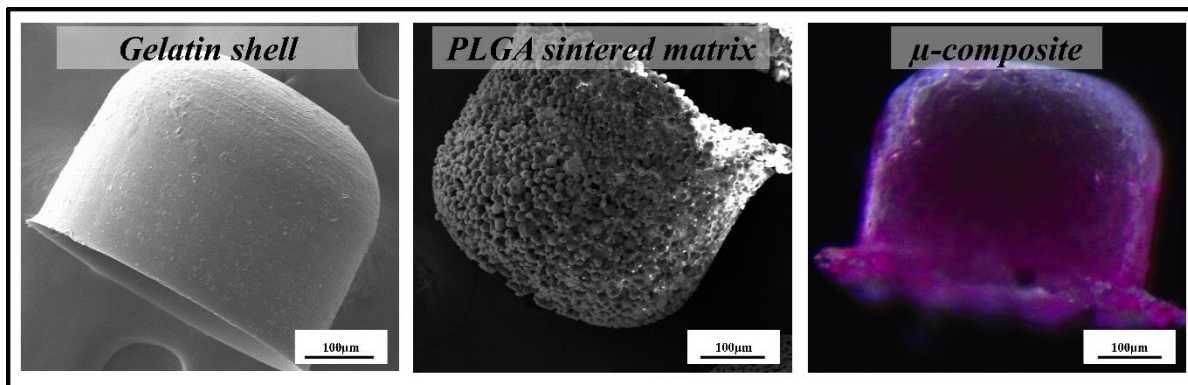


Figure5.2: SEM photographs of gelatin shell, sintered PLGA μ -scaffolds and lateral view of a μ -composite.

PLGA μ Ps sintering was carried out by using a mild vapor sintering procedure, similar to that described in [4]. The combination of these drug delivery systems with hybrid samples developed during this project may open new route to study blood vessels grow and maturation mechanisms under the spatial and temporal controlled release of bioactive molecules [4].

5.3. References

- [1]. Zhang, H.; Zhou, L.; Zhang, W. Control of scaffold degradation in tissue engineering: a review. *Tissue Eng Part B Rev.* **2014**, *20*, 492-502.
- [2]. Pan, Z.; Ding, J. Poly(lactide-co-glycolide) porous scaffolds for tissue engineering and regenerative medicine. *Interface Focus.* **2012**, *2*, 366–377.
- [3]. Kim, H. K., Chang, H. J., Park, T. G., Biodegradable polymeric microspheres with “open/closed” pores for sustained release of human growth hormone. *J. Control. Release.* **2006**, *112*, 167-174.
- [4]. De Alteriis, R.; Vecchione, R.; Attanasio, C.; De Gregorio, M.; Porzio, M.; Battista, E.; Netti, P.A. A method to tune the shape of protein-encapsulated polymeric microspheres. *Sci. Rep.* **2015**, *5*, article n° 12634.

List of publication:

- [1]. **Pedram, P.**; Mazio, C.; Imparato, G.; Netti, P.A.; Salerno, A. Bioinspired design of novel micro-scaffolds for fibroblasts guidance towards in vitro tissue building. *ACS. Appl. Mater. Interfaces*. **2021**, *13*, 9589-9603.
- [2]. De Luca, I.; **Pedram, P.**; Moeini, A.; Cerruti, P.; Peluso, G.; Di Salle, A.; Germann, N. Nanotechnology development for formulating essential oils in wound dressing materials to promote the wound-healing process: A Review. *Appl. Sci.* **2021**, *11*, article n° 1713.
- [3]. Salerno, A.; Leonardi, A. B.; **Pedram, P.**; Maio, E. Di.; Fanovich, M. A.; Netti, P. A. Tuning the three-dimensional architecture of supercritical CO₂ foamed PCL scaffolds by a novel mould patterning approach. *Mater. Sci. Eng. C.* **2020**, *109*, article n° 110518.
- [4]. Moeini, A.; **Pedram, P.**; Makvandid, P.; Malinconico, M.; Gomez d'Ayala, G. Wound healing and antimicrobial effect of active secondary metabolites in chitosan-based wound dressings: A review. *Carbohydr. Polym.* **2020**, *233*, article n° 115839.
- [5]. Salerno, A.; Cesarelli, G.; **Pedram, P.**; Netti, P.A. Modular strategies to build cell-free and cell-laden scaffolds towards bioengineered tissues and organs. *J. Clin. Med.* **2019**, *8*, article n° 1816.